Thermal field-flow fractionation and the advanced analysis of complex polymers

by

Upenyu Lucky Muza

This thesis is presented in partial fulfilment of the degree of Doctor of Philosophy in Polymer Science, from the Faculty of Science at Stellenbosch University, South Africa

Supervisor: Prof. Harald Pasch

December 2019

Thesis declarations

By submitting this thesis electronically, I the undersigned candidate declare that:

1. The entirety of the work contained herein is my own original work.
2. I am the sole author thereof (save to the extent explicitly stated otherwise).
3. Reproduction and publication thereof by Stellenbosch University will not infringe on any third-party rights.
4. Hitherto, I have not in entirety or partiality submitted any of this work to obtain any qualification.

December 2019

Upenyu Lucky Muza

Declaration on publications

The nature of work and extent of contribution by the author of this thesis in all peer reviewed publications contained herein are as follows:

Nature of work	Extent of contribution (%)
Experimental work, data analysis and discussion of results.	90
Drafting of manuscripts and responding to comments from the reviewers.	90

The nature of the work carried out by co-authors is as follows: Experimental work, data analysis, discussion of results, drafting of manuscripts and responding to comments from the reviewers. The following co-authors have contributed to the publications contained in this thesis as subsequently tabulated.

Publication	Co-authors	Contribution (%)
Core microstructure, morphology and chain arrangement of block copolymer self-assemblies as investigated by thermal field-flow fractionation.	Harald Pasch	8
	Guilaume Greyling	2
Stereocomplexation of polymers in micelle nanoreactors as studied by thermal field-flow fractionation.	Harald Pasch	8
	Guilaume Greyling	2
Thermal field-flow fractionation with quintuple detection for the comprehensive analysis of complex polymers.	Harald Pasch	10

Declaration by co-authors:

1. The declaration above accurately reflects the nature and extent of the contributions by the co-authors to the manuscripts contained in this thesis.
2. In addition to the co-authors specified above, no other authors contributed to the manuscripts in this dissertation, and
3. All parties granted their consent for the inclusion of all work contained in the manuscripts, and any potential conflicts of interest have been disclosed to all parties.

Acknowledgements

First and foremost, I would like to extend my heartfelt gratitude to my supervisor, Prof. Harald Pasch, for extending to me this wonderful learning opportunity. I am forever grateful and indebted for the mentoring as well as the academic, moral and financial support that I generously received from your person and office.

I also want to take this opportunity to thank my family for their unwavering emotional support and incomparable love and fortitude throughout my studies. I love you all so much!

Much appreciation goes to the members of Prof. Pasch's research group, friends, colleagues and the entire Department of Chemistry and Polymer science at Stellenbosch University for affording me such unparalleled academic and administrative assistance.

I give the utmost thanks and praises to the Almighty God for His divine guidance and grace in my life. Most importantly I would like to acknowledge God in my mother tongue (Chishona), and say, *ndinotenda Ishe wangu!*, meaning "thank you my Lord".

Contents

List of figures

List of tables

Abstract

Self-assemblies (SAs) and composites designed from block copolymers (BCPs) have found an important niche in nanotechnology. In order to establish commercially viable and sustainable polymeric applications for such materials in industry, there is a need to develop advanced analytical methods for their characterization. SAs being polymeric in nature inherently exhibit molecular heterogeneity, and thus their molecular properties are not specific but rather exist as distributions, which immensely impacts on their ultimate performance. As such, there is a critical need to move away from the traditional batch mode analytical techniques which only yield average property values. Instead, it is imperative to embrace separation techniques such as size exclusion chromatography (SEC) and field-flow fractionation (FFF) which have been applied for the analysis of molecular properties and the corresponding distributions. In particular, the advent of thermal field-flow fractionation (ThFFF) as a sub-technique of FFF has enabled unique separations of SAs according to both hydrodynamic size (D_h) and chemical composition (CC).

Herein, the focus of the research was directed at developing multidimensional analytical techniques for the analysis of SAs in three separate but mutually related studies. In the first case, the focus was on investigating the impact of microstructural and molecular packing differences of the core domains on the behaviour of SAs. The core microstructure and molecular density are cumulatively shown to impact on the morphology, critical micelle concentration (CMC), hydrodynamic diameter (D_h), molar mass (M_w), aggregation number (Z), elastic behaviour and thermal stability.

Secondly, ThFFF was successfully applied in the analysis of nanoreactors. Specific SAs are shown to be capable of functioning as micelle nanoreactors (MNRs) by triggering phase separated and thermally induced physical transitions within the micelle core to produce new SAs with unique properties. In essence, the MNRs are shown to circumvent the inherent precipitations associated with stereocomplexation (SC) of polymers, thus providing a vital route for studying SCs in solution.

Finally, a ThFFF-quintuple detection system (ThFFF-QD) was presented for the comprehensive analysis of SAs and other complex polymers. This novel approach used the so-called triple detection (TD), that is, differential viscometer (dVis), refractive index and (dRI) and static light scattering (SLS) detectors. TD was complimented by a second concentration detector (ultraviolet, UV) and a dynamic light scattering (DLS) detector.

The method development process for (ThFFF-QD) was based on linear, branched and isotopic polystyrenes (PSs) as model compounds. In particular, ThFFF of isotopic polystyrene analogues was fundamentally shown to exhibit gravimetric and density sensitivities. Structural information for SAs was elucidated from the Mark-Houwink (MH) and conformation plots and correlated with chemical composition, structure, compactness, molar mass, aggregation number (Z), size and intrinsic viscosity (IV).

Opsomming

Selfversamelings (SAs) en samestellings wat uit blok ko-polimere (BCPs) ontwerp is, het 'n belangrike nis in nanotegnologie gevind. Ten einde kommersieel lewensvatbare en volhoubare polimeertoepassings vir sulke materiale in die industrie te vestig, is daar 'n behoefte om gevorderde analitiese metodes vir hul karakterisering te ontwikkel. SAs se polimeriese aard toon inherent molekul ê re heterogeniteit, en dus is hul molekul ê re eienskappe nie spesifiek nie, maar bestaan dit eerder as verspreidings, wat 'n geweldige impak op hul uiteindelike gedrag het. As sodanig is daar 'n kritiese behoefte om weg te beweeg van die tradisionele bondel-modus analitiese tegnieke wat slegs gemiddelde eienskapwaardes lewer. In plaas daarvan is dit noodsaaklik om skeidingstegnieke soos grootte-uitsluitingschromatografie (SEC) en veld-vloeifraksionering (FFF) te gebruik wat aangewend is vir die analise van molekul ê re eienskappe en die ooreenstemmende verspreidings. In die besonder het die koms van termiese veld-vloeifraksionering (ThFFF) as 'n subtegniek van FFF, unieke en gesamentlike skeidings van SAs volgens beide hidrodinamiese grootte (Dh) en chemiese samestelling (CC) toegelaat.

Die fokus van die navorsings is gerig op die ontwikkeling van multidimensionele analitiese tegnieke vir die analise van SAs in drie afsonderlike, maar onderling verwante, studies. In die eerste plek is die fokus op die ondersoek van die impak van mikrostruktuur- en molekul ê re pakkingsverskille van die kernarea, op die gedrag van SAs. Daar word aangedui dat die kernmikrostruktuur en molekul ê re digtheid 'n kumulatiewe impak op die morfologie, kritiese miselkonsentrasie (CMC),

hidrodinamiese deursnee (Dh), molêre massa (Mw), samevoegingsnommer (Z), elastiese gedrag en termiese stabiliteit het.

Tweedens, is ThFFF suksesvol toegepas in die analise van nanoreaktore. Daar word aangedui dat spesifieke SAs in staat is om as miselnanoreaktore (MNRs) te funksioneer deur fase-geskeide en termies geïnduseerde fisiese oorgange binne die miselkern te aktiveer om nuwe SAs met unieke eienskappe te produseer. In wese word daar aangedui dat die MNRs die inherente neerslae, wat verband hou met stereokompleksering (SC) van polimere, omseil en dus 'n belangrike roete bied vir die bestudering van SCs in oplossing.

'n ThFFF-vyfvoudige-opsporingstelsel (ThFFF-QD) vir die omvattende analise van SAs en ander komplekse polimere is voorgestel. Hierdie nuwe benadering gebruik die sogenaamde drievoudige opsporing (TD); wat differensiële viskometer- (dVis), brekingsindeks- (dRI) en statiese ligverstrooiings- (SLS) detektors is. TD is gekomplimenteer deur 'n tweede konsentrasie detektor (ultraviolet, UV) en 'n dinamiese ligverstrooiings- (DLS) detektor.

Die metode-ontwikkelingsproses vir (ThFFF-QD) is gebaseer op lineêre, vertakte en isotopiese polistireen (PS) as modelverbindings. In die besonder, is daar fundamenteel aangedui dat ThFFF van isotopiese polistireenanaloë, gravimetriese- en digtheidsensitiwiteite uitbeeld. Strukturele inligting vir SAs is uit die Mark-Houwink (MH) en konformasiegrafieke verklaar en gekorreleer met chemiese samestelling, struktuur, kompaktheid, molêre massa, samevoegingsnommer (Z), grootte en intrinsieke viskositeit (IV).

Research outputs

Publications

1. UL Muza, GH Greyling, H Pasch. Core microstructure, morphology and chain arrangement of block copolymer self-assemblies as investigated by thermal field-flow fractionation. *Journal of Chromatography A* 1562 (2018) 87-95. DOI: 10.1016/j.chroma.2018.05.065
2. UL Muza, GH Greyling, H Pasch. Stereocomplexation of Polymers in Micelle Nanoreactors as Studied by Thermal Field-Flow Fractionation. *Analytical Chemistry* 90 (2018) 13987-13995. DOI: 10.1021/acs.analchem.8b03590
3. UL Muza, H Pasch. Thermal Field-Flow Fractionation with Quintuple Detection for the Comprehensive Analysis of Complex Polymers (just published). *Analytical Chemistry* (2019). DOI: 10.1021/acs.analchem.9b01384.

Conference presentations

1. UL Muza, GH Greyling, H Pasch. Core microstructure, morphology and chain arrangement of block copolymer self-assemblies as investigated by thermal field-flow fractionation. 19th International Symposium on Field and Flow-based Separations, Columbia, SC, 14-17 May 2018.
2. UL Muza, GH Greyling, H Pasch. A comprehensive analysis of the evolution of worm and jellyfish micelles by multi-detector thermal field-flow fractionation

(ThFFF). PISA International Conference, Stellenbosch, South Africa, 9-10 November 2017.

3. UL Muza, GH Greyling, H Pasch. Thermal field-flow fractionation and the comprehensive analysis of complex polymers. Oral presentation at the 9th International Symposium on the Separation and Characterization of Natural and Synthetic Polymers, Amsterdam, The Netherlands, 30 January - 1 February 2019.
4. UL Muza, GH Greyling, H Pasch. Stereocomplexation of Polymers in Micelle Nanoreactors as Studied by Thermal Field-Flow Fractionation. Poster presentation at the 9th International Symposium on the Separation and Characterization of Natural and Synthetic Polymers, Amsterdam, The Netherlands, 30 January - 1 February 2019.
5. UL Muza, H Pasch. Novel Thermal Field-Flow Fractionation Quintuple Detection (ThFFF - QD) for the Comprehensive Analysis of Complex Polymers. Poster presentation at the 9th International Symposium on the Separation and Characterization of Natural and Synthetic Polymers, Amsterdam, The Netherlands, 30 January - 1 February 2019.
6. UL Muza, GH Greyling, H Pasch. Stereocomplexation of Polymers in Micelle Nanoreactors as Studied by Thermal Field-Flow Fractionation. Poster presentation at the 13th International Conference on Advanced Polymers via Macromolecular Engineering, Stellenbosch, South Africa, 15 - 18 April 2019.

List of symbols and abbreviations

ABC	Amphiphilic block copolymer
ACN	Acetonitrile
AF4	Asymmetric flow field-flow fractionation
A_2	Second virial coefficient
BCP	Block copolymer
C	Concentration
CC	Chemical composition
CCD	Chemical composition distribution
CMC	Critical micelle concentration
CMD	Core microphase domain
CMT	Critical micelle temperature
dRI	Differential refractive index
dVis	Differential viscometer
D	Diffusion coefficient
DBC	Diblock copolymer
D_h	Hydrodynamic diameter

DLS	Dynamic light scattering
dn/dc	Specific refractive index increment
D_T	Thermal diffusion coefficient
f	Coefficient of friction
F	Force
FFF	Field-flow fractionation
FlFFF	Flow field-flow fractionation
FTIR	Fourier-transform infrared spectroscopy
^{1}H-NMR	Proton nuclear magnetic resonance spectroscopy
K	Boltzmann constant
L	Distance from the accumulation wall
MALDI-TOF MS	Matrix-assisted laser desorption/ionization mass spectrometry
MALS	Multiangle light scattering
MH	Mark-Houwink
MMD	Molar mass distribution
MD	Morphology distribution
M_η	Viscosity-average molar mass

M_w	Weight-average molar mass
NMR	Nuclear magnetic resonance spectroscopy
PB-PS	Polybutadiene-polystyrene block copolymer
1,2-PB-PS	1,2-polybutadiene-polystyrene block copolymer
1,4-PB-PS	1,4-polybutadiene-polystyrene block copolymer
PMMA-PS	Polymethylmethacrylate-polystyrene block copolymer
i-PMMA-PS	Isotactic polymethylmethacrylate-polystyrene block copolymer
s-PMMA-PS	Syndiotactic polymethylmethacrylate-polystyrene block copolymer
PS	Polystyrene
PSD	Particle size distributio
R	Retention ratio
R_g	Radius of gyration
R_h	Hydrodynamic radius
SA	Self-assembly
SC	Stereocomplexation
SEC	Size exclusion chromatography

SEM	Scanning electron microscopy
SLS	Static light scattering
STEM	Scanning transmission electron microscopy
T	Temperature
T_c	Cold wall temperature
t_o	Void time
t_R	Retention time
ΔT	Temperature gradient
THF	Tetrahydrofuran
ThFFF	Thermal field-flow fractionation
TEM	Transmission electron microscopy
PSD	Particle size distribution
U	Field-induced mass transfer
UV	Ultraviolet
w	Channel thickness
Z	Aggregation number

Chapter 1. Introduction

Summary

This chapter serves as a brief introduction which articulates key concepts and outlines the scope of the entire thesis. In the concluding remarks, the research aims and objectives are be formulated.

1.1 Background

The history of materials has evolved from the modest Stone and Bronze Ages to ultimately include the more sophisticated and advanced polymer age. The persistent growth of materials science and technology has been greatly influenced by advanced progress in the synthesis of complex polymers and composites with unprecedented applications in state of the art industries.[1–4] With such major advancements in materials' design and application, and with the need to maintain such positive growth, there is a prerequisite to be able to measure and define such materials at a molecular level. This process of characterization allows polymer scientists and engineers to be able to correlate the measured molecular properties to the physical and mechanical properties.[5,6] Ultimately, suitable commercial applications of numerous polymers can be recognized and established. Figure 1.1 illustrates the generic nexus between molecular, physical/mechanical properties and the final applications for polymeric materials.

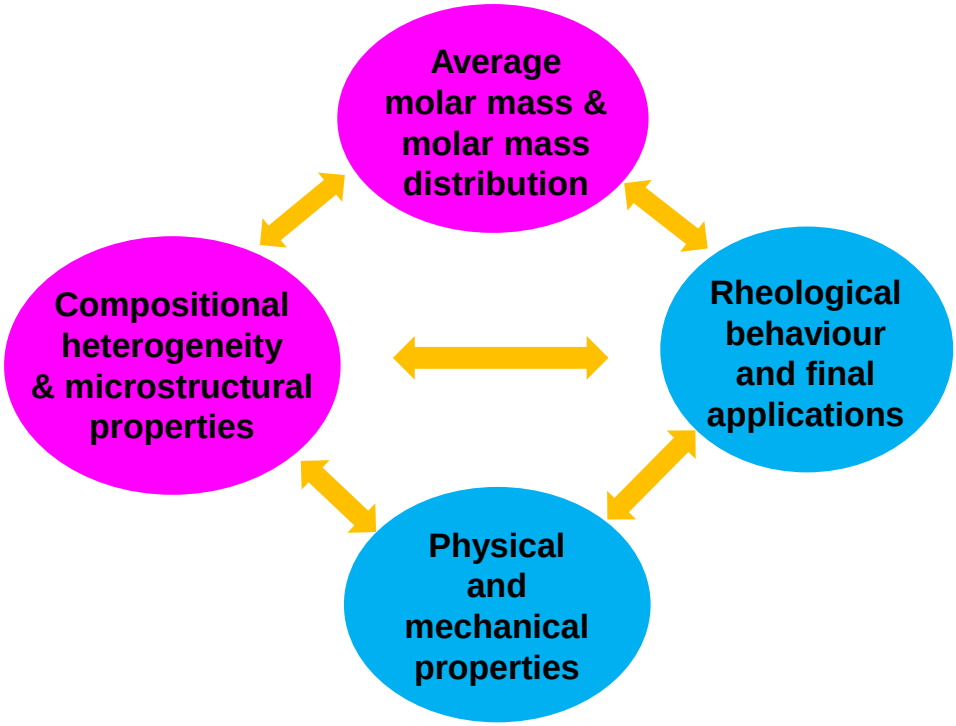

Figure 1.1. Schematic illustration of the nexus between polymer properties and applications.

Strength, elasticity, rheology, biodegradability, conductivity, thermal stability and toxicity, to mention just a few, are some of the critical physical and mechanical properties. Such properties emanate from fundamental molecular properties such as microstructure, molar mass (M_w), hydrodynamic size (D_h) and chemical composition (CC).[7–10] However, polymers are complex materials whose fundamental molecular properties exist as distributions, and as such, polymers generally present major analytical challenges. Therefore, it becomes essential to continuously develop competent and advanced analytical techniques for their characterization.

Herein, the focus is on characterizing complex polymers referred to as self-assemblies (SAs) which are prepared essentially from block copolymers (BCPs).[11,12] The schematic

illustration of a characteristic SA structure is shown in Figure 1.2. These SAs account for a wide range of nanotechnological applications in pharmaceutical, cosmetics, biomedicine, electronics, locomotive and environmental industries.[13–15]

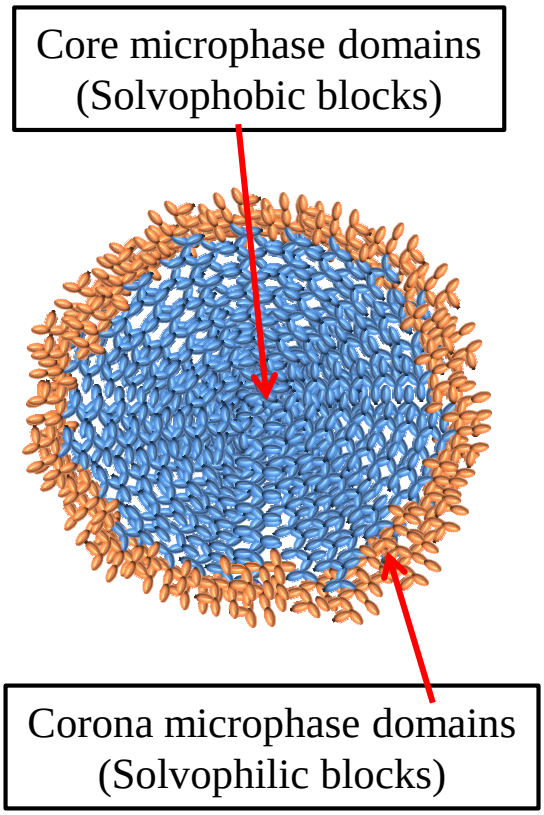

Figure 1.2. Schematic representation of self-assemblies.

The BCPs used to prepare SAs are complex polymers composed of two or more different types of polymer chains covalently bonded together. Some common BCPs are based on polystyrene (PS), whereby the PS block can be attached to polymers such as polybutadiene (PBd) and polymethylmethacrylate (PMMA). The different polymer chains and their microstructural variants are inherently diverse regarding solubility, polarity and solvent interactions, to mention just a few. In the case of two blocks, where one block is solvophilic and the other solvophobic for a particular solvent, BCPs

can phase segregate into various microphase morphologies such as spheres, cylinders and vesicles.[16,17] The solvophilic blocks segregate into corona microphase domains whilst the solvophobic blocks simultaneously segregate into the core microphase domains (CMDs).

Traditionally, bulk characterization techniques are utilised to measure the average values of fundamental molecular properties such as M_w, D_h and CC.[18–22] Widely used bulk techniques include static light scattering (SLS), dynamic light scattering (DLS), Fourier transform infrared (FTIR) spectroscopy and nuclear magnetic resonance (NMR) spectroscopy. In addition, electron microscopic techniques such as transmission electron microscopy (TEM) and scanning emission microscopy (SEM) can also be used for micrographic imaging and qualitative analysis of size and morphology.[23–25]

The generic synthesis and production protocols result in polymers or SAs with a wide variety of property distributions rather than specific values. Consequently, the measurement of average property values alone using bulk characterization techniques becomes inadequate. In order to generate advanced understanding of molecular properties and their respective distributions, separation techniques need to be applied in order to measure these distributions.[6,26] More so, separations are in essence a fundamental step in the deconvolution of complex sample compositions into constituent entities to enable a more reliable measurement of the associated molecular properties.

Classical separation techniques such as size exclusion chromatography (SEC) have been widely used to characterize a broad spectrum of complex polymers.[10,27,28] However, these techniques are column-based and have a low size limit, thus generally yield satisfactory results only for mechanically stable and not too high M_w polymers (<5x10^3 kg/mol) in solution. This renders such separation techniques unsuitable for very high molar mass and delicate polymers such as SAs, gels and large aggregates. However, modern channel-based separation techniques have evolved as complementary alternatives.[29] In particular, the advent of field-flow fractionation (FFF) techniques coupled to an array of various light scattering and spectroscopic detectors has provided for the online measurement of numerous molecular properties and the associated distributions.[30–34]

Of the FFF family, thermal field-flow fractionation (ThFFF) shall be singled out as the separation technique of choice for the entirety of this thesis. This is partially due to the accompanying high selectivity owing to the unique ability of ThFFF to simultaneously achieve separations that are according to both size and surface chemistry.[35–39] The underlying working principles of ThFFF as well as the detailed rational for selecting such a technique for the analysis of polymer SAs shall be discussed in the next chapter.

1.2 Research hypothesis

Previous studies have determined that ThFFF can be applied for the characterization of SAs in solution. In particular, elution trends of SAs were shown to be influenced by the microstructure and charge of the corona microphase domains.[40–42] Alternatively,

the microstructure of the core microphase domains (CMDs) may also impact on the solution behaviour of SAs and potentially influence ThFFF behaviour. Bearing that in mind, the present study seeks to address the following questions:

1. Can ThFFF be utilised to evaluate the impact of microstructure of the CMDs on properties such as the degree of crystallinity, elasticity, chain flexibility and topology on the elution behaviour of SAs?
2. Can microstructural differences of the cores affect compactness, thermal stability, degree of elasticity, molar mass (hence aggregation number) and hydrodynamic size (D_h) of the resultant SAs?
3. Do homopolymers and SAs of similar D_h have the same elution trends in ThFFF?

Notably, CMDs of SAs are fundamental compartments for housing solvophobic molecules in solution, thus SAs can be applied as nanoreactors for both physical and chemical in-situ processes within the core.[43–46] Therefore, for CMDs composed of specific polymers, a physical process such as stereocomplexation (SC) owing to interchain interactions of chains with different microstructures can be expected to proceed in-situ within the core. It must be noted that stereocomplexes are generally crystalline macromolecules that precipitate out of solution.[47–49] Therefore, SA nanoreactors may hypothetically provide a viable route to studying stereocomplexes in solution. As such, the following questions arise:

1. Are SAs capable of providing complimentary protocols in designing nanoreactors for the in-situ SC of stereoregular polymers within the CMDs, as characterized by multidimensional ThFFF?

2. Can these nanoreactors provide alternative pathways in micelle design and modification?
3. Can precipitation effects associated with SCs be circumvented and can such properties related to SC be retained in solution? On that same note, can SCs potentially become achievable in solvents where such phenomena are typically not feasible, courtesy of such an in-situ approach within nanoreactors?

Overall, the broad study of complex SA using ThFFF systems requires the development of robust and competent analytical methods. One alternative route is through the incorporation of additional detectors followed by optimisation of such new systems. This expands the data and information pool obtainable from a single experimental ThFFF run. In this regard, the following questions become pertinent in the development of advanced multiple detection systems for the characterization of SAs:

1. What novel detector combinations can be incorporated into the traditional ThFFF multiple detection setups for the characterization of SAs?
2. What additional information of significance on SAs is derivable from such a novel setup?

All the questions raised in this research hypothesis section have cumulatively and synergistically been applied to establish the following central objectives.

1.3 Objectives

1. In the instance where the CMDs are composed of 1,2- and 1,4-PBd microstructures, determine the influence of microstructure, morphology and chain arrangement on retention behaviour of SAs prepare from PBd-PS.
2. Investigate using ThFFF multiple detection the in-situ SC of CMDs composed of isotactic (i) and syndiotactic (s) PMMA inside MNRs composed of PS coronas.
3. Develop and apply ThFFF couple with ultraviolet (UV), differential refractive index (dRI), multiangle light scattering (MALS), differential viscometry (dVis), and dynamic light scattering (DLS) detectors, as a novel analytical method for the analysis of SAs of 1.4-PBd-PS in heptane as model compounds.

1.4 Thesis layout

This thesis is divided into five mutually related chapters as outlined below.

Chapter 1: Introduction

Chapter 2: Literature review

Chapter 3: Experimental section

Chapter 4: Results and discussion

Chapter 5: Conclusions and recommendations

Chapter 6: References

The next chapter will focus on the literature review and historical background of concern to the topical questions.

Chapter 2. Literature review

Summary

This chapter discusses the historical background and the fundamental scientific contributions of relevance to this thesis. Most importantly, gaps in knowledge of interest to the present work shall be highlighted.

2.1 Field-flow fractionation

The year 1966 saw the inception of FFF onto the scientific landscape as a complimentary alternative to liquid chromatography, and the inventor was Calvin Giddings. By design, his FFF innovation functioned on a single phase (channel) working principle in contrast to the dual phase (column) observed in chromatography.[30] The single phase separation mechanism, which is void of any packing material has rendered FFF superior for the separation of fragile macromolecules such as gels, colloids, biomolecules and self-assemblies (SA).[42,50]

In analogy to chromatography, FFF involves the use of carrier solvents for the mass transfer of differentially displaced (separated) entities for the subsequent measurement of their specific molecular properties using specialised detectors.[51] However, unlike in SEC, a larger size separation range is involved in FFF, namely from 0.001-100 µm.[29] Therefore, larger sized molecules such as proteins, SAs and large aggregates which may otherwise be impossible to separate using SEC have now found a niche with FFF.[31,52] FFF separations in general are achievable via mechanisms and working principles that shall be explained in detail in the subsequent subsection 2.2.

2.2 FFF separation principles

FFF channels are composed of micro-thin and ribbon-like structures sandwiched between a depletion and an opposite accumulation wall, within which prevails laminar and parabolic flow profiles of the pumped carrier solvent.[51,53] In order to induce separations, the flow direction of the channel is subjected to an orthogonal, easily adjustable and externally controlled field force which emanates exclusively from one extreme (depletion wall) of the channel. This instigates the mass transfer (U) of injected molecules in the direction of the field force towards the other extreme end of the channel (accumulation wall).[30,53]

Owing to different molecules having variable responses to a particular field force, a potential is created for the differential displacement of molecules inside the active channel. The one directional field force-induced mass transfer will naturally create concentration gradients, and as a result a counteracting diffusional mass transfer (D) is prompted, whose rate is exclusively known to be a function of molecular size. Ultimately, the concurrent forces driving mass transfer of molecules inside the channel will balance out, and clusters of molecules having respective average equilibrium layer values (l_1,l_2 ...) will correspond to specific retention times (t_R) and physicochemical properties, as illustrated in Figure 2.1.[30,54]

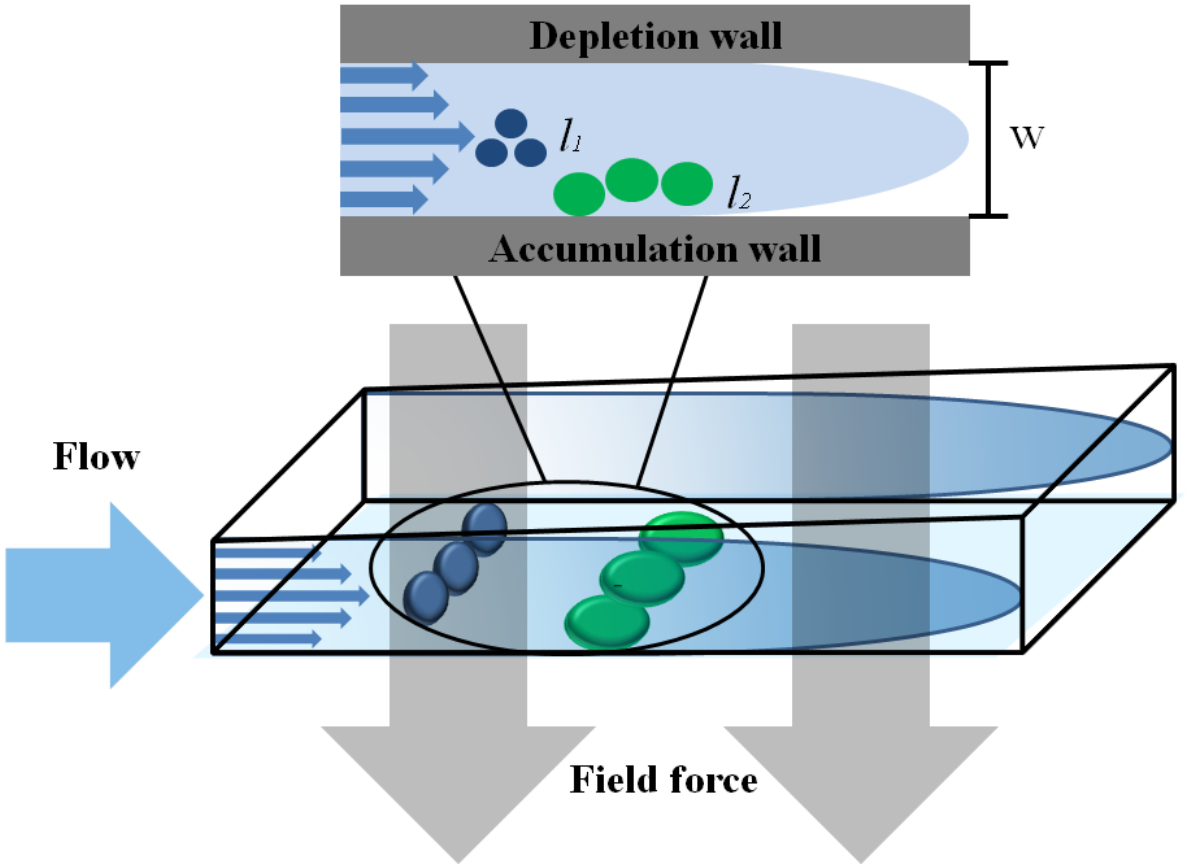

Figure 2.1. Schematic illustration of the FFF separation mechanism.

If the thickness of the channel is *w*, the ratio between *l* and *w* can be expressed as a dimensionless parameter λ (Equation 2.1):

$$\lambda = \frac{l}{w} \qquad \textit{Equation } 2.1.$$

As already alluded to, retention correlates to the equilibrium layers (l_n) within the channel, therefore λ can also be expressed as a ratio between the system volume and retention times (t_0) and (t_R), respectively, as shown in Equation 2.2:

$$\lambda = \frac{t_0}{t_R} \qquad \textit{Equation } 2.2.$$

Therefore, the retention factor (R), which describes the ratio between (t_0) and (t_R) can be defined by Equation 2.3:

$$\frac{t_R}{t_0} = \frac{w}{l} = R \qquad Equation\ 2.3.$$

if the field force (F) is given by Equation 2.4; where k is the Boltzmann constant, and T is the temperature:

$$F = \frac{6\,k\,T}{R\,w} \qquad Equation\ 2.4.$$

Therefore, the relationship between the retention behaviour and F experienced by a single molecular entity within a cluster of molecules at any equilibrium layer (l) can be given by the expression in Equation 2.5:[29,30,55]

$$\frac{t_R}{t_0} = \frac{F\,w}{6\,k\,T} \qquad Equation\ 2.5.$$

The following sub-section shall outline the protocols observed in the nomenclature of sub-techniques of FFF.

2.3 FFF sub-techniques

The nomenclature for FFF sub-techniques primarily rests upon the specific external field force utilised to achieve separations, as illustrated in Table 2.1.

Table 2.1. The nomenclature for FFF sub-techniques.

Sub-technique	Acronym	External field force
Thermal FFF	ThFFF	Thermal gradient
Flow FFF	FlFFF	Flow
Asymmetrical flow FFF	AF4	Flow
Sedimentation FFF	SdFFF	Gravitation
Electrical FFF	EFFF	Electrical current

For the work at hand and as already referenced to in the concluding remarks of the previous chapter, emphasis shall be given to a sub-technique of FFF called ThFFF. Accordingly, the following subsection shall detail the specific working principles and mechanisms thereof.

2.4 Thermal field-flow fractionation

ThFFF makes use of a thermal gradient as the external field force to establish the differential displacement of molecules inside the channel. The channel in this specific sub-technique is constructed from a micrometer-thin ribbon-like material that is air-tightly sandwiched between two rectangular metallic plates.[37] When active, the bottom plate is always maintained at ambient temperatures by an externally operated cooling system. Flexible amounts of thermal energy can be applied to the top plate such that ultimately an array of preconceived thermal gradients can be established. Figure 2.2 illustrates the schematic of the ThFFF mechanism and working principle.

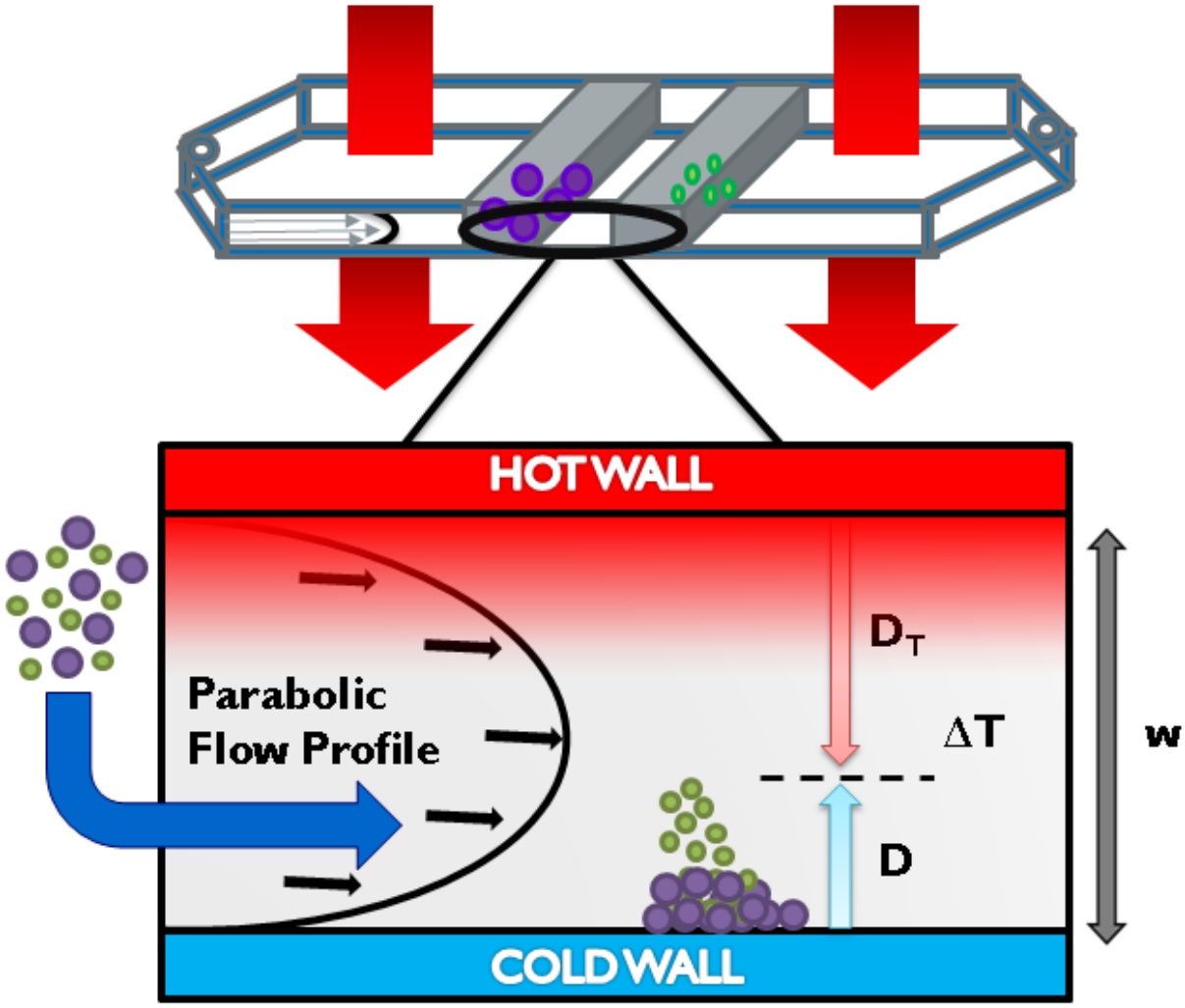

Figure 2.2. Schematic illustration of the ThFFF mechanism and working principle.

Molecules injected into the channel experience the thermal gradient, which generally drives them down the temperature gradient towards the colder plate, commonly referred to as the accumulation wall.[56] This thermal migration of molecules can be described by a technical term defined as the thermal diffusion coefficient (D_T).[57] The one directional accretion of molecules at the accumulation wall naturally creates an active concentration gradient, whereupon, opposing molecular migrations are

established owing to passive ordinary diffusion (Brownian motion). The term diffusion coefficient (D) can be used to describe this particular mass transfer of molecules as a function of the concentration gradient.

Owing to the poorly understood concept of D_T, the thermal migration velocity (U) of the molecules can be defined in simple terms as follows (Equation 2.6):[38,57,58]

$$U = D\left[\frac{D_T}{D} + \gamma\right]\frac{\Delta T}{w} \qquad Equation\ 2.6.$$

Where γ is thermal expansion coefficient of the solvent and $\Delta T/w$ is the thermal gradient (assuming uniformity across the entire channel). At steady-state conditions, $|U| = F/f$, where "F" is the force exerted on the molecules inside the channel and "f" is the frictional force coefficient. From the Nernst-Einstein relationship, $f = kT/D$, thus, F can be expressed as (Equation 2.7):

$$F = |U|\, f = k\,T\,\frac{|U|}{D} \qquad Equation\ 2.7.$$

The value of γ is generally ignored as it is insignificant relative to D_T/D, therefore, F can be evaluated from Equation 2.8 as shown below:

$$F = k\,T\left[\frac{D_T}{D}\right]\frac{\Delta T}{w} \qquad Equation\ 2.8.$$

The relationship between retention and mass transfer can then be deduced from Equation 2.9 as follows:[30]

$$\frac{t_R}{t_0} = \frac{D_T\,\Delta T}{D} \qquad Equation\ 2.9.$$

D can be calculated from the Einstein-Stokes law (Equation 2.10), where η is the solvent viscosity, and D_h is the polymer hydrodynamic diameter:

$$D = \frac{kT}{3\prod \eta D_h} \qquad Equation\ 2.10.$$

Ultimately an approximation of D_T can subsequently be evaluated from ThFFF experiments.[37,59] At generally high M_w as in the case of SAs, D_T is known to be independent of M_w and entirely dependent on the surface chemistry of polymers.[60,61] Therefore, the availability of D_T data can enable for the compositional analysis of SAs analysed by ThFFF.

ThFFF is generally a technique of choice when aprotic organic solvents as the carrier liquid are involved, although a few cases have been reported where aqueous solvents have been successfully utilised.[42,62] The superiority of ThFFF as a separation technique primarily rests upon the following beneficial attributes:

1. The achievable separations can be a function of either size or peripheral chemical structure, or both the latter and former properties simultaneously.
2. Optimum operational conditions are easily attainable in the method development process.
3. The experimental set-up is relatively simple.
4. Sample recoveries are very high, closely approaching 100%.

The first attribute recognizes ThFFF as a technique with multiple sensitivities, which makes it more suitable for the separation of complex polymer systems in general.[63–65] A brief discussion on the history ThFFF as a unique technique for the separation

and characterization of SAs and other pertinent complex polymers to this study shall be outlined in the subsequent sub-section.

2.5 ThFFF characterization of complex polymers

Advanced separation systems for the characterization of complex polymers typically involve experimental setups that are a combination of different (information-rich) detectors. Basic multiple detection involves the combination of UV, SLS, dRI and DLS detectors, to mention just a few, in order to generate information on composition, absolute M_w, D_h and the respective distributions thereof.[66,67] Furthermore, additional information on D and D_T can also be obtained.

It has been shown that for block copolymers of polystyrene-poly(n-butylacrylate) and polystyrene-polymethylacrylate with similar percentage compositions, respectively, the ThFFF separations were dependent on comonomer content when using a thermodynamically good solvent.[35] More so, the separations were shown not to be entirely dependent on the sizes of the different types of copolymers. This strongly demonstrated the dual sensitivity of ThFFF towards both size and CC. A number of similar observations have been reported by different other authors.[37,39,68] However, in other studies on BCPs, the separations were shown to be dependent on the size of the preferentially more soluble blocks when selective solvents were used.[38,57,58] More recently, polystyrene-polyethylene oxide (PS-PEO) block copolymers and PS homopolymers were shown to co-elute when the PS homopolymers in question were of comparable M_w to the PS blocks of the respective PS-PEO copolymers.[63] The proposed hypothesis stipulates that BCPs tend to phase segregate when dissolved in

selective solvents, such that the insoluble blocks constitute CMDs which are "shielded" from the solvent by the soluble blocks which dominate the peripheral compositions. In the postulated phase segregation, the less soluble blocks attain collapsed coil conformations and their contribution to size in solution is insignificant, whereas, the more soluble blocks exist as random coils whose influence on the overall size is profound.

In general, the setup and calculations involved in extrapolating compositional information from data generated from multiple detection techniques can be tedious when analysing complex polymers. In view of that, other than just multiple detector couplings, ThFFF has been hyphenated to a number of composition-sensitive detectors such as ^{1}H NMR,[33] matrix-assisted laser desorption/ionization time-of-flight mass spectrometry (MALDI-TOFMS),[69] and FTIR.[70] Consequently, quantitative and qualitative information on microstructural distributions can be derived from a single measurement using one hyphenated technique. However, these hyphenated techniques are generally very expensive compared to the standard concentration and light scattering detectors.

In summary, there has been a limited number of advanced studies reporting on the characterization of SAs by exploiting ThFFF-hyphenations and -multiple detection systems. Available ThFFF literature on SAs reports on the overall measurement of M_w, CC, particle size and morphology and the respective distributions.[42,50] The tacticity of the corona of some SAs has been proven to influence the observed ThFFF behaviour.[40,41] However, in general, tacticity-oriented research on SA systems using

ThFFF primarily focused on the corona chemistry. On the other hand, the tacticity of the equally important core may have a substantial and perhaps indirect influence on ThFFF behaviour. This assertion is yet to be specifically addressed in a detailed study.

The importance of the SA core also stems from its renowned application as a facile storage compartment for hydrophobic drugs in the design of targeted drug delivery systems.[44,71–73] Cancer drugs, for example, can be attached to biodegradable polymers, and under specific conditions this polymer-drug composite can phase segregate to form SAs with the drugs ideally forming the cores and the polymer forming the shells, respectively. These polymer-drug composite SAs can be designed and functionalized such that the drug can be delivered and released to targeted cells when the SAs are subjected to specific external stimuli.

The phase segregation of SAs allows for otherwise insoluble drugs or polymers to be kept in solution for further manipulation at nanoscopic levels. As such, SAs can function as in-situ nanoreactors with the core as the centre for physical or chemical reactions.[45,46,74] However, a range of molecular information regarding these nanoreactors is crucial for their design and application, and multiple detection ThFFF can be considered as a suitable alternative and complementary technique for such characterizations.

One form of multiple detection, the so-called "triple detection", has been widely used in SEC and AF4 separations.[75–77] Triple detection is a combination of a differential capillary viscometer (dVis), SLS, and concentration detection, which allows for the measurement and determination of the following parameters: intrinsic

viscosity (IV), viscosity radii ($R_{g\eta}$ and R_η), Mark-Houwink (MH) parameters, viscosity molar mass (M_η), R_g and absolute M_w. From specific relations between some of the aforementioned parameters, corresponding plots can be established to determine properties such as branching, topology and the degree of branching. The conformation and MH plots, that is, log R_g vs. log M_w and log IV vs. log M_w, respectively, can potentially be used to obtain topological information and compactness of SAs.

To the best of our knowledge, the coupling of ThFFF with a triple detection system is yet to be reported, let alone for the characterization of SAs. However, the coupling of ThFFF-dRI-Vis,[78] and ThFFF-dRI-SLS,[40,64,65] have separately been reported. Most importantly, the cumulative and strategic coupling of the above-mentioned detectors for the ultimate goal of achieving comprehensive analysis of SAs remains to be explored.

The next chapter shall outline the design and development of experimental techniques and protocols. The output is aimed at redressing some of the gaps in knowledge that have been highlighted in the literature review.

Chapter 3. Experimental work

Summary

The instrumentation as well as all the technical and experimental protocols are outlined in this chapter.

3.1 ThFFF conditions

Separations were performed using the TF2000 (Postnova Analytics, Germany) instrument and online measurements were performed using the following detectors: multi-angle laser scattering (MALS), (PN3070, Postnova Analytics, Germany) with multiple measuring angles over a range of 35-145^{o} and M_w calculations were obtained by manipulating the TF2000 software and using the Zimm plot, differential refractive index (dRI), (PN 3140, Postnova Analytics, Germany), dVis (PN3310), UV (PN 3212 at 254 nm, Postnova Analytics, Germany) and a zetasizer nano-series (Malvern Instruments, Worcestershire, UK) with built-in data processing software for dynamic light scattering (DLS) at an angle 175^{o} for back scattering detection.

For each measurement, in excess of 100 µL of sample was manually injected into a 100 µL capillary sample loop to ensure capillary flooding, and each analysis was performed in triplicate. Predetermined sample concentrations and thermal gradients were used as required to avoid overloading and allow adequate separations. A stable cold wall temperature was maintained at about ≈ 25 ℃ by an external chiller (Unichiller, Monitoring and Control Laboratories, South Africa). The appropriate

carrier solvents for all respective measurements were pumped by an isocratic pump (PN 1130, Postnova Analytics, Germany).

3.2 Basic self-assembly preparation

Figure 3.1 shows a schematic representation of the basic method applied in preparing the SAs. The respective BCPs were directly dissolved in a selective solvent for one block at temperatures ranging from 25-150 ℃ over a period of 10-30 minutes. The BCP + selective solvent solutions were allowed to cool and then left for a minimum of one week acclimatizing time prior to analysis.

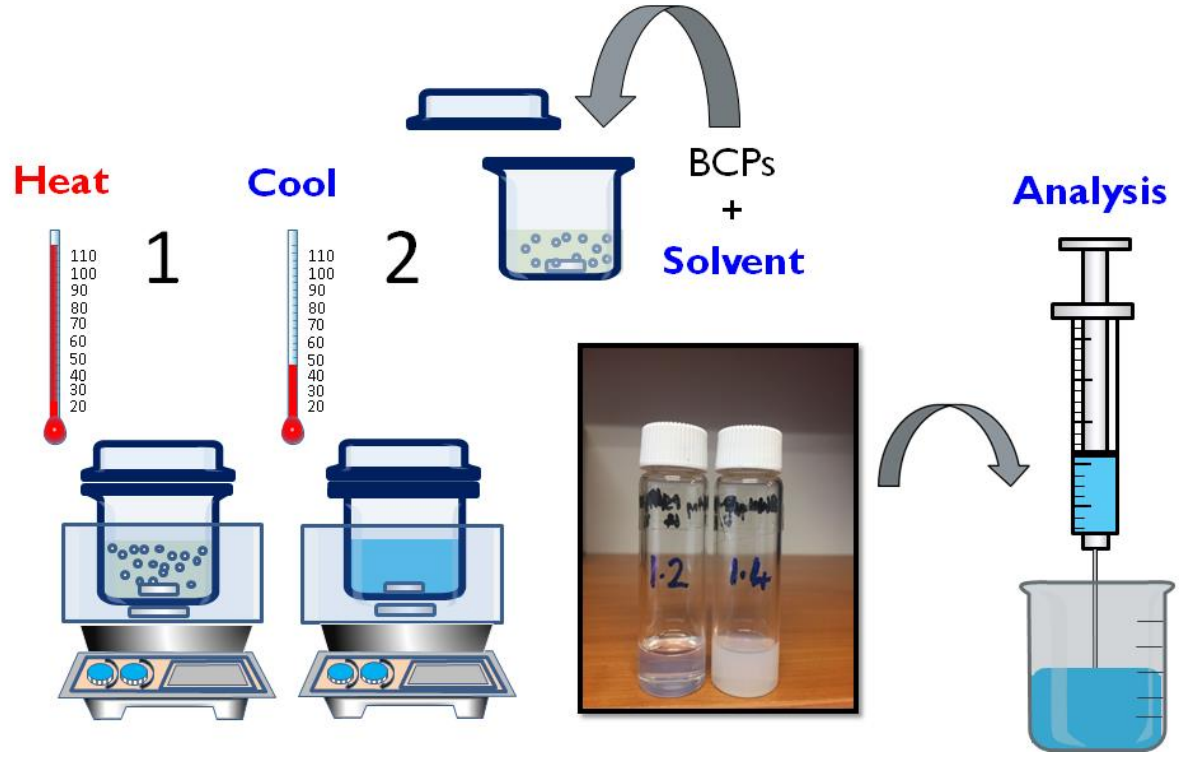

Figure 3.1. Schematic illustration of the basic preparation of self-assemblies.

3.3 Offline DLS

The Zetasizer Nano S (Malvern Panalytical, United Kingdom) was used to perform a triplicate of runs per measurement. A glass cuvette with an open round aperture was utilized for all measurements using 1 mL sample volumes at temperatures ranging from 20-60 ℃. The sample concentrations ranged from 0.1-2.0 mg/mL, as deemed appropriated for specific experiments. Prior to all measurements, a five minute equilibrium time was programmed on the instrument. Relevant solvent viscosity values were used accordingly, as required by the DLS software (Zetasizer software 7.11). From the DLS software, D_h was reverse calculated from the diffusion coefficient (D) in accordance with the Stokes-Einstein equation shown below (Equation 3.1), where k, T and η represent Boltzmann's constant, temperature and solvent viscosity, respectively.

$$D_h = \frac{k\,T}{3 \prod \eta\, D} \qquad \textit{Equation } 3.1.$$

3.4 ^{1}H NMR

Spectra were recorded using a 400 MHz Varian Unit Inova NMR spectrometer (Agilent/Varian, Palo Alto, California, USA). The measurements were carried out with a 5 mm dual broadband pulsed field gradient probe. 256 scans were performed with a relaxation delay of 1 s and acquisition time of 2.56 s. Data processing was carried out using Mestrenova software (version 11.0.2).

3.5 ATR-FTIR

All FTIR spectra were recorded in the absorbance mode using a Thermo Nicolet iS10 Spectrometer (Thermo Scientific, Waltham, MA) equipped with a diamond crystal. Each background and sample scan were performed 64 times with a spectral resolution of 4 cm^{-1} over a range of 700-4000 cm^{-1}. Scientific OMNIC software (version 8.1) was utilised for data collection and processing.

3.6 TEM

The Zeiss MERLIN FE-SEM (Oberkochen, Germany) equipped with a Zeiss five-diode scanning transmission electron detector (Zeiss STEMA) was used for TEM imaging. Instrument control was performed using the Zeiss Smart SEM software. Beam conditions during analysis were a 20 kV accelerating voltage, 250 pA probe current, and a working distance of approximately 4 mm. All TEM micrographs were imaged in the bright field mode.

3.7 SEC analysis.

Comparative SEC studies were carried out using a Waters GPC (Milford, USA) comprising of the following components: Waters 2487 dual wavelength UV detector, Waters 1515 isocratic HPLC pump, Waters 410 differential refractometer (at temperature of 30 ℃), Waters 717 plus autosampler, Waters in-line degasser. Column set-up: Two PLgel 5 μm Mixed-C columns and a PLgel 5 μm guard column, column temperature 30 ℃, eluent system: THF (HPLC grade, BHT stabilized) at a flow rate of 1 mL/min at pressure of 941 psi. Concentration of samples: 2 mg/mL.

Calibration: Narrow polystyrene standards with a molecular weight range of 580-3 187 000 g/mL.

Chapter 4. Results and discussion

Summary

In this chapter, results that are published in international peer reviewed journals are discussed in detail as a tri-series of papers. An introductory section is presented prior to attaching each respective publication. The overall conclusions on the cumulative results are presented in a separate chapter.

4.1 Core microstructure, morphology and chain arrangement of block copolymer self-assemblies as investigated by thermal field-flow fractionation (Part 1).

This particular study is complementary to previous ThFFF studies where the emphasis was on investigating the impact of the corona microstructure on the micelle properties and retention behaviour.[40] It is shown that two types of vesicles both having PS shells, and either 1.2- or 1.4-PBd cores (prepared from respective PS-PBd block copolymers with symmetrical PS and PBd block sizes) are successfully separated by ThFFF. Properties that depend on microstructure such as the degree of crystallinity, elasticity, chain flexibility and topology of PS-b-PBd SAs are correlated to molecular structure, and the overall ThFFF retention behaviour is investigated.

Stereoregular 1.2-PBd isomers are more crystalline and rigid than the 1.4(cis)-isomers and, as such, the resultant vesicles are shown to have different degrees of core crystallinity, elasticity, and flexibility, which consequently impacts on the respective sizes, as illustrated in Figure 4.1. In an unexpected turn, the solvophobic PBd cores exhibit ^{1}H NMR resolution. This behaviour can be explained by the low T_g of PBd and

the subsequent better mobility, thus the higher signal intensities in the ^{1}H NMR spectrum.

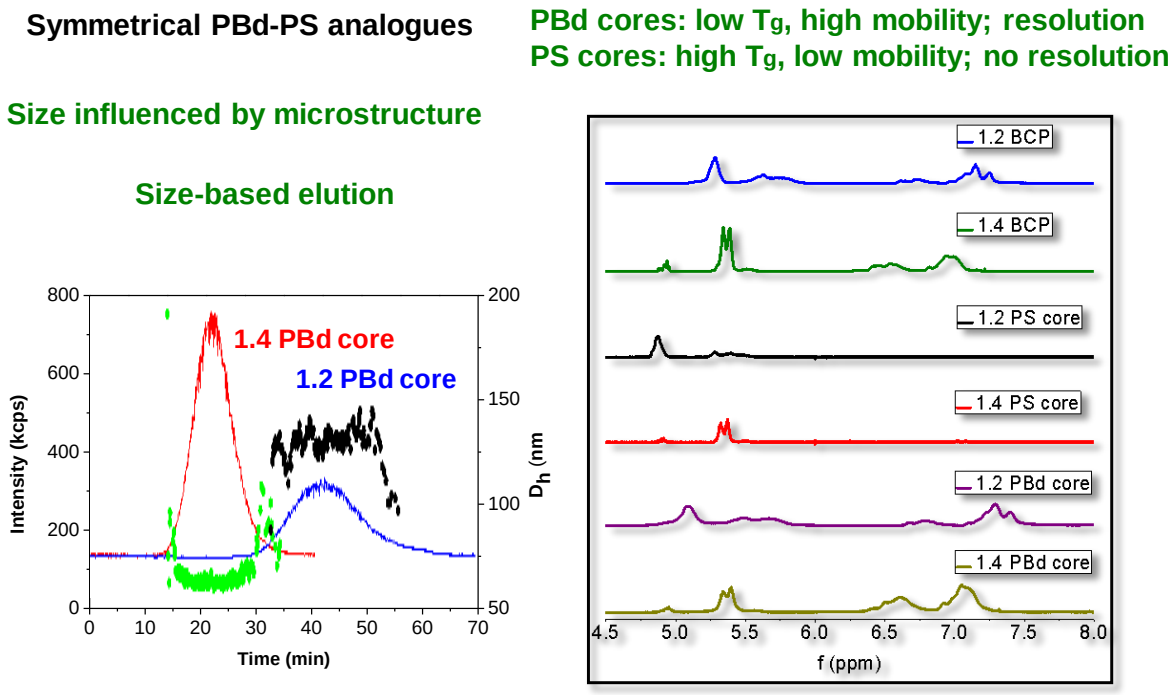

Figure 4.1. Graphical presentation for the study: Influence of microstructure (of the cores) on the ThFFF elution behaviour, and impact of T_g on ^{1}H NMR resolution for self-assemblies prepared from symmetrical PBd-PS block copolymer analogues.

As a result, D_h, M_w, aggregation number (Z), and critical micelle concentration (CMC) of these vesicles are shown to be sensitive to the core microstructure, therefore, demonstrating the potential of microstructural differences of the cores as platforms for providing tuneable pathways for designing specific SAs. Furthermore, it was established that for vesicles and homopolymers of similar surface chemistry and D_h, ThFFF was sensitive towards the inherent differences in morphology and chain arrangement, and thus the two polymeric species were successfully separated. These results are illustrated in Figure 4.2.

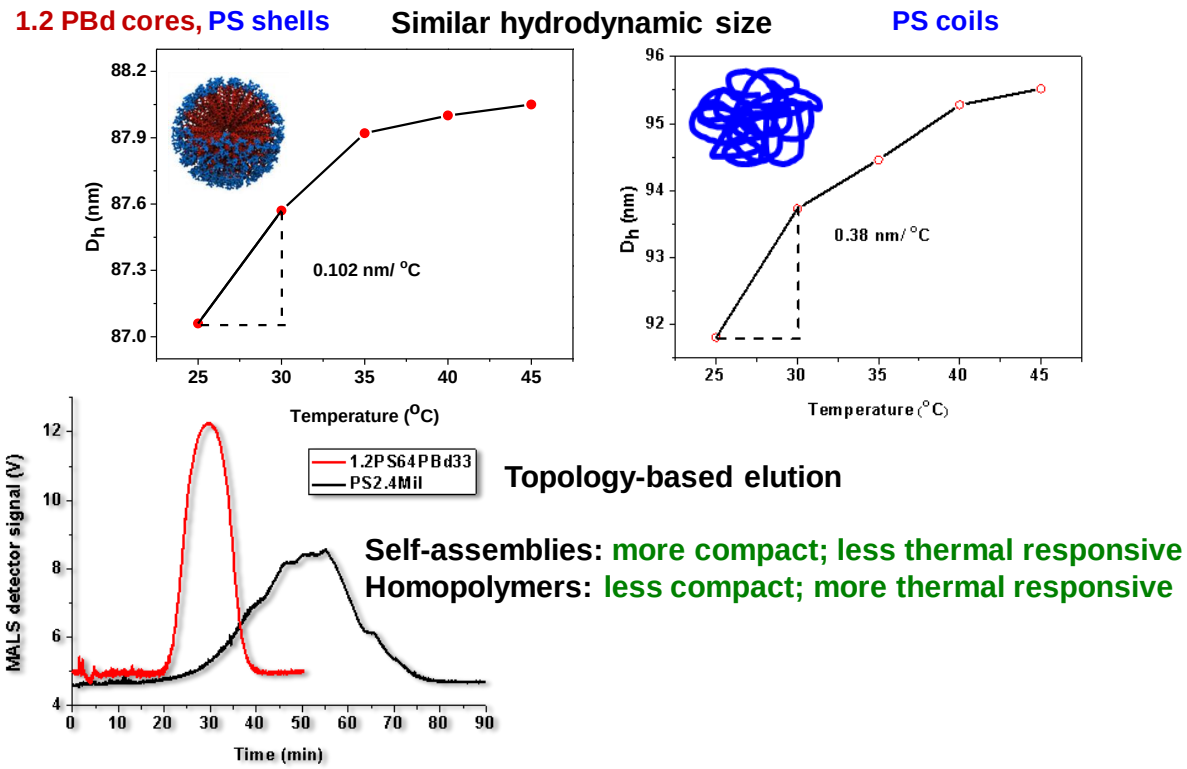

Figure 4.2. Graphical presentation for the study: Topology-based ThFFF separations for vesicles and homopolymers of similar hydrodynamic size and surface chemical composition.

Journal of Chromatography A, 1562 (2018) 87–95

Contents lists available at ScienceDirect

Journal of Chromatography A

journal homepage: www.elsevier.com/locate/chroma

Core microstructure, morphology and chain arrangement of block copolymer self-assemblies as investigated by thermal field-flow fractionation

U.L. Muza, G. Greyling, H. Pasch *

Department of Chemistry and Polymer Science, University of Stellenbosch, PO Box X1, 7600 Stellenbosch, South Africa

ARTICLE INFO

Article history:
Received 2 April 2018
Received in revised form 22 May 2018
Accepted 27 May 2018
Available online 28 May 2018

Keywords:
Thermal field-flow fractionation
Block copolymers
Micelles
Vesicles
Self-assemblies

ABSTRACT

The self-assembly of block copolymers (BCPs), as a result of solvent selectivity for one block, has recently received significant attention due to novel applications of BCPs in pharmaceuticals, biomedicine, cosmetics, electronics and nanotechnology. The correlation of BCP microstructure and the structure of the resulting self-assemblies requires advanced analytical methods. However, traditional bulk characterization techniques are limited in the quest of providing detailed information regarding molar mass (M_w), hydrodynamic size (D_h), chemical composition, and morphology for these self-assemblies. In the present study, thermal field-flow fractionation (ThFFF) is utilised to investigate the impact of core microstructure on the resultant solution properties of vesicles prepared from polystyrene-polybutadiene block copolymers (PS-b-PBd) with 1,2- and 1,4-polybutadiene blocks, respectively. As compared to investigations on the impact of the corona microstructure, the impact of core microstructure on micellar properties has largely been neglected in previous work. In *N,N*-dimethylacetamide (DMAc) these BCPs form vesicles having PS shells and PBd cores. D_h, M_w, aggregation number, and critical micelle concentration of these micelles are shown to be sensitive to the core microstructure, therefore, demonstrating the potential of microstructural differences to be used for providing tuneable pathways to specific self-assemblies. It is shown that micelles prepared from BCPs of similar PS and PBd block sizes are successfully separated by ThFFF. It is further demonstrated in this study that PS-b-PBd vesicles and PS homopolymers of identical surface chemistry (PS) and comparable D_h in DMAc, can be separated by ThFFF.

1. Introduction

The evolution of self-assembled structures from block copolymers (BCPs) in solution, being primarily a result of solvent selectivity for one block, has received much attention due to novel applications of self-assembled structures in pharmaceuticals, biomedicine, cosmetics, electronics and oil recovery [1–3]. These self-assembled structures can be spheres, cylinders or vesicles depending on various molecular factors such as the hydrophobic-hydrophilic (or more generally solvophobic-solvophilic) block ratio, chemical composition and molar mass. On the other hand, solution factors such as solvent type and thermodynamic quality, temperature, pH, ionic strength and concentration also determine what type of self-assembled structure is formed. In addition to these effects, microstructural differences in BCPs are also known to influence physical and chemical properties. This was shown by Schmelz et al. and Du et al. who demonstrated that when the BCPs in solution are heated above the crystallization temperature of the core forming block, the resultant micelle morphologies can be manipulated via controlling the temperature at which crystallization occurs [4,5]. Furthermore, investigations on polyethylene glycol (PEO)-based BCP micelles with either ε-caprolactone (ε-CPL) or ε-decalactone (ε-DCL) as the hydrophobic blocks in aqueous solvents illustrated the influence of M_w and chemical composition (CC) of the core [6]. It was shown that the resultant amorphous or crystalline core, as induced by varying the M_w and CC of the micelle core, had an influence on properties such as the critical micelle concentration (CMC) and morphology [6].

The correlation of BCP microstructure to the structure of the resulting self-assemblies requires advanced analytical methods. Traditional bulk characterization techniques like electron microscopy, light scattering and spectroscopy are limited in the

* Corresponding author.
E-mail address: hpasch@sun.ac.za (H. Pasch).

https://doi.org/10.1016/j.chroma.2018.05.065
0021-9673/

quest of providing detailed information regarding molar mass (M_w), hydrodynamic size (D_h), chemical composition, and morphology for self-assemblies. Moreover, column-based techniques like size exclusion chromatography (SEC) can provide information on M_w, D_h and the associated distributions, however, fragile self-assemblies can be shear-degraded by interactions with the SEC column [7,8]. Thus, in order to fully comprehend and understand the behaviour of self-assemblies in solution, there is a need to establish robust characterization techniques capable of defining micelles at molecular level with regard to M_w, D_h, CC, and morphology.

Most recently, thermal field-flow fractionation (ThFFF) has been shown to be a versatile tool capable to separate and characterize micelles according to CC and size, microstructure and morphology [9–11]. ThFFF is a sub-technique of field-flow fractionation (FFF) that makes use of a thermal gradient as the driving force to separate analytes across a narrow channel clamped between two metallic plates [12]. In ThFFF, the temperature gradient is achieved by heating the one plate (hot wall) and cooling the other (the cold accumulation wall). The aspect ratio of the plates is such that a parabolic flow profile of the carrier solvent is established along the channel. Moreover, the thermal gradient drives analyte molecules away from the hot wall towards the cold/accumulation wall by the process of thermal diffusion. This in turn creates a concentration build-up of the analyte molecules at the accumulation wall, thereby triggering a counteracting concentration diffusion motion [13,14]. The thermal and concentration diffusion processes eventually balance out and the analyte molecules are differentially distributed across the channel. Thus, depending on the analytes position in the concentration gradient, they will reside in different velocity flow streams and elute at different times from the channel. Thermal diffusion, as described by the thermal diffusion coefficient (D_T), is sensitive to surface chemistry, while on the other hand, concentration diffusion, as described by the diffusion coefficient (D), is sensitive to size (D_h) [13,15]. As a result, separations according to D_h and CC are possible by ThFFF in one measurement [16,17].

ThFFF has previously been applied to separate and characterize poly(methyl methacrylate)-b-polystyrene (PMMA-b-PS) micelles with isotactic and syndiotactic coronas as a function of corona composition [18]. The CMC was found to be dependent on the tacticity of the PMMA corona. Micelles with the syndiotactic PMMA (sPMMA) corona exhibited lower CMC values than the isotactic equivalent owing to the better capability of the more flexible sPMMA blocks to pack together in the corona. Polystyrene-b-polybutadiene (PS-b-PBd) micelles of different PBd corona microstructures (1.2- and 1.4-PBd) have been shown via ThFFF to exhibit similar micelle-vesicle transition trends as a function of temperature gradients [9]. The corona microstructure was thus shown to have no significant impact on the resultant morphology.

Notably, in all previous ThFFF studies, emphasis has been on investigating the impact of the corona microstructure on the micelle properties [9,11,18]. It is against this background that the present study aims to utilise ThFFF to evaluate the impact of core microstructure on properties such as the degree of crystallinity, elasticity, chain flexibility and topology on the retention behaviour of PS-b-PBd self-assemblies. Since the stereoregular 1.2-PBd isomer is more crystalline and rigid than the 1.4(cis)-isomer, it is expected that self-assemblies with PBd cores having 1.2- and 1.4-isomeric structures should have different degrees of core crystallinity, elasticity and flexibility which would have an impact on morphology. This study describes the application of ThFFF coupled online to multiangle laser light scattering (MALLS), differential refractive index (dRI) and dynamic light scattering (DLS) detectors to determine the influence of microstructure, morphology and chain arrangement of the PBd core on retention behaviour of PS-b-PBd self-assemblies in ThFFF.

Table 1
Sample code names and isomeric contents of the PS-PBd block copolymers and PS homopolymers. PS-polystyrene, PBd-polybutadiene.

Sample[1]	Code name	PBd content	Dispersity[2]
1.2-PS_{66}-PBd_{75}	1.2-PS66-PBd75	1.2 > 90%	1.09
1.4-PS_{65}-PBd_{80}	1.4-PS65-PBd80	1.4 > 90%	1.14
1.2-PS_{66}-PBd_{75}	1.2-PS64-PBd33	1.2 > 90%	1.08
PS_{1400}	PS 1.4Mil	0	1.10
PS_{2400}	PS 2.4Mil	0	1.10

[1] subscript numbers indicate molar masses in kg/mol.
[2] as M_w/M_n.

2. Materials and methods

2.1. Materials

All standards were purchased from Polymer Source (Montreal, Canada) and were used as received. The subscripts represent the molar masses for the respective blocks in kg/mol (Table 1).

HPLC grade *N,N*-dimethylacetamide (DMAc) (Sigma Aldrich, South Africa) was used as received for preparing the self-assemblies and as the carrier solvent. ^{1}H NMR spectra (see Section 2.4.) was recorded using deuterated DMAc (DMAc-d_9), deuterated cyclohexane (cycloxane-d_{12}) and HPLC grade heptane. All solvents were purchased from Sigma Aldrich, South Africa.

2.2. ThFFF conditions

Measurements were performed using the TF2000 (Postnova Analytics, Landsberg, Germany) coupled in series to the following detectors, MALLS (7 angles over a range of 35–145° using Zimm plot) (PN3070, Postnova Analytics), dRI (PN 3140, Postnova Analytics) and a zetasizer nano-series (Malvern Instruments, Worcestershire, UK) with built-in data processing software was used for dynamic light scattering (DLS) detection at an angle 175° (back scattering detection). In excess of 100 μL of 1 mg/mL of the sample was manually injected into a 100 μL capillary sample loop to insure capillary flooding, and each analysis was performed in triplicate. A temperature drop (ΔT) of 25 °C was applied for all fractionations and an external chiller (Unichiller, Monitoring and Control Laboratories, South Africa) maintained a stable cold wall temperature at about ≈ 25 °C. The carrier solvent for all measurements, (DMAc), was pumped by an isocratic pump (PN 1130, Postnova Analytics) at a flow rate of 0.2 mL/min. Values for D_T were calculated according to:

$$D_T = \frac{6Dt_R}{\Delta T t_0}$$

where D is the diffusion coefficient as determined by DLS, t_R and t_0 are the respective retention and void times of the sample and ΔT is the temperature difference between the hot and cold wall [12].

2.3. Micelle preparation

1.2- and 1.4-isomeric PS-PBd block copolymers of similar PS and PBd block molar masses are separately and directly dissolved in DMAc at a temperature of 70 °C for 30 min. Complete dissolution was confirmed by dynamic light scattering (DLS) experiments, whereby, stable and reproducible unimodal peaks are observed. The expected result is two different types of micelles, both having PS coronas, but one type having a 1.2-PBd core and the other having 1.4-PBd core.

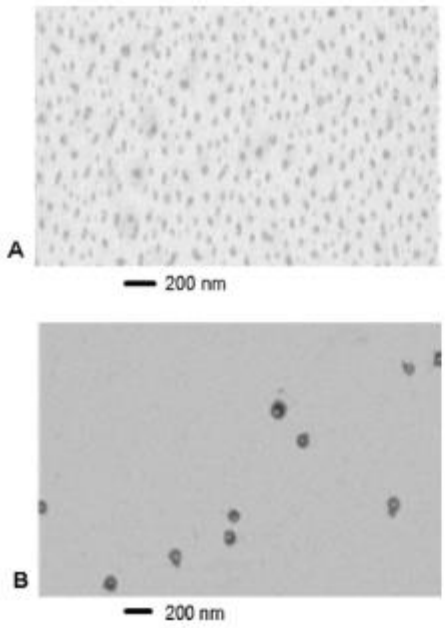

Fig. 1. TEM micrographs of (A) 1.2-PS-PBd and (B) 1.4-PS-PBd vesicles.

2.4. ^1H NMR

A 400 MHz Varian Unit Inova NMR spectrometer (Agilent/Varian, Palo Alto, California, USA) was utilised. The measurements were carried out with a 5 mm dual broadband pulsed field gradient probe. 256 scans were performed with a relaxation delay of 1 s and acquisition time of 2.56s.

2.5. TEM

A Zeiss five-diode scanning transmission electron detector (Zeiss STEMA Detector) and Zeiss Smart SEM software were used to generate the STEM images from a Zeiss MERLIN FE-SEM (Oberkochen, Germany). Beam conditions during analysis were a 20 kV accelerating voltage, 250 pA probe current, and a working distance of approximately 4 mm. All micrographs were imaged in the bright field mode. The staining agent used, osmium tetraoxide, reacts preferentially with PBd to give a more intense colour and to provide contrast between the PS and PBd microphase regions.

3. Results and discussion

The self-assembly of the PS-PBd BCPs in DMAc is expected to result in microphase separation in which PS, the soluble block, forms the peripheral regions (the corona), and PBd, the insoluble block, forms the core regions. Fig. 1 shows the TEM micrographs of the PS-PBd self-assemblies and it appears that both types of self-assemblies exhibit vesicle morphologies but the 1.4-PS-PBd vesicles are larger in size. Therefore, the core microstructure appears to have no significant impact on the overall morphology in much the same way as the corona microstructure, as reported by Greyling et al [9].

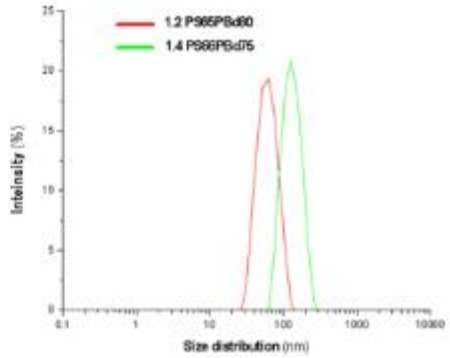

Fig. 2. Superimposed DLS hydrodynamic z-average size distribution curves for the vesicles: 1.2-PS-PBd (red) 64.1 ± 0.2 nm, and 1.4-PS-PBd (green) 120.1 ± 0.7 nm. (For interpretation of the references to colour in this figure legend, the reader is referred to the web version of this article.)

In general, the size of the vesicles should be directly dependent on the size (molar mass) of the soluble and corona-forming block and to a lesser extent on the total molar mass of the BCP [19]. This is due to the fact that (assumingly) the insoluble block forms a collapsed core. The size of the core, however, depends on the thermodynamic quality of the solvent. In the present case the respective blocks of the two types of vesicles have comparable molar masses. Accordingly, the differences in the total sizes of the vesicles can only be explained by the differences in the microstructure of the PBd blocks. The significant size differences of the two types of vesicles can be attributed to the following microstructure-related properties: PS-PBd with a high content of the stereo-regular 1.2-PBd content has a higher T_g (≈−20 °C) and should constitute a more compact core capable of attaining a higher aggregation number and remain stable [20,21]. However, this also restricts the mobility of the chains when aggregating which results in the observed relatively lower sizes. Under similar thermal conditions, the 1.4-PBd microphase regions with a lower T_g (≈−100 °C) are generally expected to be less compact and more elastic and thus having a lower elastic modulus [20,21]. Notably, the susceptibility to stretching of the 1.4-PBd core is expected to affect the solvophobic-solvophilic balance significantly, which has been shown to be one of the key factors governing changes in size and/or morphology [22,23].

3.1. Offline DLS analysis

For more quantitative information on the vesicles, offline DLS was applied firstly to measure the sizes in solution, and secondly to determine the respective CMCs by measuring size in solution as a function of BCP concentration. The DLS measurements in Fig. 2 corroborate the TEM results and confirm that the D_h value for the 1.4-PS-PBd vesicles is larger compared to the D_h value for the 1.2-PS-PBd vesicles. The measured CMCs at 25 °C show significant differences with values of 0.15 mg/mL and 0.30 mg/mL for 1.2- and 1.4-PS-PBd vesicles, respectively. In support of this observation, Glavas et al. reported that the CMCs of aqueous micelles prepared from PEO-b-ε-PCL with amorphous ε-PCL cores (PCL-polycaprolactone), were significantly higher compared to the CMCs of PEO-ε-PDL micelles (PDL-polydecalactone) with semi-crystalline ε-PDL cores [6]. This shows that the difference in the degree of crystallinity of the cores as imposed by the differences in core microstructure may also have a significant impact on the

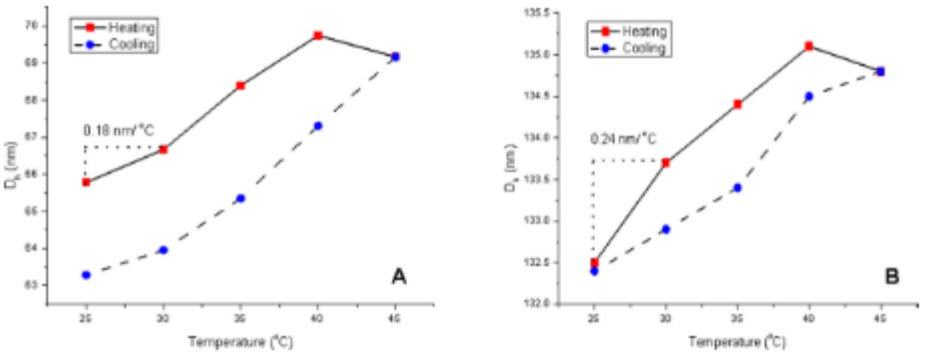

Fig. 3. Thermo-responsive behaviour of 1.2-PS-PBd (A) and 1.4-PS-PBd (B) at a concentration of 1 mg/mL. Red squares show the z-average size of the vesicles during the heating cycle while the blue circles show the size of the vesicles during the cooling cycle. (For interpretation of the references to colour in this figure legend, the reader is referred to the web version of this article.)

CMC, as observed in this case. In general, the lower CMC of the 1.2-PS-PBd vesicles indicates a better thermodynamic stability of the vesicles due to their specific core microstructure.

The thermo-responsive behaviour of the vesicles shall be investigated by monitoring the changes in size as a function of temperature at similar concentrations. The thermo-responsive behaviour is an important variable as it relates to chain flexibility and elasticity of the vesicles.

Both types of vesicles show an increase in size with heating and in order to quantify this observation, the slope of the linear change in size between 25 and 30 °C was measured. This temperature range was selected as it most accurately describes the conditions the vesicles experience at the cold wall during analysis. It was found that the 1.4-PS-PBd micelles exhibit a steeper change in size with temperature with a slope of 0.24 nm/°C, as compared to 0.18 nm/°C for 1.2-PS-PBd micelles. The more pronounced thermo-responsive behaviour of 1.4-PS-PBd micelles implies higher chain flexibility and elasticity that can be attributed to the lower degree of crystallinity of 1.4-PBd relative to 1.2-PBd. The higher chain flexibility results in greater chain swelling and stretching of the 1.4-PBd isomer as a function of temperature. Therefore, 1.4-PS-PBd vesicles are quantitatively shown to have higher susceptibility to changes in the solvophobic-solvophilic balance, as expected. Furthermore, for the1.4-PS-PBd vesicles the temperature dependent changes in size can be defined as reversible, as evident from the cooling curve, which shows that the vesicles ultimately attain size values similar to the initial ones. In order to obtain additional insight into the thermo-responsive behaviour of the vesicles, ^{1}H NMR analysis at various temperatures was performed (Fig. 3).

3.2. ^{1}H NMR analysis

^{1}H NMR analysis was first carried out for the two BCPs in cyclohexane, and then for their respective vesicles with PBd cores in DMAc. Secondly, the inverse self-assemblies with compact PS cores and PBd coronas were prepared and analysed for comparison. The inverse self-assemblies were prepared using the co-solvent method, with heptane as the selective solvent [24,25]. The overlayed spectra of the BCPs and all the self-assemblies are presented in Fig. 4. For the BCPs, the corresponding proton signals for PBd and PS are observed as expected at around 4.7–5.4 ppm and 6.5–7.3 ppm, respectively. For the BCPs in cyclohexane, the molar ratios for the PBd blocks as determined from peak integral ratios are 54 mol% and 53 mol% for 1.2- and 1.4-PBd, respectively. These

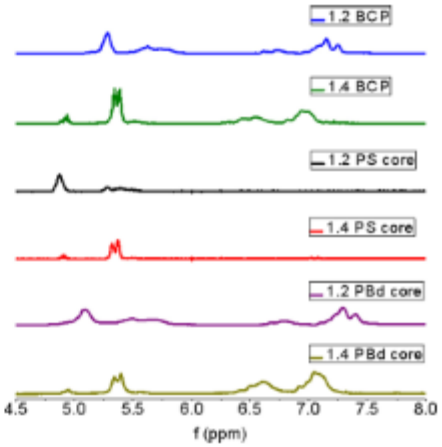

Fig. 4. ^{1}H NMR spectra of 1.2-PS-PBd (blue) and 1.4-PS-PBd (green) BCPs, 1.2- (black) and 1.4-PS-PBd (red) self-assemblies with PS cores and 1.2- (purple) and 1.4-PS-PBd (olive) vesicles with PBd cores. (For interpretation of the references to colour in this figure legend, the reader is referred to the web version of this article.)

values are in close agreement with the nominal values provided by the supplier.

It is known that the ^{1}H NMR spectra of self-assemblies with compact cores typically display intense signals for the corona polymer whilst the signals for the core polymer are very broad and have very low intensities. 12–14 This trend is typically observed for self-assemblies where the core polymer has a high T_g and, thus, has a glassy and compact (solid like) nature, as is the case for the self-assemblies with PS cores [15,16]. The compact and solid-like cores typically have very low mobility and solubility, and consequently produce very broad ^{1}H NMR signals with very low intensities. In contrast to this type of self-assemblies, for the vesicles having PBd cores with very low T_g (≈ −20 °C to −100 °C), the cores are expected not to be as compact and solid-like. The expected better mobility should result in higher intensity PBd core signals, as clearly reflected in Fig. 5.

Both vesicles show pronounced proton signals at lower temperatures for the core-forming PBd blocks, although (as expected) the

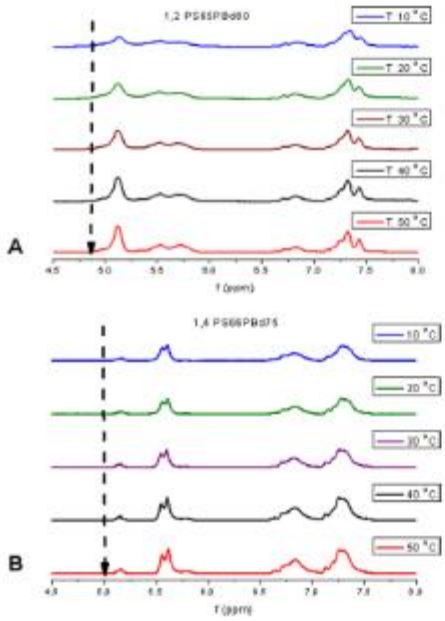

Fig. 5. Temperature-dependent ^{1}H NMR spectra for (A) 1.2-PS-PBd and (B) 1.4-PS-PBd vesicles in DMAc-d_9. Indicated in blue, green, purple, black and red are the spectra collected at temperatures of 10, 20, 30, 40 and 50 °C, respectively. Arrow indicates the temperature increase. (For interpretation of the references to colour in this figure legend, the reader is referred to the web version of this article.)

signals for the corona-forming PS are evidently more intense. This is clear proof for the previous statement that PBd as the core polymer (1.2-PBd as well as 1.4-PBd) is more flexible and mobile compared to PS being the core. The intensities for both the PS and PBd peaks moderately improve as a function of temperature. This trend can be attributed to a number of temperature related factors such as, improved mobility, solubility and, therefore, increased relaxation times [28–31]. Furthermore, both peaks become less broad and sharper.

A plot of the respective PS and PBd molar ratios as a function of temperature (as calculated from the ^{1}H NMR peak integrals) was produced to quantitatively corroborate the aforementioned ^{1}H NMR spectral trends, as illustrated in Fig. 6. The molar ratios of both 1.2- and 1.4-PBd are below the expected ^{1}H NMR determined nominal values of 54% and 53% respectively, which means that the PBd units are not fully solvated across such a temperature range (unlike in a good solvent), hence self-assemblies are still in existence.

As expected, the molar ratios of 1.2-PBd cores for 1.2-PS-PBd vesicles show an increasing trend as a function of temperature due to thermally induced mobility and solubility. The observed trend ultimately approaches a plateau phase around 30–50 °C, as the overall temperature induced effects on the PS coronas and 1.2-PBd cores are balanced. In contrast, the molar ratios of the 1.4-PBd cores for the 1.4-PS-PBd vesicles do not show any increasing trend with temperature. Moreover, the 1.4-PBd cores show relatively lower molar ratio values ranging from 0.33–0.35, as compared to 0.35–0.48 for 1.2-PBd for the 1.2-PS-PBd vesicles. These trends can be related to the associated highly aggregated nature, and thus relatively lower solubility, mobility and relaxation times of the much larger 1.4-PBd cores.

3.3. ThFFF of the vesicles in DMAc

Having established the general behaviour of the vesicles in bulk, the next step was to separate and characterize the vesicles with multi-detector ThFFF. The two vesicle types have significantly different retention times, and therefore, can potentially be separated from each other as shown in Fig. 7. The respective ThFFF data are summarised in Table 2. Since both self-assemblies have similar morphologies (vesicles), a separation based on morphology can be ruled out. Furthermore, the fact that the thermal diffusion coefficients (D_T) are similar indicates that separation is not due to chemical differences of the corona polymer (PS in both cases). As is shown by the differences in the normal diffusion coefficients (D), the aggregation numbers (Z) and the hydrodynamic diameters (D_h), the separation in the present case is based on the size differences between the two types of vesicles [9–11].

The shape factor, as defined by the R_g/R_h ratio, shows that both vesicles have values within the expected range for vesicles (≈1.5) [26,27]. The 1.2-PS-PBd vesicles have smaller D_h, which explains the observed lower retention time as compared to 1.4-PS-PBd vesicles with much larger D_h and, hence, a higher retention time [10–12]. Accordingly, the micelles with the largest D_h (1.4-PS-PBd)

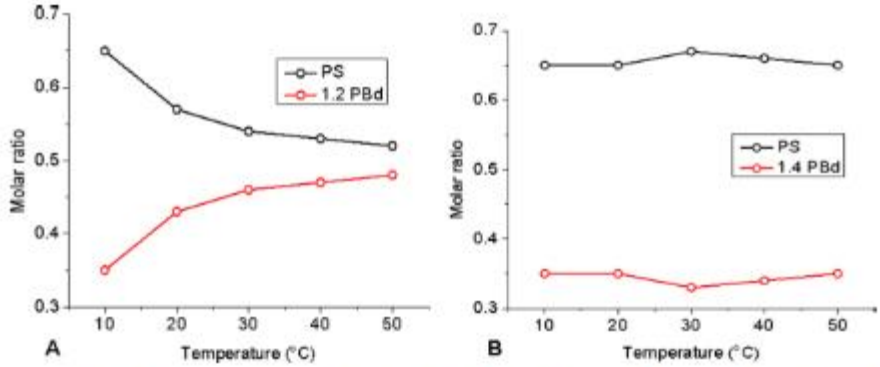

Fig. 6. Temperature dependent ^{1}H NMR spectra for (A) 1.2-PS-PBd and (B) 1.4-PS-PBd vesicles in DMAc-d_9 where the PS and PBd peak integrals are shown in black and red, respectively. (For interpretation of the references to colour in this figure legend, the reader is referred to the web version of this article.)

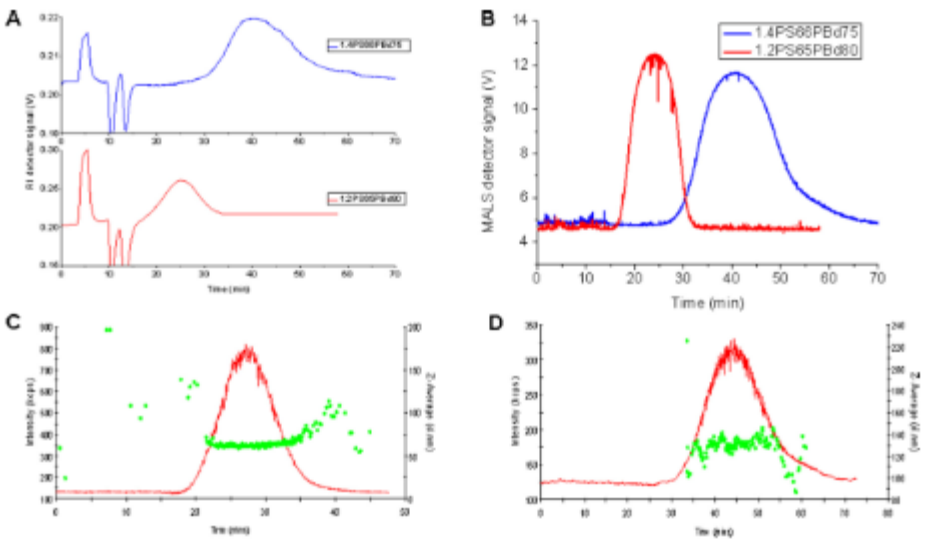

Fig. 7. Superimposed ThFFF RI (A) and MALLS (B) fractograms for 1.2-PS-PBd and 1.4-PS-PBd vesicles. Graphs (C) and (D) represent the respective DLS fractograms, where the green symbols represent the z-average size distributions. t_0 = 13.3 min. (For interpretation of the references to colour in this figure legend, the reader is referred to the web version of this article.)

Table 2
ThFFF data for 1.2-PS-PBd and 1.4-PSPBd vesicles.

Sample code	t_R (min)	$M_w \times 10^3$ (kg/mol)	Z	D_h (nm)	$D \times 10^{-8}$ (cm2/s)	$D_T \times 10^{-8}$ (cm2/s K)	R_G/R_h
1.2-PS-PBd	24.1 ± 0.1	2.64 ± 0.01	33.0 ± 1.0	63.0 ± 0.2	0.70 ± 0.01	0.026 ± 0.002	1.67 ± 0.02
1.4-PS-PBd	42.4 ± 0.3	28.3 ± 0.3	354 ± 12	131.0 ± 1.0	0.34 ± 0.02	0.022 ± 0.001	1.51 ± 0.04

record the lowest D values due to the inverse relationship between the two parameters.

The most important question to be answered is, if the separation of the two types of vesicles is solely based on size. As has been seen in previous work, the microstructure of the corona polymer has a pronounced effect on separation in ThFFF [9,11]. So far it is not known, however, if the microstructure of the core polymer may have a similar effect.

To try and answer this question, the ThFFF behaviour of 1,2-PS-PBd self-assemblies of different hydrodynamic sizes was compared to that of specific PS homopolymers. These PS homopolymers had hydrodynamic sizes that were comparable to the sizes of the self-assemblies. In this setup, the effect of core chemistry is factored out and the comparison is based on entities with similar sizes and surface chemistries.

3.4. ThFFF of 1.2-PS-PBd self-assemblies and PS homopolymers of similar sizes

The selected self-assemblies and homopolymers of similar D_h are shown in Table 3, with D_h measured by offline DLS. The respective homopolymers have broader size distributions compared to the self-assemblies, although both species have the same average sizes as depicted in Fig. 8. The results of the respective ThFFF seperations are summarised in Table 4. As expected, broader ThFFF fractogram peaks are observed for the homopolymers (Fig. 9), in a trend similar to the offline DLS size distribution peaks shown in Fig. 8.

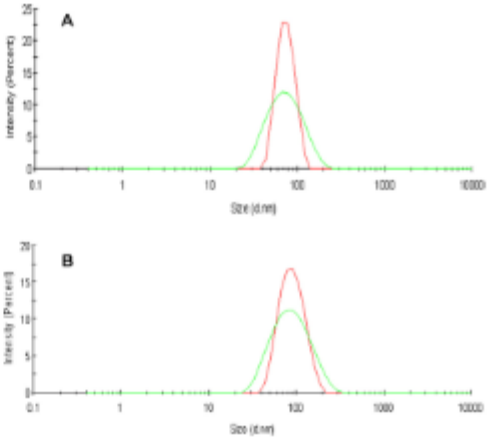

Fig. 8. DLS z-average size distribution by intensity for (A) PS 1.4Mil (green) and 1.2-PS65-PBd75 (red); and (B) PS 2.4Mil (red) and 1.2-PS64-PBd33 (green). (For interpretation of the references to colour in this figure legend, the reader is referred to the web version of this article.)

Figs. 10 and 11 show comparisons of the ThFFF behaviour of the BCP vesicles and the corresponding PS homopolymers. As pointed

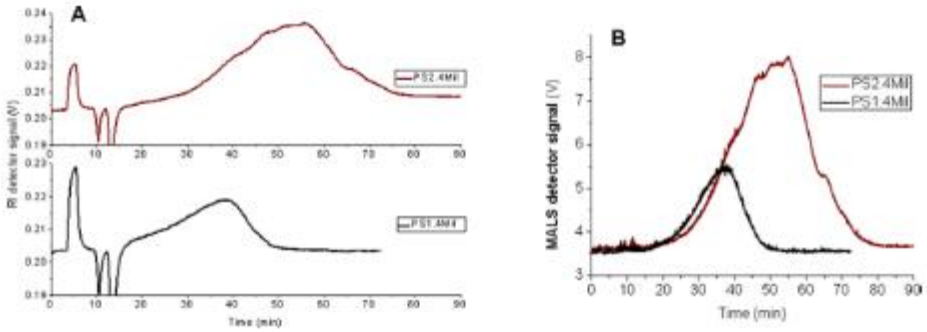

Fig. 9. Superimposed ThFFF RI (A) and MALLS (B) fractograms for PS 1.4Mil and PS 2.4Mil. t_0 = 13.3 min.

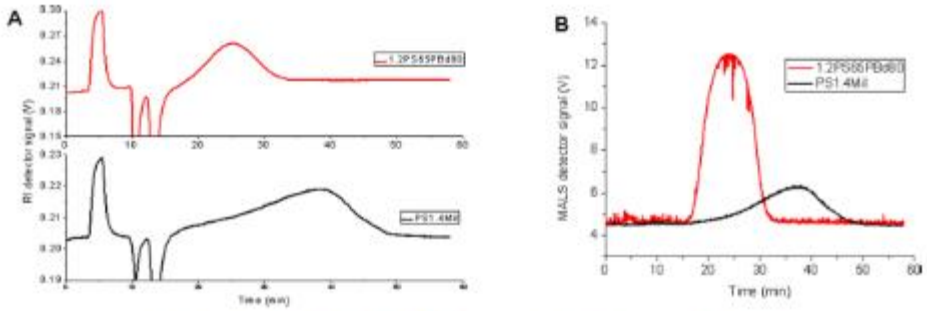

Fig. 10. Superimposed ThFFF RI (A) and MALLS (B) fractograms for PS 1.4Mil and 1.2 PS85PBd80. t_0 = 13.3 min.

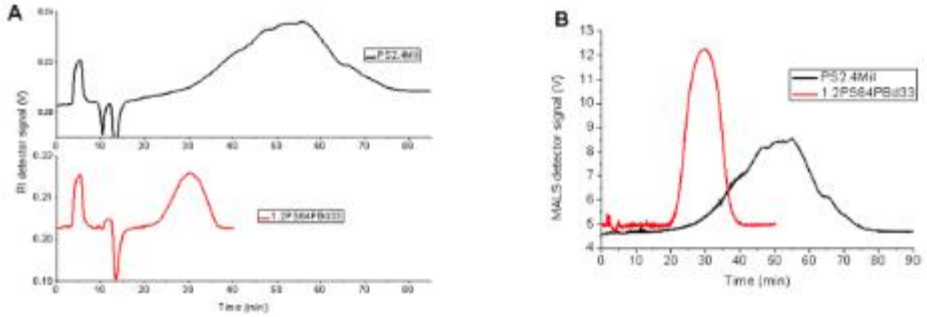

Fig. 11. Superimposed ThFFF RI (A) and MALLS (B) fractograms for PS 2.4Mil and 1.2 PS64PBd33. t_0 = 13.3 min.

Table 3
Hydrodynamic sizes of 1.2-PS-PBd self-assemblies and PS homopolymers.

Sample	Code	D_h (nm)
1.2-PS_{85}-PBd_{75}	1.2-PS80-PBd75	64.1 ± 0.2
$PS_{1400000}$	PS 1.4Mil	63.7 ± 0.4
1.2-PS_{64}-PBd_{33}	1.2-PS64-PBd33	94.3 ± 2.2
$PS_{2400000}$	PS 2.4Mil	92.7 ± 1.1

out before, comparisons are based on similar hydrodynamic sizes but different molecular structures.

The calculated shape factors for the PS homopolymers are of typical Gaussian coils and are comparable to literature values for PS chains of similar sizes [28]. As expected, the shape factors for the self-assemblies confirm the presence of vesicles [26]. When now comparing the vesicles and the homopolymers of similar solution sizes, it is evident that the homopolymers generally have much larger retention. These unexpected results brings into question whether or not surface chemistry or rather a combination of the latter with morphology and chain arrangement could be impacting on the observed separations. The calculated D_T values can partially explain this observation since D_T is known to be sensitive to surface chemistry. The calculated D_T values for the homopolymers are shown to be more or less similar. The minor differences may be emanating from the chain entanglement effects which are ampli-

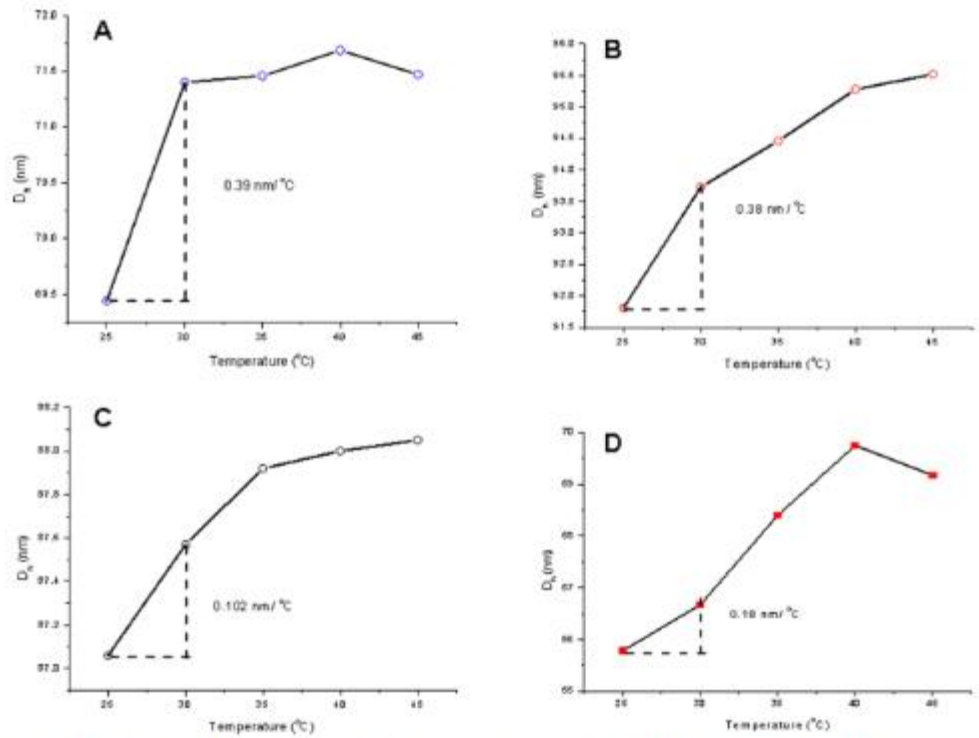

Fig. 12. Variable temperature DLS producing z-average size distribution graphs for PS 1.4Mil (A), PS 2.4Mil (B), 1.2-PS66PBd75 (C) and 1.2 PS64PBd33 (D).

Table 4
ThFFF data for PS-PBd self-assemblies and PS homopolymers of comparable sizes (D_h).

Sample code	t_R (min)	$M_W \times 10^3$ (kg/mol)	Z	D_h (nm)	$D \times 10^{-8}$ (cm2/s)	$D_T \times 10^{-8}$ (cm2/s K)	R_G/R_h
1.2-PS66-PBd75	24.1 ± 0.1	2.64 ± 0.01	33.0 ± 1.0	63.0 ± 0.2	0.70 ± 0.01	0.026 ± 0.001	1.67 ± 0.02
PS 1.4Mil	37.6 ± 0.4	1.52 ± 0.06	-	62.3 ± 0.2	0.71 ± 0.02	0.040 ± 0.002	1.81 ± 0.03
1.2-PS64-PBd33	30.4 ± 0.3	7.47 ± 0.64	226 ± 12	80.2 ± 2.1	0.55 ± 0.01	0.025 ± 0.001	1.63 ± 0.03
PS 2.4Mil	54.8 ± 2.1	2.66 ± 0.13	-	77.3 ± 1.1	0.57 ± 0.03	0.047 ± 0.003	1.89 ± 0.01

fied for the larger molar mass polymer chains. Chain entanglement effects may also be responsible for the observed band broadening.

The D_T values for the two types of vesicles are almost identical, which confirms that the corona compositions are identical. Therefore, the differences in retention of the two vesicles are strictly size based, as expected. It is also interesting to note that the molar mass of the core block (apparently) does not influence thermal diffusion. However, it is apparent that different D_T values are obtained for the vesicles and the corresponding PS homopolymers that have the same corona chemistry. This could mean that the core chemistry may be contributing to the overall surface chemistry (although of a very low volume/volume ratio), and thus affecting thermal diffusion. However, this is not the case. If this was true, then the corresponding PB signals in the NMR spectra would have been stronger. Furthermore, as shown by Köhler et al., the inner parts of a polymer coil do not participate in thermophoresis (and thus do not influence D_T) as the flow lines only penetrate into a thin surface layer of the coil [29]. Similar trends in D_T were also observed from conformation-based elution studies of PS-b-PEO in THF [30]. THF is a selective solvent for PS, and thus PS chains were expected to form a solvated shell around collapsed PEO chains, and thus behaving as "unimicelles". PS homopolymers were shown to have similar retention and D_T values with PS-b-PEO having PS blocks of a comparable size. The following paragraph shall try and explain the observed trends in retention and D_T values between the PS homopolymers and the vesicles in the present study.

The retention behaviours of the self-assemblies (and thus D_T) are not directly influenced by the core chemistry. Rather, it is the influence by the flow shear forces acting on the molecules and the differences in how they react to these forces that determines their retention, which in turn influences the value of D_T. D_T is actually indirectly influenced by how the homopolymer can deform in the channel due to the flow shear forces acting on it. It can be assumed that homopolymers can easily deform, and be pushed closer to the cold wall than the vesicles and thus exhibit longer retention in the channel. The longer retention results in greater D_T values. On the other hand, the vesicles cannot deform like the homopolymers and thus elute earlier. This is the most likely reason why D_T is different, and not due to the core chemistry. This can be shown experimentally with variable temperature DLS, as illustrated in Fig. 12, were

the PS homopolymers generally display a larger change in size per unit temperature, especially in the temperature range of 25 and 30 °C.

The slope of the change in size as a function of temperature was taken between 25 and 30 °C as this temperature range most accurately describes the conditions the vesicles and homopolymers experience at the cold wall during analysis. Thus, Fig. 12 shows that the homopolymers can more readily undergo changes in conformation as compared to the vesicles. This observation can explain why the two species distinctly separate under the conditions inside the channel despite the comparable solution sizes.

4. Conclusion

ThFFF was successfully applied in the separation and characterization of PS-b-PBd vesicles with 1,2- and 1,4-PBd cores, respectively. The core microstructure was shown to impact on the D_h, M_w, Z, and CMC of the vesicles, thus demonstrating the potential application of microstructural differences for providing designed BCP self-assemblies. Furthermore, it was established that for the vesicles and homopolymers of similar surface chemistry and D_h, ThFFF was sensitive towards the inherent differences in morphology and chain arrangement, and thus the two polymeric species were successfully separated.

References

[1] P. Bhargava, J.X. Zheng, R.P. Quirk, S.Z.D. Cheng, J. Polym. Sci. Part B. Polym. Phys. 44 (24) (2006) 3605–3611.
[2] Y. Zhang, Y.M. Lam, J. Nanosci. Nanotechnol. 6 (12) (2006) 3877–3881.
[3] A.B. Ebrahim Attia, Z.Y. Ong, J.L. Hedrick, P.P. Lee, P.L.R. Ee, P.T. Hammond, Y.Y. Yang, Curr. Opin. Colloid Interface Sci. 16 (3) (2011) 182–194.
[4] J. Schmelz, M. Karg, T. Hellweg, H. Schmalz, ACS Nano 12 (2011) 9523–9534.
[5] Z. Du, J. Xu, Z. Fan, Macromol. Rapid Commun. 29 (2008) 467–471.
[6] L. Glavas, P. Olse, K. Odelius, A. Albertsson, Biomacromolecules 14 (2013) 4150–4156.
[7] Z. Grubišic-Gallot, J. Sedláček, Y. Gallot, J. Liq. Chromatogr. Relat. Technol. 21 (10) (1998) 2459–2472.
[8] M.G. String, H.H. Teo, C. Price, C. Booth, J. Chromatogr. 388 (1987) 421–427.
[9] G. Greyling, H. Pasch, Macromolecules 49 (2016) 1882–1889.
[10] U.L. Muza, G. Greyling, H. Pasch, Anal. Chem. 89 (2017) 7216–7224.
[11] G. Greyling, H. Pasch, Polym. Int. 66 (2017) 745–751.
[12] M.E. Schimpf, K. Caldwell, J.C. Giddings, in: M.E. Schimpf, K. Caldwell, J.C. Giddings (Eds.), Field-Flow Fractionation Handbook, Vol. 4, Wiley-Interscience, New York, USA, 2000.
[13] M.E. Schimpf, J.C. Giddings, Macromolecules 20 (7) (1987) 1561–1563.
[14] M.E. Schimpf, J.C. Giddings, J. Polym. Sci. Part B Polym. Phys. 28 (13) (1990) 2073–2080.
[15] M.E. Schimpf, J.C. Giddings, J. Polym. Sci. Part B Polym. Phys. 27 (6) (1989) 1317–1332.
[16] F. Messaud, R.D. Sanderson, J.R. Runyon, T. Otte, H. Pasch, S.K.R. Williams, Prog. Polym. Sci. 34 (4) (2009) 351–368.
[17] J.R. Runyon, S.K.R. Williams, J. Chromatogr. A 1218 (38) (2011) 6774–6779.
[18] G. Greyling, H. Pasch, J. Chromatogr. A 1414 (2015) 163–172.
[19] Z. Tuzar, P. Kratochvíl, Adv. Colloid Interface Sci. 6 (3) (1976) 201–232.
[20] G. Natta, P. Corradini, J. Polym. Sci. 20 (1956) 251–266.
[21] G. Natta, F. Danusso (Eds.), Stereoregular Polymers and Stereospecific Polymerisation, 1st ed., Oxford, Pergamon, 1967.
[22] S. Jain, F.S. Bates, Science 300 (5618) (2003) 460–464.
[23] S. Jain, F.S. Bates, Macromolecules 37 (4) (2004) 1511–1523.
[24] G. Riess, Prog. Polym. Sci. 28 (7) (2003) 1107–1170.
[25] T. Liu, L.-Z. Liu, B. Chu, Formation of Amphiphilic Block Copolymer Micelles in Nonaqueous Solution, Woodhead Publishing Limited, Cambridge, UK, 2000.
[26] W. Burchard, Advances in Polymer Science, vol. 143, Springer, Berlin, 1999, pp. 114–194.
[27] M.L. Mansfield, J.F. Douglas, S. Irfan, E. Kang, Macromolecules 40 (2007) 2575–2589.
[28] I. Terzaoka, Polymer Solution, John Wiley & Sons, New York, USA, 2002.
[29] K.I. Morozov, K. Werner, Langmuir 30 (2014) 6571–6576.
[30] N. Ngara, M. Brand, H. Pasch, Macromol. Chem. Phys. (2015) 1355–1364.

4.2 Stereocomplexation of polymers in micelle nanoreactors as studied by multiple detection thermal field-flow fractionation (Part 2).

Stereoregular polymers can be chemically or physically manipulated to form unique crystalline stereocomplexes (SC)s that consequently precipitate out of solution. This paper demonstrates that micellar nanoreactors (MNR)s can be used to provide a viable route for studying SC in solution. A schematic representation of the SC of PMMA is given in Figure 4.3. While i-PMMA and s-PMMA separately exhibit random coil conformations in solution, blends of the two polymers form stereocomplexes under specific well-defined conditions.

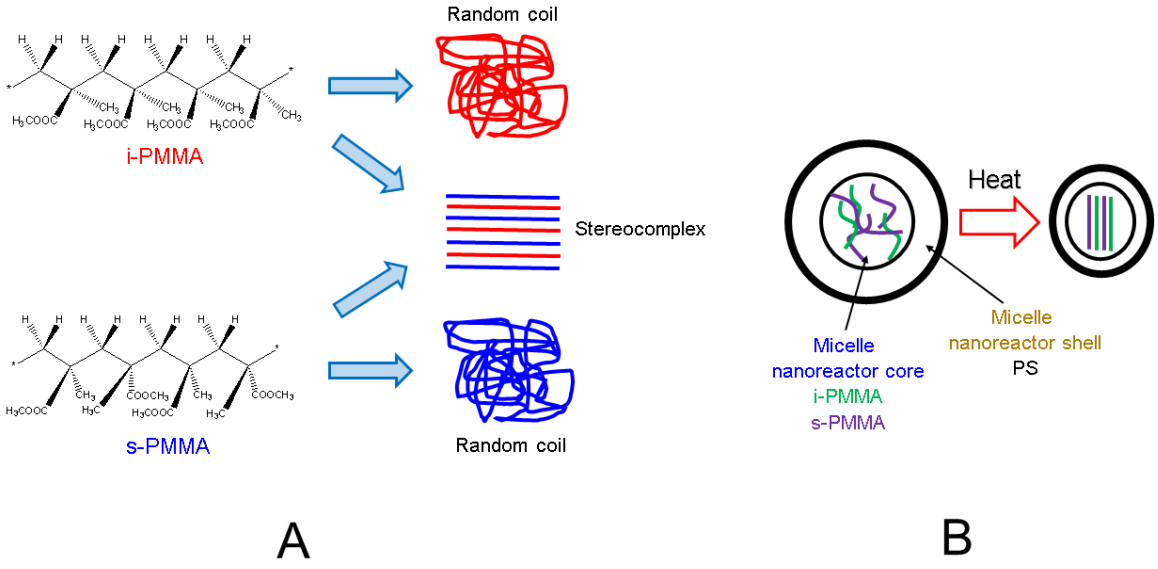

Figure 4.3. Schematic representation of the stereocomplexation of isotactic and syndiotactic PMMA.

As shown in Figure 4.4, significant changes in ATR-FTIR signal intensities, signal shifts and remarkable size changes are used as probes for SC. In addition to providing the

expected hydrodynamic size measurements, DLS studies performed on the micelles and MNRs were also aimed at studying solubility.

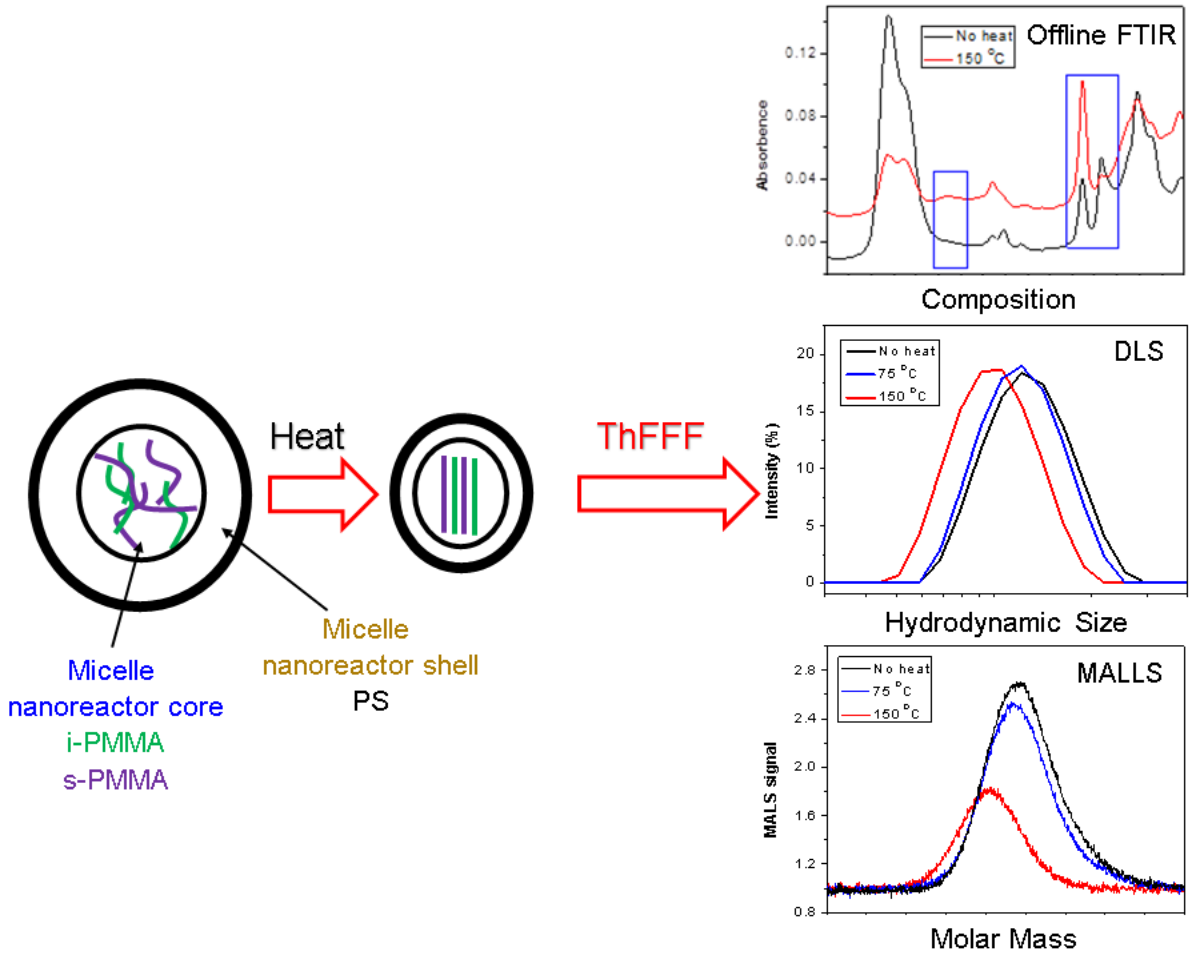

Figure 4.4. Graphical presentation of the analytical approach for the study: Stereocomplexation of polymers in micelle nanoreactors as studied by multiple detection thermal field-flow fractionation.

The primary confirmation for the solubility of the MNRs is obtained from the data "quality reports" and "expert advice" generated in the results sheets of all size measurements. "Good" quality is reported throughout as expected for soluble and homogeneous solutions without any "sedimentation" and such scenario is not

typical for cases involving precipitation. Another confirmation for solubility is obtained from the fact that unimodality of the size distributions is consistently measured, more so within the nanometer range, where any precipitation would be rather expected to be in the micrometer size range. It is expected that the surface chemistry of all the MNRs is similar, being composed of PS shells. Therefore, any elution trends of these MNRs should strictly be based on their sizes, as is demonstrated in this work and illustrated in Figure 4.4.

The associated article and supplementary information for this study are presented as follows.

analytical chemistry

Article

Cite This: Anal. Chem. 2018, 90, 13987−13995

pubs.acs.org/ac

Stereocomplexation of Polymers in Micelle Nanoreactors As Studied by Multiple Detection Thermal Field-Flow Fractionation

Upenyu L. Muza, Guilaume Greyling, and Harald Pasch*

Department of Chemistry and Polymer Science, University of Stellenbosch, 7602 Matieland, South Africa

Supporting Information

ABSTRACT: In this study the thermally induced in situ stereocomplexation (SC) of binary blends of symmetrical isotactic and syndiotactic polymethymethacrylates (i- and s-PMMAs) inside micellar nanoreactors (MNR) with polystyrene (PS) shells is investigated using thermal field-flow fractionation (ThFFF) as a separation technique. The MNRs are prepared from three systematic binary blending ratios of pure micelles of i-PMMA-PS and s-PMMA-PS in a nonsolvent for PMMAs in order to produce mixed micelles with a binary microstructural composition of the interior PMMA cores. The SC of these stereoregular PMMA cores inside the MNRs is shown to be thermally induced as a function of annealing temperatures from room temperature up to 150 °C. This SC is initially confirmed by Fourier transform infrared spectroscopy (FTIR), whereby signal shifts are observed in the carbonyl absorption regions. These signal shifts are as a result of SC interactions between adjacent ester and alpha-methyl groups. Furthermore, temperature-dependent dynamic light scattering (DLS) results show that MNRs with more SC domains have a much more drastic reduction in size. Additional corroboration is provided by multiple detection ThFFF results which show significant differences in retentions and sizes between MNRs with stereocomplexed cores and those without. Ratios of i-PMMA:s-PMMA in the order of 1:1, 1:2, and 2:1 were investigated with all ratios exhibiting thermal annealing induced SC, of which the 1:2 ratio is shown to have the highest predisposition to SC.

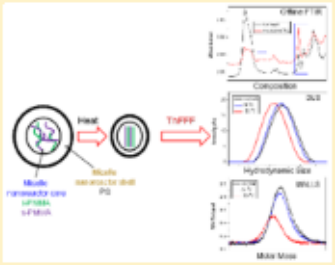

INTRODUCTION

Polymer stereocomplexes are defined through stereoselective interactions between two complementing stereoregular polymers that interact and form a new entity, exhibiting new properties in comparison to the parent polymers. The main interactions are proposed to rely on stereoselective van der Waals forces. Stereocomplexes of poly(methyl methacrylate) (PMMA) homo- and blockcopolymers, poly(lactic acid) (PLA) homo- and blockcopolymers, and between D-configured PLA and L-configured peptides have been described.[1]

The stereocomplexation (SC) of isotactic and syndiotactic poly(methyl methacrylate) (i- and s-PMMA) has been applied in designing novel and advanced materials such as ultrathin films, microcellular foams, hollow fiber dialyzers, thermoplastic elastomers, polymerization templates, and supramolecular nanospheres/networks. Factors such as the binary blending ratio, molar mass, solvent, concentration, annealing temperature, and complexation time are known to influence the SC.[2−6] The SC in PMMA is in principle a result of the intricate interchain interactions of adjacent ester and α-methyl groups.[7,8]

Although the first SC studies on PMMA were reported in the late 1950s,[9] molecular dynamics and mechanism of formation of the SC remain ambiguous to date.[10,11] It is known that relative to i-PMMA the geometrical configuration of s-PMMA favors more molecular interactions and the formation of closely packed chains which results in higher glass transition temperature (T_g).[12] In general, tacticity differences are known to impact the blending compatibility and T_g of polymers. Binary blends of symmetrical i- and s-PMMA were found to undergo SC across the entire composition range as investigated by Schroeder et al.[2] i- and s-PMMA of different molar masses were also shown to exhibit similar trends.[13] These results concur with earlier findings by Krause and Roman.[14] However, contrasting results were reported by Bauer et al., who concluded that i-PMMA and s-PMMA binary systems were in fact immiscible. It must be noted, however, that in the case of contrasting findings different sample molar masses and analytical techniques were employed.[15] A schematic representation of SC of PMMA is given in Figure 1A. While i-PMMA and s-PMMA separately exhibit random coil conformations in solution, blends of the two polymers form stereocomplexes under specific well-defined conditions.

Stereocomplexation studies of i- and s-PMMA have largely been confined to bulk characterization techniques such as X-ray diffraction, thermal analysis, and microscopy. This is mainly due to the fact that upon complex formation the samples become insoluble and precipitate. Preceding investigations have focused on homopolymer or block copolymer

Received: August 8, 2018
Accepted: November 12, 2018
Published: November 12, 2018

DOI: 10.1021/acs.analchem.8b03590
Anal. Chem. 2018, 90, 13987−13995

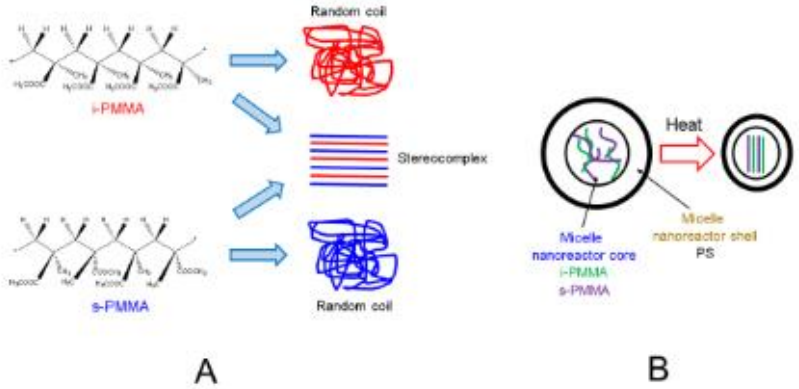

Figure 1. Stereocomplex formation of i-PMMA and s-PMMA in solution (A) and in micelle nanoreactors (B).

(BCP) blends.[3,4,16−19] Kawauchi et al. investigated the stereocomplexation into self-aggregated large clusters of i- and s-PMMA chains functionalized with fullerene end groups.[10]

To date SC investigations have not been conducted on self-assembling BCPs such as amphiphilic BCPs. There is special interest regarding in situ SC in cores of micelles that are composed of i- and s-PMMA blocks. The in situ SC can be approached by designing micellar nanoreactors (MNRs) from the self-assembly of two BCPs having i- and s-PMMA as the core-forming blocks, respectively, in a nonsolvent for PMMA.[20−22] As a result, these MNRs will have an internal core of stereoregular PMMAs inside the shells of the solvophilic blocks (polystyrene in the present case). By considering various ratios of i- and s-PMMA blocks in the core, reactions such as SC can be conducted inside the MNRs by optimizing critical parameters such as reaction time, temperature, catalyst, and pH (see schematic presentation in Figure 1B). It must be noted henceforth that although "nanoreaction" generally refers to a chemical process, for this study the term shall be used in reference to a physical process (SC).

In situ SC will allow the resultant SC properties to be retained in solution as opposed to the inevitable precipitation effects observed in the SC of stereoregular PMMA homopolymers. As SC occurs only in specific solvents, the in situ SC approach using specifically designed MNR can enable SCs to occur even when using solvents that are generally incompatible with the system. This study will, for the first time, investigate the in situ SC of cores composed of i- and s-PMMA inside MNRs composed of polystyrene (PS) shells using thermal field-flow fractionation (ThFFF).

ThFFF is a subtechnique of FFF that has the capabilities of fractionating according to surface chemical composition (CC) and hydrodynamic size (D_h).[23] By coupling ThFFF with an array of detectors, one is able unravel fundamental information on molar mass, CC, D_h, and the respective distributions.[24,25] These molecular properties are critical properties in any polymeric material's design and application. It must be noted that asymmetrical flow field-flow fractionation (AF4) is the more popular and commonly used FFF subtechnique for the separation and characterization of gels, SAs, and large aggregates.[26−29] However, ThFFF can represent a complementary analytical alternative, bearing in mind the attractiveness of the relatively simpler and well-defined dimensions of the separation channel thereof.[23] In addition, in the present case the fractionation power of ThFFF is enhanced by using multiple offline and online detectors that provide quantitative information on diffusion coefficients and hydrodynamic diameters.

ThFFF setup and operation have been described before in a number of reviews.[23] Sample retentions in ThFFF are governed by the balance between the normal diffusion coefficient (D) and the thermal diffusion coefficient (D_T). The latter has been experimentally proven to be a function of CC, while the former (D) is well known to be influenced by D_h (Stokes−Einstein equation).[30−32] Other fractionation techniques such as size exclusion chromatography (SEC) have been rendered unsuitable for the characterization of self-assemblies owing to the tendency of the column to shear degrade the sensitive self-assemblies.[33] Moreover, polymeric self-assemblies range from around 10^3 kg/mol and above in molar mass, which generally is above the separation limit of SEC and makes the technique unsuitable for highly aggregated and larger molar mass species. Accordingly, ThFFF has developed into a robust alternative analytical technique for large and delicate self-assemblies.[34,35]

EXPERIMENTAL SECTION

Materials. All samples shown in Table 1 were purchased from Polymer Source (Montreal, Canada) and were used as received. The subscript represents the molar mass for the respective blocks in kg/mol.

Table 1. BCP and Micelle Code Names (where the subscripts represent $M_w \times 10^3$ g/mol), Tacticity Content, and Critical Micelle Concentrations (CMC) of the Prepared Self-Assemblies

block copolymer	tacticity content (mol %)	micelle code name	CMC (mg/mL)
i-PMMA$_{85}$-PS$_{80}$	92.6	i-PMMA-PS	0.015
s-PMMA$_{83}$-PS$_{80}$	81.3	s-PMMA-PS	0.017

DOI: 10.1021/acs.analchem.8b03500
Anal. Chem. 2018, 90, 13987−13995

Table 2 shows MNR code names as well as the associated i-PMMA to s-PMMA ratios and nanoreactor temperatures.

Table 2. MNR Code Names, i-PMMA to s-PMMA Ratios, and Nanoreactor Temperatures

nanoreactor code name	i-PMMA:s-PMMA ratio	nanoreactor temperature (°C)
1.1 RT	1:1	room temperature (RT)
1.1 T75	1:1	75
1.1 T150	1:1	150
1.2 RT	1:2	RT
1.2 T75	1:2	75
1.2 T150	1:2	150
2.1 RT	2:1	RT
2.1 T75	2:1	75
2.1 T150	2:1	150

Preparation of Micelles and MNRs. Two symmetrical BCPs, namely, i-PMMA-PS and s-PMMA-PS, were separately and directly dissolved in *p*-cymene (a nonsolvent for PMMA) at a temperature of 150 °C for 5 min. The core microstructure is shown not to significantly influence the critical micelle concentrations (CMCs) as shown by the values recorded in Table 1. The micellar solution was left for 1 week acclimatizing time. Thereafter, the MNRs were prepared from 1:1, 1:2, and 2:1 binary blending ratios of the pure micelles. Three sets of aliquots were further prepared from each of the respective ratios. One set was left at room temperature over a period of 1 week. The other two sets of aliquots were set at temperatures of 75 and 150 °C for 15 min, respectively.

ThFFF Conditions. Measurements were performed using the TF2000 instrument (Postnova Analytics, Germany) coupled in series to the detectors MALLS (PN3070, Postnova Analytics, Germany), dRI (PN 3140, Postnova Analytics, Germany), and a Zetasizer Nano series (Malvern Instruments, Worcestershire, UK) with built-in data processing software which was used for dynamic light scattering (DLS) detection at an angle of 175° (back-scattering detection). An excess of 100 μL of sample was manually injected into a 100 μL capillary sample loop to ensure capillary flooding, and each analysis was performed in triplicate. A temperature drop (ΔT) of 20 °C was applied for all fractionations, and an external chiller (Unichiller, Monitoring and Control Laboratories, South Africa) maintained a stable cold wall temperature at about ~21 °C. The carrier solvent, *p*-cymene (Sigma-Aldrich, South Africa), was pumped by an isocratic pump (PN 1130, Postnova Analytics, Germany) at a flow rate of 0.3 mL/min.

MALLS data was processed using the TF2000 software (Postnova analytics, Germany) over 7 scattering angles from the range of 35−145°. The Zimm plot was utilized to obtain molar mass (M_w) and the radius of gyration (R_g). The degree of compactness was assessed by calculating the apparent density (ρ_{app}) from the following equation; where $V(R_g)$ represents the volume of a sphere with a radius identical to R_g.[26,36]

$$\rho_{app} = \frac{M_w}{V(R_g)}$$

The following assumptions are made regarding the separations reported herein this study. (1) ThFFF is rendered applicable for this specific sample system because the surface chemistry of the micelles and MNRs is deemed identical;[37] accordingly, their respective D_T values are expected to be constant.[38−40] (2) Consequently, D becomes the only variable of concern regarding the observed ThFFF separations.

Offline DLS. Three runs were performed per measurement using a glass cuvette with an open round aperture at a temperature of 26.7 °C and using 1 mL sample volumes at respective concentrations of 2 mg/mL. Five minute equilibrium times were programmed prior to all measurements. A solvent viscosity value of 0.774 cP was used. From the DLS software (Zetasizer software 7.11), D_h was reverse calculated from the diffusion coefficient (D) in accordance with the Stokes−Einstein equation shown below, where k, T, and η represent the Boltzmann's constant, temperature, and solvent viscosity, respectively.

$$D = \frac{kT}{3\pi\eta D_h}$$

Attenuated Total Reflectance Fourier Transform Infrared Spectroscopy (ATR-FTIR). A Thermo Nicolet iS10 Spectrometer (Thermo Scientific, Waltham, MA) equipped with a diamond crystal was used for the FTIR analysis of thin films of the pure micelles and MNRs. Each sample was scanned 64 times with a spectral resolution of 8 cm^{-1} over a range of 700−4000 cm^{-1}. Data collection and processing was performed using Scientific OMNIC software (version 8.1).

RESULTS AND DISCUSSION

In the first step of this work, BCP micelles were prepared that have a PS corona and a PMMA core. The core is composed of either i-PMMA or s-PMMA blocks that, under the conditions of preparation, are in random coil conformation. The formation of self-assemblies from the respective symmetrical BCPs is confirmed by batch-mode DLS, where size distributions typical for self-assemblies and aggregations are recorded in the range from 100 to 150 nm (Figure 2).[37] Both

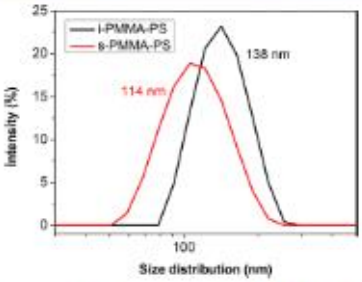

Figure 2. Z-average D_h distributions (offline) of i-PMMA-PS (black) and s-PMMA-PS (red).

distribution curves show unimodality which infers the existence of single and not multiple size distributions in solution. The self-assemblies with i-PMMA cores are shown to have larger D_h compared to the ones with s-PMMA cores.

A similar trend has previously been observed for self-assemblies prepared in a similar manner from symmetrical BCPs of polybutadiene-polystyrene BCPs with 1.2- and 1.4-polybutadiene cores, respectively.[41] The observed differences in size should be emanating from variations in molecular

DOI: 10.1021/acs.analchem.8b03500
Anal. Chem. 2018, 90, 13987−13995

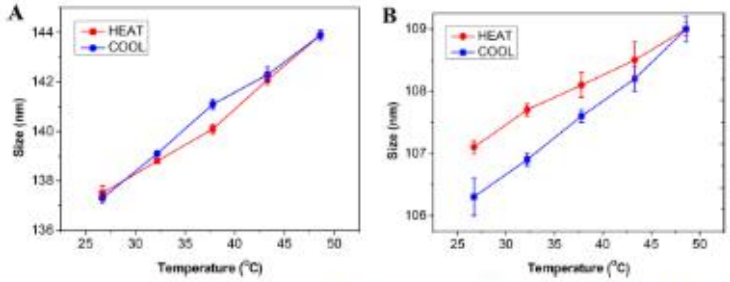

Figure 3. Z-average D_h as a function of temperature for (A) i-PMMA-PS and (B) s-PMMA-PS, where the red and blue curves represent the respective heating and cooling trajectories.

Table 3. Molar Mass (M_w), Aggregation Number (Z), Hydrodynamic Diameter (D_h), Retention Time t_R, Shape Factor (R_g/R_h), and Apparent Density (ρ_{app}) for the Pure Micelles

sample	$M_w \times 10^3$ (kg/mol)	Z	D_h (nm)	t_R (min)	R_g/R_h	$\rho_{app} \times 10^{-4}$ (1/nm^3)
i-PMMA-PS	17.7 ± 0.6	295	137.5 ± 0.7	26.3 ± 0.4	0.80 ± 0.04	4.23
s-PMMA-PS	5.2 ± 0.1	87	113.5 ± 0.7	23.3 ± 0.1	0.75 ± 0.01	2.69

properties of the core forming blocks as imposed by their microstructural differences. In this context, remarkable differences exist between the glass transition temperatures (T_g) of either i- and s-PMMA or 1,2- and 1,4-PBd, and as a result significant differences in chain flexibility of the respective cores are expected. Thus, under similar experimental conditions, these self-assemblies will naturally have significant differences in their respective solvophobic−solvophilic balance index, which in turn is essential in governing the size and morphology of self-assemblies.[37,42]

The differences in chain flexibility as imposed by the microstructural differences can be investigated by batch-mode DLS through measuring differential size changes as a function of temperature (Figure 3). As expected, i-PMMA-PS self-assemblies have a steeper slope for size change vs temperature owing to their lower T_g and thus higher chain flexibility (see Figure S1 in Supporting Information). On the other hand, s-PMMA cores in s-PMMA-PS micelles should have a higher T_g and are expected to be more compact and less flexible. Hence, the lower slope in the size vs temperature plot for s-PMMA-PS is as expected (see Figure S2 in Supporting Information).

The ThFFF analysis of the two types of micelles reveals that the higher D_h of i-PMMA-PS self-assemblies corresponds to higher molar mass and retention, as summarized in Table 3 and depicted in Figure 4. However, similar topologies are observed regardless of the microstructural differences of the cores for both self-assemblies, as similar shape factors (R_g/R_h) are recorded that are typical for spherical micelles (~0.8).[43−45] It must be noted that Mozorov et al. have previously reported in detail that the thermal diffusion of polymers is only influenced by very ultrathin peripheral layers of their surface chemistry.[46] Therefore, microstructural differences between the cores of the two respective micelles (and later on MNRs) are expected not to affect their thermal diffusion and hence are inconsequential to the observed retention trends inside the channel.

The apparent density (ρ_{app}) of the micelles as expressed in the more appropriate form of aggregation number (Z) per unit volume can be calculated from the quotient of Z and the

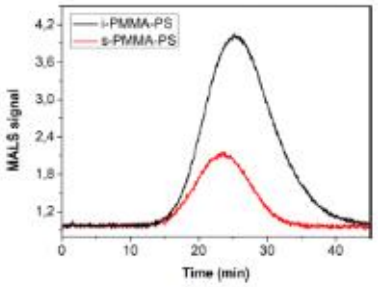

Figure 4. ThFFF fractograms for i-PMMA-PS (black) and s-PMMA-PS (red) micelles. Detector signal: MALS. Void time: 7.6 min.

associated volume as obtained from R_g. Z values are obtained from M_w(micelle)/M_w(PS). The i-PMMA-PS micelles are shown to have the largest ρ_{app} value of the two. This characteristic may also be emanating from the fact that i-PMMA chains in the core of i-PMMA-PS micelles have a lower T_g; thus, more intricate chain interactions are expected to be predominant, which results in more aggregation per unit volume. Thus, i-PMMA-PS micelles can be described to be the more compact of the two spherical morphologies.[26]

Thereafter, mixed micelles were prepared from three binary blending protocols of the respective i- and s-PMMA-PS pure micelles in 1:1, 1:2, and 2:1 ratios in order to investigate the stereocomplexation (SC) of the "mixed" stereoregular cores. By triggering SC reactions of the two different PMMA components of the mixed cores inside the PS shells as a function of known SC parameters such as reaction time and temperature, the mixed micelles can essentially be considered as nanoreactors.[20] These MNR shall be investigated for the in situ SC of their stereoregular i- and s-PMMA mixed cores.

For SC to take place at room temperature (RT), a 7 day equilibrium time was allowed prior to analysis. FTIR spectra measured after equilibrium shows near perfect overlays for both the pure and the mixed micelles as shown in Figure 5. For

DOI: 10.1021/acs.analchem.8b03500
Anal. Chem. 2018, 90, 13987−13995

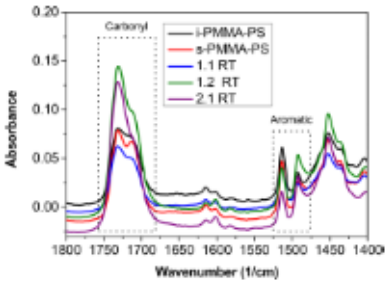

Figure 5. Superimposed ATR-FTIR absorbance spectra for the pure micelles and mixed-micelle nanoreactors (MNRs) at room temperature.

all of the samples the expected carbonyl and aromatic functionalities exhibit strong and perfectly overlaying signals at 1675−1750 and 1475−1525 cm^{-1}, respectively.[47] Therefore, no new signals or signal shifts were detected that would support the formation of SC of the mixed cores inside the nanoreactors.[48,49]

Furthermore, batch-mode DLS and ThFFF results show no drastic changes in size and ThFFF retention time between the pure micelles and the MNRs as would be anticipated in the event of any SC (Table 4 and Figure S3 in Supporting Information). Rather, the mixed micelles are shown to generally possess the average sizes and retention times of the pure parent micelles.[25] The 1:2 ratio has a higher concentration of the smaller s-PMMA-PS micelles and thus exhibits the lowest D_h and molar mass values, while the 2:1 ratio contains more of the larger i-PMMA-PS micelles and hence the largest D_h and molar mass (Table 4). Accordingly, the retention of the micelles corresponds to the size trends, whereby the 2:1 ratio records the highest retention time and 1:2 the lowest. It must be generally noted that D_h results obtained by bulk DLS and ThFFF are very comparable, which highlights the reliability of the complementary use of both techniques.

As a follow up to the inability of the cores to undergo SC at RT conditions, heat was applied to the nanoreactors to provide activation energy and thermal stimulus to induce in situ SC of the cores. Thermal annealing has previously been applied in SC of stereoregular PMMAs in the bulk state.[16,50] Temperatures of 75 and 150 °C are applied to the nanoreactors on a hot plate with vigorous agitation for 5 min. These two particular temperatures are ideal. (1) Each corresponds to the temperatures just above the T_gs for i- and s-PMMA. This approach allowed for measuring the annealing-induced SC as a function of a specific thermochemical property. (2) Annealing temperatures are within the boiling point limits of the solvent (*p*-cymene).

The FTIR spectra of the MNRs shown in Figure 6 at the two temperature extremes, that is, at RT as lowest and 150 °C as highest, displays a remarkable decrease in the intensity of the carbonyl signals and the development of a new and broad signal around 1650 cm^{-1}. This new signal can be attributed to a signal shift of the original carbonyl signal due to the formation of SC domains from ester and methyl functionalities of i- and s-PMMA block inside the MNR core.[5,8,11] SC in essence lowers the vibrational energy of the carbonyl groups, which explains the decrease in signal intensities and signal shifts from higher energy wavenumbers (1675−1750 cm^{-1}) to the observed lower energy wavenumber of 1650 cm^{-1}. The carbonyl signal shift is more intense for the 1:2 ratio followed by 1:1 and 2:1 ratios. Subsequently, the 1:2 ratio can be regarded as the most ideal for this particular case of SC of i- and s-PMMA inside the nanoreactors. This is in agreement with previous studies on stereoregular PMMA homopolymers.[5,11]

Additional evidence is provided by batch DLS measurements which indicate size reduction trends as a function of temperature for all of the nanoreactors after thermal annealing (Figure 7). Moderate size reductions (~10−20 nm) occur at the transition from RT conditions to 75 °C. Much more significant size reductions between 30 and 40 nm are observed when the maximum annealing temperature (150 °C) is applied to the nanoreactors. These drastic changes in size are sufficiently significant to deduce the occurrence of thermally induced SC of the mixed cores in the nanoreactors. More intense SC-related size changes are observed at 150 °C as compared to 75 °C since 150 °C is above the T_g of both i- and s-PMMA, and thus, more intricate chain interactions are likely to happen. Second, higher temperatures are generally related to higher levels of kinetic and activation energy which enables stronger chain interactions that are required for SC.[50] As a result, SC domains are formed by the PMMA cores and the solvophobic−solvophilic balance is changed to favor smaller micelles with much more compact cores. Thus, the SC domains have the advantage of stabilizing the micelles.[51]

In support of the batch DLS, ThFFF analysis reveals that in addition to the decrease in D_h as a function of temperature, so are molar masses and ThFFF retention times (Table 5 and Figure 8). This is first due to the smaller D_h being expected to have lower retention times in the normal mode of elution. Second, lower aggregation numbers of the unimers and thus lower molar masses correspond to lower D_h. No topological changes as a function of temperature or blending ratios are observed as shape factor values between 0.7 and 0.8 are consistently determined.

For the i-PMMA to s-PMMA ratios in the core, the largest size changes per unit original length and the lowest final size

Table 4. Summarized Batch Mode DLS and ThFFF Results for the Pure Micelles and MNRs[a]

sample	batch D_h (nm)	$M_w \times 10^5$ (kg/mol)	D_h (nm)	t_R (min)	R_g/R_h
i-PMMA-PS	138.1 ± 0.2	17.7 ± 0.6	137.5 ± 0.7	26.3 ± 0.4	0.80 ± 0.04
s-PMMA-PS	114.0 ± 0.1	5.2 ± 0.1	113.5 ± 0.7	23.3 ± 0.1	0.75 ± 0.01
1:1 RT	123.2 ± 0.1	10.3 ± 0.3	122.9 ± 0.8	25.1 ± 0.1	0.72 ± 0.03
1:2 RT	117.6 ± 0.1	6.62 ± 0.11	117.0 ± 0.5	24.3 ± 0.2	0.84 ± 0.00
2:1 RT	126.7 ± 0.2	12.0 ± 0.1	126.5 ± 0.3	25.2 ± 0.2	0.79 ± 0.02

[a]Hydrodynamic size (D_h), molar mass (M_w), retention time (t_R), and shape factor (R_g/R_h). ΔT = 30 °C.

DOI: 10.1021/acs.analchem.8b03590
Anal. Chem. 2018, 90, 13987−13995

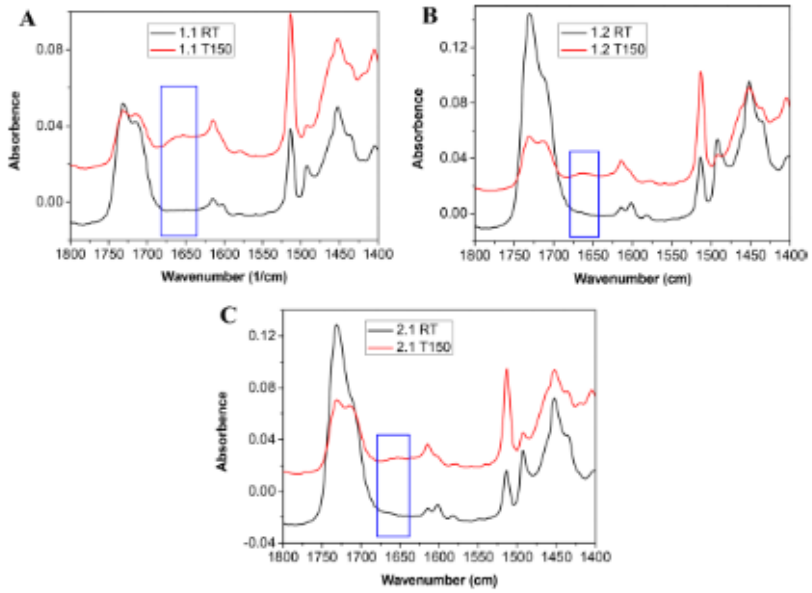

Figure 6. Superimposed ATR-FTIR absorbance spectra at RT (black) and 150 °C (red) for (A) 1:1, (B) 1:2, and (C) 2:1 mixed MNRs.

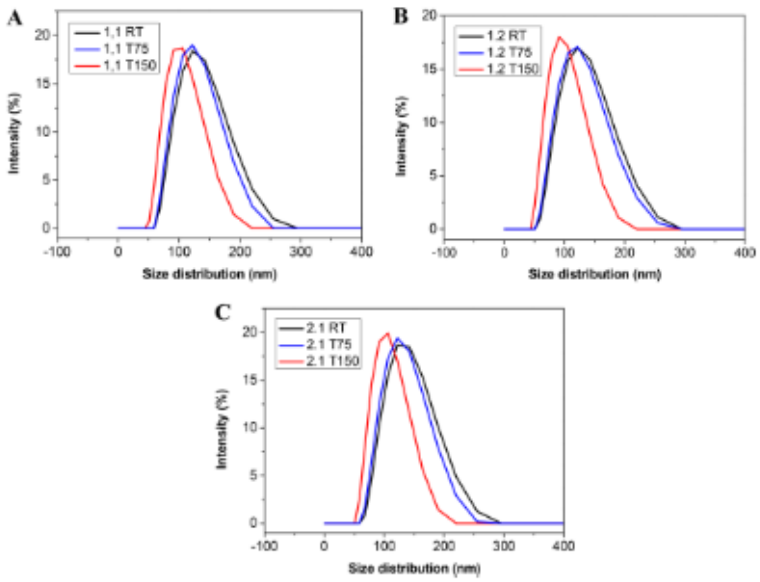

Figure 7. Superimposed Z-average D_h distribution graphs (offline) for (A) 1:1, (B) 1:2, and (C) 2:1 mixing ratios MNRs at room temperature (black), 75 °C (blue), and 150 °C (red).

values for the MNRs after SC are observed in the ratio order of 1:2, 1:1, and 2.1, as summarized in Table 6 and depicted in Figure S4 of the Supporting Information. This trend may be attributed to the fact that the 1:2 and 1:1 ratios in particular

DOI: 10.1021/acs.analchem.8b03590
Anal. Chem. 2018, 90, 13987−13995

Table 5. Summarized ThFFF Results for the MNRs for a Range of Annealing Temperatures[a]

sample	$M_w \times 10^5$ (kg/mol)	D_h (nm)	t_R (min)	R_g/R_h
1.1 RT	10.3 ± 0.3	122.9 ± 0.8	25.1 ± 0.1	0.77 ± 0.03
1.1 T75	6.88 ± 0.01	115.6 ± 0.1	24.4 ± 0.1	0.70 ± 0.05
1.1 T150	4.71 ± 0.04	94.5 ± 0.4	21.2 ± 0.1	0.72 ± 0.03
1.2 RT	6.62 ± 0.11	117.0 ± 0.5	24.3 ± 0.2	0.84 ± 0.00
1.2 T75	4.89 ± 0.08	109.0 ± 0.2	23.3 ± 0.1	0.76 ± 0.06
1.2 T150	3.07 ± 0.11	87.9 ± 0.1	20.5 ± 0.1	0.77 ± 0.03
2.1 RT	12.0 ± 0.1	126.5 ± 0.3	25.2 ± 0.2	0.79 ± 0.02
2.1 T75	8.25 ± 0.12	121.1 ± 0.6	24.8 ± 0.1	0.81 ± 0.01
2.1 T150	6.00 ± 0.08	99.5 ± 0.5	23.0 ± 0.3	0.74 ± 0.03

[a]Molar mass (M_w), hydrodynamic size (D_h), retention time (t_R), and shape factor (R_g/R_h). ΔT = 30 °C.

have previously been shown to be ideal for the SC of i- and s-PMMA, compared to other ratios.[3−5,11,17] Most importantly, the $\Delta\ \rho_{app}$ percentage for the 1:2 ratio is observed to be the highest of the three with a value almost double that of the respective 1:1 and 2:1 ratios. The $\Delta\ \rho_{app}$ percentage values of the latter and former ratios are seen to be comparable. As such, the 1:2 ratio can be regarded as the most ideal one for generating the most compact MNRs from the SC conditions under consideration.

Kinetics of the Stereocomplexation. In the quest to understand the effect of time on SC, kinetic studies were performed by measuring size changes over time for a specific annealing temperature. The mixing ratio of 1:1 was chosen for mixing the pure micelles to form MNRs, and thermal annealing was carried out at a temperature of 100 °C. Such a temperature is expected to be high enough to induce substantial changes in size and still remain low enough to avoid thermal degradation over a reasonable experimental time frame. DLS measurements were then performed in different intervals until no significant changes in size were observable as shown in Figure 9.

Table 6. Percentage Change in Size (D_h and M_w) and Apparent Density (ρ_{app}) from Room Temperature to 150 °C for the MNRs

sample range	ΔD_h (%)	ΔM_w (%)	$\Delta\ \rho_{app}$ (%)
1.1 RT-1.1 T150	23.1	54.3	23.3
1.2 RT-1.2 T150	25.0	58.2	42.1
2.1 RT-2.1 T150	21.3	50.0	24.8

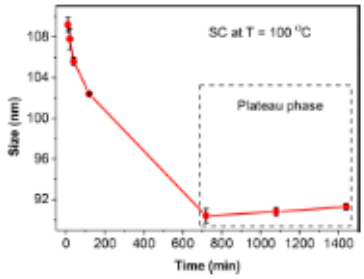

Figure 9. Z-average D_h change as a function of time for MNRs produced from a 1:1 ratio of the pure micelles at an annealing temperature of 100 °C.

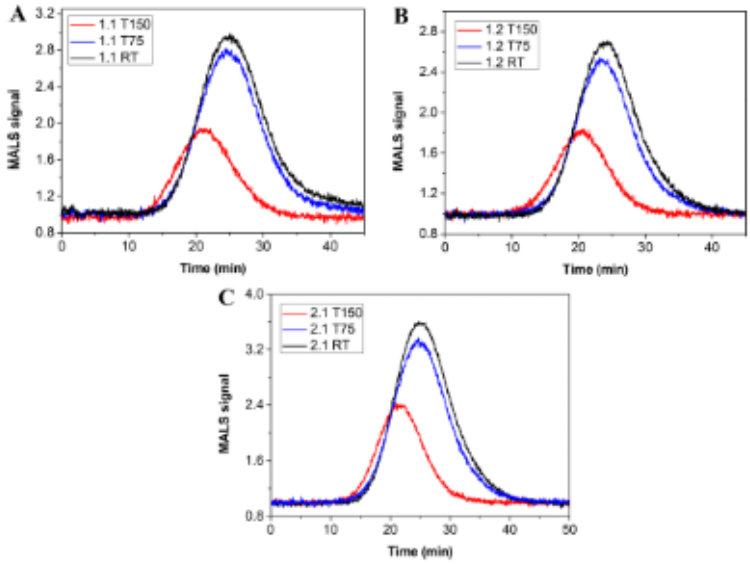

Figure 8. Superimposed ThFFF-MALS graphs for (A) 1:1, (B) 1:2, and (C) 2:1 mixing ratios MNRs at room temperature (black), 75 °C (blue), and 150 °C (red). Void time: 7.6 min

DOI: 10.1021/acs.analchem.8b03590
Anal. Chem. 2018, 90, 13987−13995

The size changes follow a rather linear pattern from 10 to 40 min, and beyond this interval the trend begins to follow a dipping trajectory which eventually plateaus after 720 min. This signifies that significant size changes per unit time as induced by SC (annealing temperature 100 °C) are obtained in the first 40 min. The plateau phase suggests that the limit for thermally induced SC has been reached as governed by the temperature-induced mobility and energy of adjacent chains.

CONCLUSION

Block copolymer (BCP) self-assemblies are shown to be potentially capable of providing complementary protocols in designing thermally driven nanoreactions for the in situ stereocompexation (SC) of stereoregular PMMAs within the core microphase, as characterized by a combination of multiple detection ThFFF (to provide fractionation) and DLS and FTIR (to provide size and composition information, respectively). These nanoreactions are shown to provide alternative pathways in micelle design and modification, where microstructural differences of the PMMA cores are also shown to affect compactness, thermal stability, degree of elasticity, molar mass (hence aggregation number), and hydrodynamic size of the resultant micelles.

Moreover, precipitation effects associated with SCs are circumvented, and as such, properties related to SC can generally be retained in solution. On that same note, SCs can thus potentially become achievable in solvents where such phenomena are typically not feasible via the in situ approach within nanoreactors.

ASSOCIATED CONTENT

Supporting Information

The Supporting Information is available free of charge on the ACS Publications website at DOI: 10.1021/acs.analchem.8b03590.

Supplementary DLS results and other fractograms for all ThFFF separations (PDF)

AUTHOR INFORMATION

Corresponding Author

*E-mail: hpasch@sun.ac.za.

ORCID

Guilaume Greyling: 0000-0001-6513-9669

Harald Pasch: 0000-0003-1132-3393

Notes

The authors declare no competing financial interest.

ACKNOWLEDGMENTS

We thank the National Research Foundation of South Africa (NRF) and the Department of Chemistry and Polymer Science at Stellenbosch University for funding.

REFERENCES

(1) Slager, J.; Domb, A. J. *Adv. Drug Delivery Rev.* **2003**, *55* (4), 549–583.

(2) Schroeder, J. A.; Karasz, F. E.; MacKnight, W. J. *Polymer* **1985**, *26*, 1795–1800.

(3) Schomaker, E.; Challa, G. *Macromolecules* **1989**, *22*, 3337–3341.

(4) Serizawa, T.; Hamada, K.; Kitayama, T.; Fujimoto, N.; Hatada, K.; Akashi, M. *J. Am. Chem. Soc.* **2000**, *122*, 1891–1899.

(5) Kumaki, J.; Kawauchi, T.; Okoshi, K.; Kusanagi, H.; Yashima, E. *Angew. Chem., Int. Ed.* **2007**, *46*, 5348–5351.

(6) Christofferson, A. J.; Yiapanis, G.; Ren, J. M.; Qiao, G. G.; Satoh, K.; Kamigaito, M.; Yarovsky, I. *Chem. Sci.* **2015**, *6*, 1370–1378.

(7) Spěváček, J.; Schneider, B. *Colloid Polym. Sci.* **1980**, *258* (5), 621–625.

(8) Gu, Q.; Song, R.; Shen, D. *Polym. Bull.* **2000**, *44*, 533–538.

(9) Fox, T. G.; Garrett, B. S.; Goode, W. E.; Gratch, S.; Kincaid, J. F.; Spell, A.; Stroupe, J. D. *J. Am. Chem. Soc.* **1958**, *80* (1), 1768–1769.

(10) Kawauchi, T.; Kumaki, J.; Yashima, E. *J. Am. Chem. Soc.* **2006**, *128* (32), 10560–10567.

(11) Yashima, E.; Ousaka, N.; Taura, D.; Shimomura, K.; Ikai, T.; Maeda, K. *Chem. Rev.* **2016**, *116*, 13752–13990.

(12) Karasz, F. E.; MacKnight, W. J. *Macromolecules* **1968**, *1* (6), 537–540.

(13) Chang, L.; Woo, E. M. *Polym. Chem.* **2010**, *1*, 198–202.

(14) Krause, S.; Roman, N. J. *J. Polym. Sci., Part A: Gen. Pap.* **1965**, *3* (4), 1631–1640.

(15) Bauer, R. G.; Bletso, N. C. *Polym. Prepr.* **1969**, *10*, 632.

(16) Schomaker, E.; Challa, G. *Macromolecules* **1988**, *21*, 2195–2203.

(17) Deuring, H.; Alberda van Ekenstein, G.; Challa, G. *Macromolecules* **1995**, *28*, 1952–1958.

(18) Mizumoto, T.; Sugimura, N.; Moritani, M. *Macromolecules* **2000**, *33*, 6757–6763.

(19) Ebrahim Attia, A. B.; Ong, Z. Y.; Hedrick, J. L.; Lee, P. P.; Ee, P. L. R.; Hammond, P. T.; Yang, Y. Y. *Curr. Opin. Colloid Interface Sci.* **2011**, *16* (3), 182–194.

(20) Vriezema, D. M.; Comellas Aragones, M.; Elemans, J. A. A. W.; Cornelissen, J. J. L. M.; Rowan, A. E.; Nolte, R. J. M. *Chem. Rev.* **2005**, *105* (4), 1445–1490.

(21) Khullar, P.; Singh, V.; Mahal, A.; Kumar, H.; Kaur, G.; Bakshi, M. S. *J. Phys. Chem. B* **2013**, *117*, 3028–3039.

(22) Bakshi, M. S. *Adv. Colloid Interface Sci.* **2014**, *213*, 1–20.

(23) Schimpf, M. E.; Caldwell, K.; Giddings, J. C. *Field-Flow Fractionation Handbook*; Schimpf, M. E., Caldwell, K., Giddings, J. C., Eds.; Wiley-Interscience: New York, 2000; Vol. 4.

(24) Shiundu, P. M.; Munguti, S. M.; Ratanathanawongs Williams, S. K. *J. Chromatogr. A* **2003**, *984*, 67–79.

(25) Greyling, G.; Pasch, H. *Macromolecules* **2016**, *49*, 1882–1889.

(26) Glantz, M.; Hakansson, A.; Lindmark Mansson, H.; Paulsson, M.; Nilsson, L. *Langmuir* **2010**, *26* (15), 12585–12591.

(27) Hupfeld, S. *Size Characterisation of Liposomes Using Asymmetrical Flow Field-Flow Fractionation Factors Influencing Fractionation and Size Determination*; University of Tromsø, 2009.

(28) Leeman, M.; Storm, M. U.; Nilsson, L. *LCGC Eur.* **2015**, *28*, 642–651.

(29) Meisterjahn, B.; Wagner, S.; von der Kammer, F.; Hennecke, D.; Hofmann, T. *J. Chromatogr. A* **2016**, *1440*, 150–159.

(30) Kassalainen, G. E.; Ratanathanawongs Williams, S. K. *Anal. Chem.* **2003**, *75* (8), 1887–1894.

(31) Nguyen, M.; Beckett, R. *Anal. Chem.* **2004**, *76* (8), 2382–2386.

(32) Hiller, W.; Van Asweegen, W.; Hehn, M.; Pasch, H. *Macromolecules* **2013**, *46* (7), 2544–2552.

(33) Styring, M. G.; Teo, H. H.; Price, C.; Booth, C. *J. Chromatogr.* **1987**, *388*, 421–427.

(34) Greyling, G.; Pasch, H. *Polym. Int.* **2017**, *66*, 745–751.

(35) Muza, U. L.; Greyling, G.; Pasch, H. *Anal. Chem.* **2017**, *89*, 7216–7224.

(36) Raak, N.; Abbate, R.; Lederer, A.; Rohm, H.; Jaros, D. *Separations* **2018**, *5*, 14.

(37) Alexandridis, P.; Lindman, B. In *Amphiphilic Block Copolymers: Self-Assembly and Applications*, 1st ed.; Alexandridis, P., Lindman, B., Eds.; Elsevier: Amsterdam, 2000.

(38) Schimpf, M. E.; Giddings, J. C. *Macromolecules* **1987**, *20* (7), 1561–1563.

(39) Schimpf, M. E.; Giddings, J. C. *J. Polym. Sci., Part B: Polym. Phys.* **1989**, *27* (6), 1317–1332.

(40) Schimpf, M. E.; Giddings, J. C. *J. Polym. Sci., Part B: Polym. Phys.* **1990**, *28* (13), 2673–2680.

DOI: 10.1021/acs.analchem.8b03590
Anal. Chem. 2018, 90, 13987–13995

(41) Muza, U. L.; Greyling, G.; Pasch, H. *J. Chromatogr. A* **2018**, *1562*, 87–95.
(42) Liu, T.; Liu, L.-Z.; Chu, B. *Formation of Amphiphilic Block Copolymer Micelles in Nonaqueous Solution*; Woodhead Publishing Limited: Cambridge, UK, 2000.
(43) Ford, N.; Havard, T.; Wallace, P. *Int. GPC Symp.* **1996**, 460–483.
(44) Mansfield, M. L.; Douglas, J. F.; Irfan, S.; Kang, E. *Macromolecules* **2007**, *40*, 2575–2589.
(45) Wen, Y. H.; Lin, P. C.; Hua, C. C.; Chen, S. A. *J. Phys. Chem. B* **2011**, *115*, 14369–14380.
(46) Morozov, K. I.; Köhler, W. *Langmuir* **2014**, *30*, 6571–6576.
(47) Tretinnikov, O. N.; Ohta, K. *Macromolecules* **2002**, *35*, 7343–7353.
(48) O'Reilly, J. M.; Mosher, R. A. *Macromolecules* **1981**, *14*, 602–608.
(49) Dybal, J.; Štokr, J.; Schneider, B. *Polymer* **1983**, *24*, 971–980.
(50) Wunderlich, B. *Thermal Analysis of Polymeric Materials*; Springer: Berlin, 2005.
(51) Owen, S. C.; Chan, D. P. Y.; Shoichet, M. S. *Nano Today* **2012**, *7* (1), 53–65.

DOI: 10.1021/acs.analchem.8b05500
Anal. Chem. 2018, 90, 13987−13995

Stereocomplexation of Polymers in Micelle Nanoreactors as Studied by Multiple Detection Thermal Field - Flow Fractionation.

Upenyu L. Muza, Guilaume Greyling, Harald Pasch

Supplementary Information:

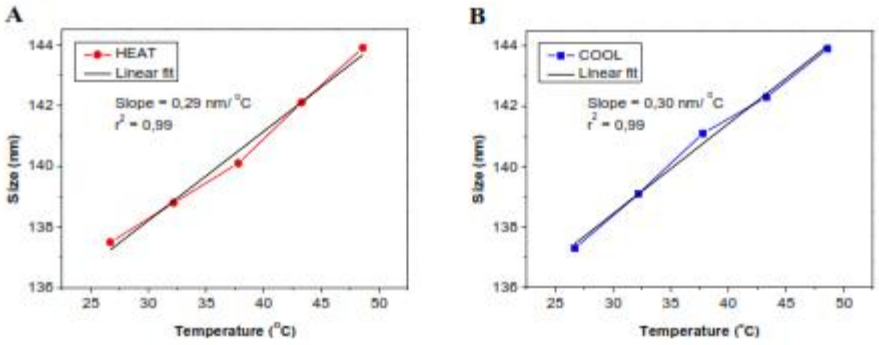

Figure S1. Z-average D_h as a function of temperature for i-PMMA-PS where red and blue curves represent the respective heating and cooling trajectories. Linear fit for (A) heating curve and (B) cooling curve.

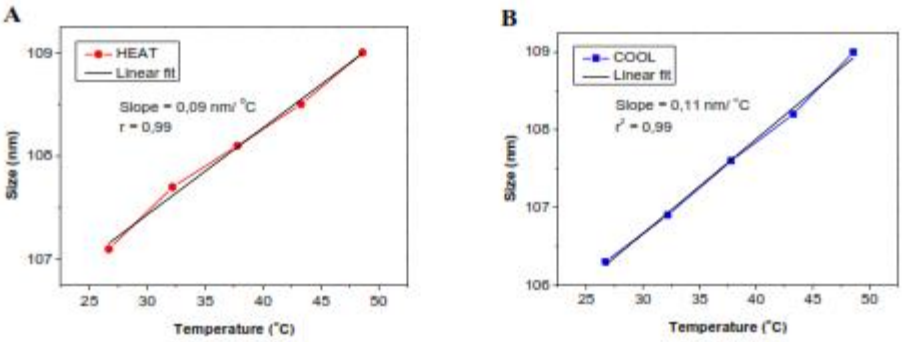

Figure S2. Z-average D_h distribution as a function of temperature for s-PMMA-PS where red and blue curves represent the respective heating and cooling trajectories. Linear fit for (A) heating curve and (B) cooling curve.

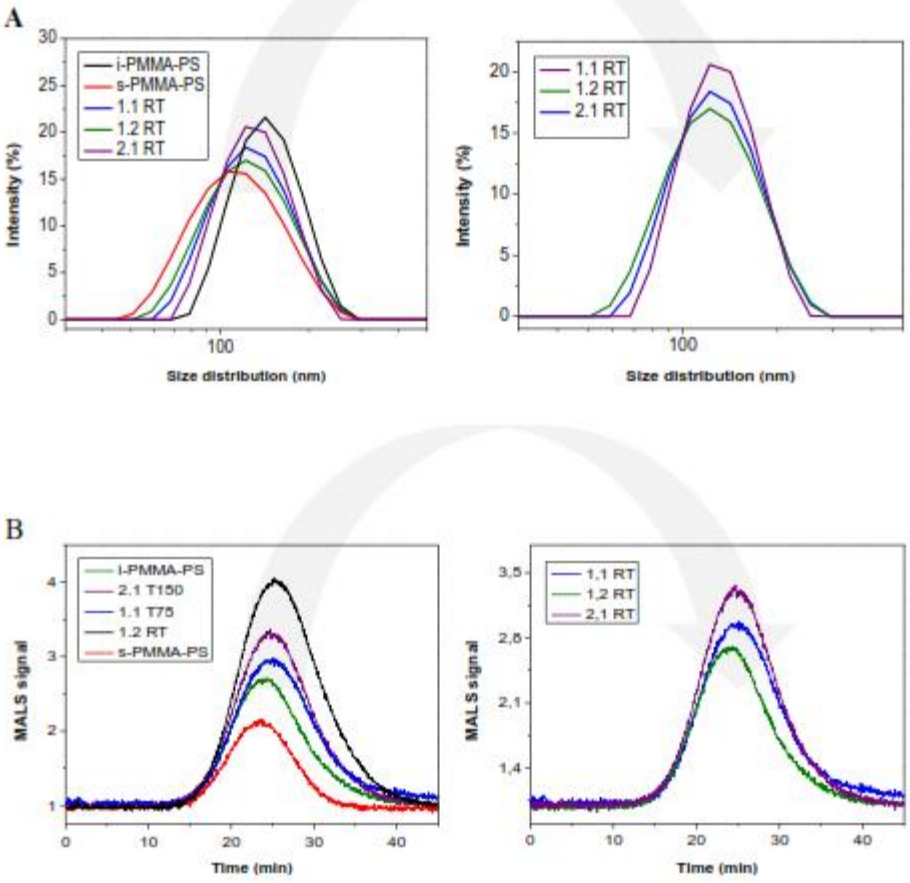

Figure S3. (A) Superimposed Z-average D_h distribution graphs and (B) ThFFF fractograms for the pure micelles and MNRs at room temperature. Detector: MALS. Void time: 7.6 min

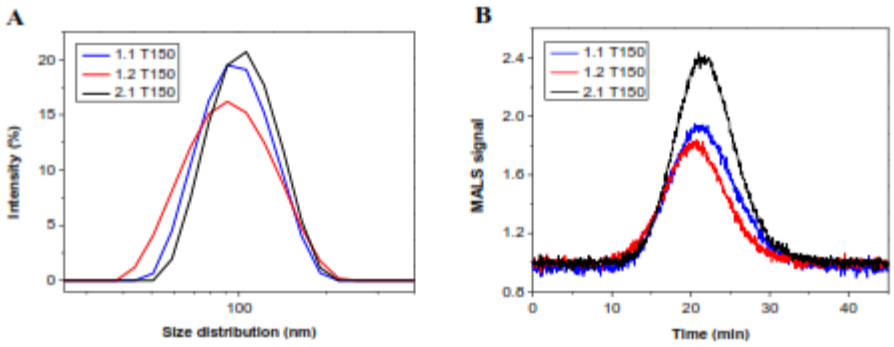

Figure S4. Superimposed (A) size distribution graphs and (B) ThFFF-MALS graphs for (A) 1:1, (B) 1:2 mixing ratios. Detector: MALS. Void time: 7.6 min

4.3 Thermal field-flow fractionation with quintuple detection for the comprehensive analysis of complex polymers (Part 3).

The so called tripled detection (TD) approach is presented for the first time for ThFFF, with the additional and complimentary support from two other detectors in the form of ultraviolet (UV) and dynamic light scattering (DLS), to formulate a unique quintuple detection (QD) system for the characterization of complex polymers. This ThFFF-QD system has the following coupling of detectors in series, UV, multiangle light scattering (MALS), differential refractive index (dRI) and DLS, with the differential viscometer (dVis) connected parallel to the dRI. The method development of ThFFF-QD is achieved using star, linear, protonated (PSH) and deuterated (PSD) polystyrenes (PS) as model compounds. Figure 4.5 illustrates a graphical presentation of the analytical method thereof.

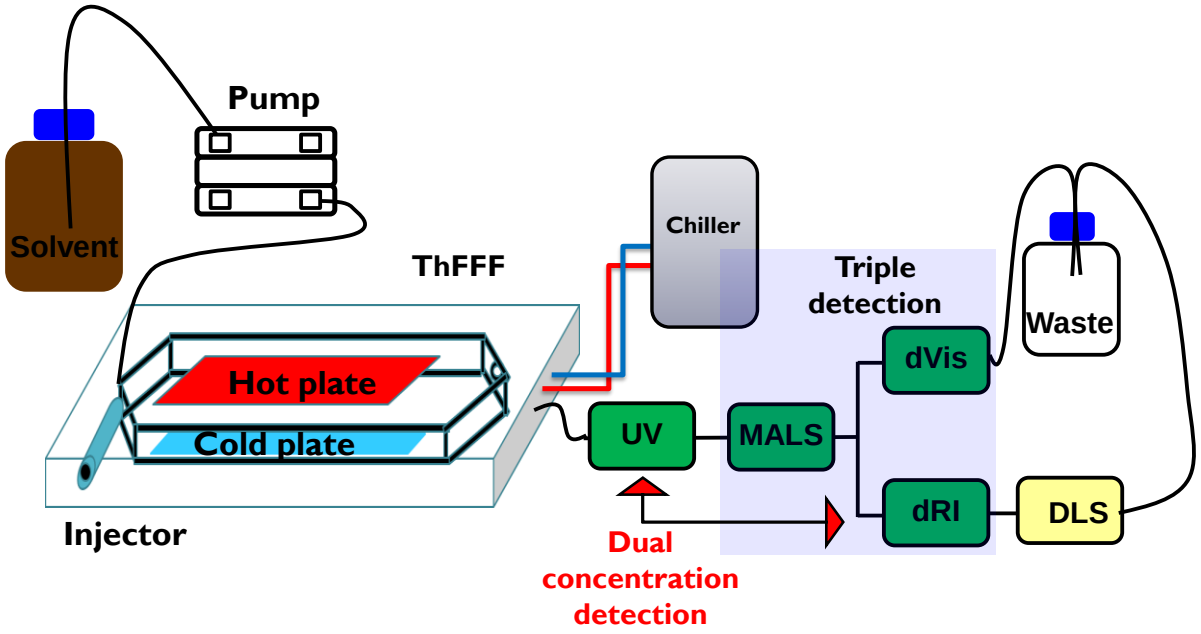

Figure 4.5. Graphical presentation for the study: Thermal field-flow fractionation with quintuple detection for the comprehensive analysis of complex polymers.

Comparable and complimentary information regarding size, structure and molar mass (M_w) is concurrently obtained, thereby enabling a comprehensive analysis plus a self-validation protocol. Comparable values of coefficients of diffusion (D) and thermal diffusion (D_T) are obtained from the respective size values measured from dVis and DLS, respectively. As expected, size exclusion chromatography (SEC) of the isotopic PSs having similar molar masses produces co-elution, however, the alternative ThFFF separations provide higher resolution. As expected, all the calculated D_Ts are comparable. However, significant resolution is observed for the separation of isotopic PSs, and such resolution cannot be explained by the inherent minor size differences.

On the other hand, significant differences in intrinsic viscosities (IVs) exist between the isotopic PS analogues, and notably the IVs share similar trends as a function of elution. To explain the elution trends, ThFFF can be hypothesized to exhibit sensitivity to gravimetric/density differences of the isotopic PS analogues. In the extended application of ThFFF-QD for the characterization of block copolymer (BCP) self-assemblies (SAs), the IVs and their respective distributions are shown to be measurable. In a novel approach, complimentary structural information from the online analysis of SAs is elucidated from the Mark-Houwink (MH) and conformation plots, respectively. The prowess of the strategic five detector combinations is illustrated in Figure 4.6.

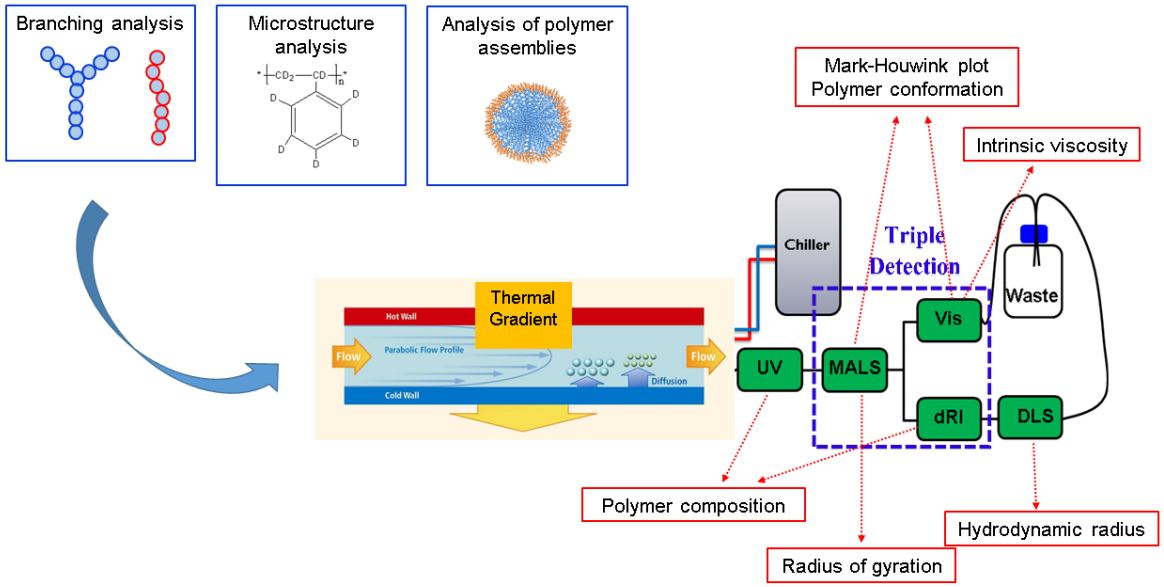

Figure 4.6. Schematic presentation of a ThFFF system equipped with five information-rich detectors for the fractionation and analysis of complex polymers.

The utility of MH and conformation plots allows for the reliable derivation of polymer structure in solution as a function of M_w. The respective slopes of these plots yield valuable structural information. In a good solvent, random linear coils, hyperbranched and hard spheres are known to have slope values of 0.55, 0.3-0.5 and 0.33 for the conformation plot, and 0.7, 0.3-0.5 and 0 for the MH plot, respectively. Moreover, for 1.4-PBd-PS in heptane, the SA of the solvophobic PS to form core microphases within the solvophilic 1.4-PBd nanoshells is applied in order to derive UV detection calibrations of the inherently insoluble PS. This enables compositional analysis of such nanocarrier systems by applying the principles of dual concentration detection, where dRI permits total concentration detection of the entire 1.4-PBd-PS entity, whilst UV detection at a wavelength of 254 nm is only sensitive to PS.

analytical chemistry

Article

Cite This: Anal. Chem. XXXX, XXX, XXX−XXX

pubs.acs.org/ac

Thermal Field-Flow Fractionation with Quintuple Detection for the Comprehensive Analysis of Complex Polymers

Upenyu L. Muza and Harald Pasch*

Department of Chemistry and Polymer Science, University of Stellenbosch, 7602 Stellenbosch, South Africa

ABSTRACT: With a constantly increasing complexity of macromolecular structures, advanced polymer analysis faces new challenges with regard to the comprehensive analysis of these structures. Today it goes without saying that comprehensive polymer analysis requires selective and robust fractionation methods in combination with a set of information-rich detectors. Thermal field-flow fractionation (ThFFF) has proven to be a powerful technique for the fractionation of complex polymers as well as polymer assemblies. In the present study, ThFFF is coupled to a set of five detectors to simultaneously provide quantitative information on a number of important molecular parameters, including molar mass, molecular size, chemical composition, molecular topology, intrinsic viscosity, and normal and thermal diffusion coefficients. The five-detector setup includes a triple detector device (multiangle light scattering (MALS), differential refractive index (dRI), and differential viscometer (dVis)) that is coupled to an ultraviolet (UV) detector for dual concentration detection and an online dynamic light scattering (DLS) detector. Triple detection consisting of MALS, dRI, and dVis provides information on molar mass, molecular size, and molecular topology. Dual concentration detection offers compositional analysis from a combination of UV and dRI detectors, whereas DLS provides information on diffusion coefficients and hydrodynamic radii. The power of this novel quintuple detector ThFFF (ThFFF-QD) is documented for three important fields of application, namely, the comprehensive analysis of (1) linear and star-shaped polymers, (2) hydrogenated and deuterated polymers, and (3) block copolymer self-assemblies. These applications highlight the novel approach of determining the most relevant molecular parameters, including Mark−Houwink and conformation plots, simultaneously in a single experiment.

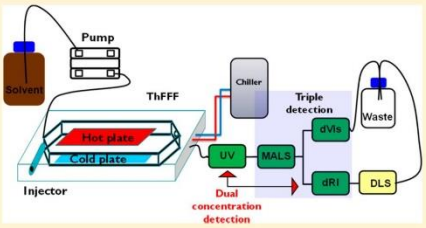

The physical properties of complex polymeric materials are primarily a function of the integral molecular properties, including molar mass, chemical composition, microstructure, and molecular topology.[1] These molecular properties typically exhibit distributions, and therefore, the application of batch-mode analytical techniques to comprehensively characterize such complexity is rather limited. Batch-mode techniques only yield average values regarding specific molecular parameters.[2] Selective fractionation methods that are sequentially coupled to multiple detection devices enable a more accurate acquisition of crucial information regarding multiple molecular parameters and their distributions.[1−3]

Column-based methods such as size-exclusion chromatography (SEC) have classically been applied to conduct fractionations of polymers with molar masses (M_w) < 10^4 kg/mol. Difficulties arise when it comes to higher M_w (>10^4 kg/mol) and delicate structures such as self-assemblies (SAs), gels, and large aggregates, where interactions with the column may result in the shear degradation.[4] The advent of field-flow fractionation (FFF) as a complementary technique has provided a less-harsh channel-based platform to circumvent such drawbacks. The channel is void of any packing material and is thus essential for the separation of larger and more delicate materials.[5−8] To date, FFF has successfully been applied for the separation and characterization of gels, SAs, and large aggregates.[9,10]

FFF separations are analogous to chromatography in that the fundamental working principles are flow-based. In contrast to column-based fractionations, an empty channel (with no stationary phase) is used.[10] The flow drives the injected sample through the channel where fractionations are achieved by applying an external field perpendicular to the flow profile.[11] The external field fundamentally causes a differential displacement of the sample across the channel based on (but not limited to) hydrodynamic size (D_h), density, charge, or chemical composition.[11] The characteristic laminar flow inside the channel allows for faster elution of sample components at the center of the flow profile. Sample components distributed closer to the channel walls elute last in what is referred to as the normal mode of elution.[12,13] After the fractionation in the FFF channel, an array of detectors can be implemented for a successive detection of relevant molecular parameters and their distributions. For this present study, separations shall be performed using thermal field-flow fractionation (ThFFF), a subtechnique

Received: March 18, 2019
Accepted: April 30, 2019
Published: April 30, 2019

DOI: 10.1021/acs.analchem.9b01384
Anal. Chem. XXXX, XXX, XXX−XXX

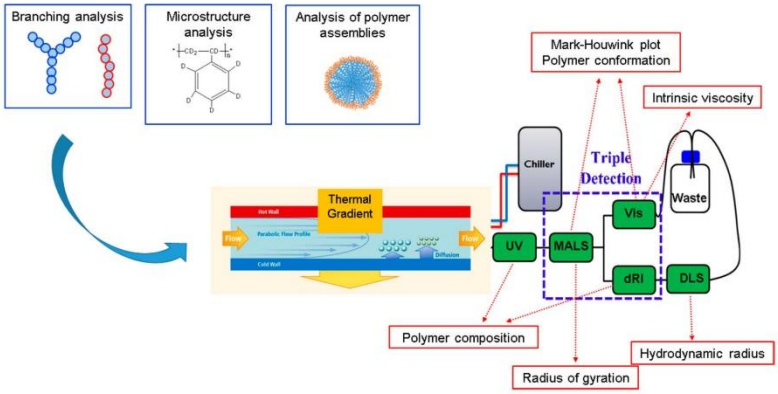

Figure 1. Schematic presentation of a ThFFF system equipped with five information-rich detectors for the fractionation and analysis of complex polymers.

of FFF that employs a thermal gradient across the channel as the external force.[11,14]

The thermal gradient instigates a thermal-induced mass transfer of molecules from the hot wall to the cold/accumulation wall. The accumulation of molecules at the cold wall creates a concentration gradient, which results in the countercurrent diffusion of molecules. Naturally smaller molecules diffuse faster than larger ones and thus attain equilibrium at relatively higher elevations from the cold wall. The mobile phase in the channel has a parabolic flow profile, and as such, smaller molecules are generally swept away by faster moving streamlines and, hence, elute faster in the normal mode of elution. Notably, in ThFFF, sample recoveries closely approach 100%, making it a better alternative in instances where maximum sample recoveries are imperative.

This study presents (for the first time) a ThFFF system with a unique combination of detectors that is capable of obtaining a wide range of molecular information on complex polymers. The proposed ThFFF quintuple detection system (ThFFF-QD) is composed of a triple detector system (light scattering, viscosimetry, and refractive index) combined with a UV detector and dynamic light scattering (DLS). This novel multidetector setup shall be presented, and its merits for the analysis of complex samples shall be showcased.

The centerpiece of this modular system is a triple detector device that encompasses multiangle light scattering (MALS), differential refractive index (dRI), and differential viscometer (dVis) detectors. A combination of MALS and dRI enables the determination of absolute M_w and molecular size in the form of the radius of gyration (R_g). Additionally, information on topology can be derived from the relationship between R_g and M_w (eq 1), where K and ν are empirical constants for a specified polymer−solvent system.

$$R_g = KM_W^{\nu} \tag{1}$$

At lower M_w (<50 kg/mol), R_g as measured by MALS becomes increasingly unreliable due to the isotropic scattering effect by smaller molecules.[15] Alternatively, dVis can be used to measure complementary sizes such as the viscosity-based radius of gyration and radius, $R_{g\eta}$ and R_{η}, respectively. $R_{g\eta}$ and R_{η} are defined by eqs 2 and 3, where the terms $[\eta]$, N_A, and Φ represent intrinsic viscosity, Avogadro number, and Flory constant, respectively.[16]

$$R_{\eta} = \left(\frac{3[\eta]M_w}{10\prod N_A}\right)^{1/3} \tag{2}$$

$$[\eta] = \Phi\left(\frac{R_{g\eta}^{\ 3}}{M_w}\right) \tag{3}$$

A combination of dVis and dRI allows for the measurement of the specific viscosity and ultimately $[\eta]$. $[\eta]$ can be related to M_w for a given solvent and temperature using the Mark−Houwink (MH) expression (eq 4), where K and α are empirical constants.[17]

$$[\eta] = KM_w^{\ \alpha} \tag{4}$$

The conformation and MH plots can be applied to derive complementary information on topology as a function of M_w.

The dual concentration detection of the multidetector system is based on UV and dRI. UV is not universally applicable as a concentration detector and is only suitable for the analysis of materials with photoactive chromophores. Even more, UV detection is not suitable in cases where the solvent and analyte have the same cutoff wavelengths and thus absorb in the same regions of the UV spectrum. On the other hand, dRI is a universal concentration detector. Therefore, when some species of interest in a complex sample are UV-active, UV-dRI detection can be applied for the compositional analysis of the eluting species.[1]

Finally, online DLS detection has been added to the system to enable the analysis of diffusion coefficients (D) and hydrodynamic sizes R_h.[18,19] Furthermore, the thermal diffusion coefficient (D_T) and the shape factor (ρ) can be calculated using eqs 5 and 6, respectively. In eq 5, t_R and t_0 are retention and void times, respectively, and ΔT is the temperature difference between the hot and cold walls of the ThFFF channel.[11] Notably, $D_{T\eta}$, the viscosity-based analogue for thermal diffusion coefficient, can be calculated from eq 5 using D_{η}, the diffusion coefficient associated with R_{η}. D_T is one essential parameter in ThFFF as it relates to the chemical composition (CC) of the

DOI: 10.1021/acs.analchem.9b01384
Anal. Chem. XXXX, XXX, XXX−XXX

analyte.[14,20−22] This gives ThFFF an advantage over other FFF techniques in that the separations are a function of both D_h and CC.

$$D_T = \frac{6Dt_R}{\Delta T t_0} \quad (5)$$

$$\rho = \frac{R_g}{R_h} \quad (6)$$

It is the idea of the present work to create a modular instrument system that is capable of addressing different tasks in the fractionation and analysis of complex polymers. Using ThFFF as the fundamental fractionation device, multiple information-rich online detectors shall provide specific and selective structural information. The principal idea of this system together with a number of proposed applications is presented in Figure 1.

The addition of an online viscometer (dVis) to other information-rich detectors enables the online measurement of absolute M_w, CCs, R_h, viscosity-based sizes ($R_{g\eta}$ and R_η), and $[\eta]$ for complex polymers and ultimately for SAs. $[\eta]$ and the respective sizes can subsequently be used to derive information on molecular density, shape, and structure of SAs as well as their respective distributions.[23−25] In general, online viscometry is applied in polymer analysis when investigating branching and branching distributions.[26−29] By conceptualizing the aggregation number (Z) as a form of branching, SAs can in principle be regarded as pseudobranched materials. To some point their solution properties can be expected to exhibit parallel trends with branched materials. The characterization of branching allows for the study and understanding of the correlation between molecular parameters and the associated mechanical, rheological, and viscoelastic properties.[30,31]

In this study, the proposed novel ThFFF-UV-dRI-MALS-dVis-DLS multiple detection represents an unprecedented advanced system for highly detailed and comprehensive analysis of (but not limited to) block copolymer SAs in a single measurement. To illustrate the versatility of such a system, multitopological and isotopic polystyrenes (PSs), respectively, are fractionated and analyzed. SAs prepared from 1.4-polybutadiene-*block*-polystyrene (1.4-PBd-PS) shall be used as the model to demonstrate the wealth of molecular information that can be obtained by ThFFF-QD.

■ EXPERIMENTAL SECTION

Materials. The polymers described in Table 1 were used in this study.

The subscripts represent the M_w of the polymers in kg/mol as provided by the suppliers. PS250 kDa and PS102 kDa were supplied by Postnova, Germany, and TSK Toyo Soda MFG, Japan, respectively. All deuterated homopolymers were obtained from PSS, Germany, and the block copolymers (BCPs) were purchased from Polymer Source, Canada. All materials were used as received.

Table 1. Description of Polymer Samples Used

sample	description	code name	dispersity (M_w/M_n)
PS_{250}	linear	PS250 kDa	2.50
$PS_{97.6}$	3-arm star	PS98 kDa	1.07
PSH_{102}	100% protonated	PSH102 kDa	1.02
PSD_{111}	100% deuterated	PSD111 kDa	1.02
PSH_{200}	100% protonated	PSH200 kDa	1.01
PSD_{211}	100% deuterated	PSD211 kDa	1.06
$1.4\text{-}PBd_{25}\text{−}PS_{34}$	BCP	1.4-PBd-PS	1.20

Preparation of SAs. The 1.4-PBd-PS BCPs were directly dissolved at 80 °C in heptane, a selective solvent for the 1.4-PBd block. Consequently, the resultant SAs were assigned to have PS cores and 1.4-PBd shells.

ThFFF Conditions. All measurements were carried out using the TF2000 instrument (Postnova Analytics, Landsberg, Germany) coupled to the following detectors: UV (PN 3212 at 254 nm), MALLS (PN3070), dVis (PN3310), and dRI (PN 3140), all from Postnova Analytics, Landsberg, Germany. A Zetasizer Nano series (Malvern Instruments, Worcestershire, U.K.) with built-in data-processing software was used for DLS detection at a back-scattering detection angle of 175°. Sample volume in excess of 100 μL was manually injected into a 100 μL capillary sample loop to ensure complete capillary flooding. For statistical purposes, each analysis was performed in triplicate. Respective temperature gradients (ΔT) of 80 and 30 °C per channel thickness of 127 μm were applied for the fractionation of homopolymers and SAs, respectively. An externally controlled chiller (Uber Unichiller, Monitoring and Control Laboratories, South Africa) was used to maintain an isothermal and stable cold wall temperature at ~22 and 26 °C, for an applied ΔT of 30 and 80 °C, respectively. For specific experiments outlined in text, the following carrier solvents were pumped by an isocratic pump (PN 1130, Landsberg, Postnova Analytics) at a flow rate of 0.5 mL/min: tetrahydrofuran (THF), cyclohexane (CH), and heptane (all from Sigma-Aldrich, South Africa).

SEC Analysis. Comparative SEC studies were carried out using a Waters GPC comprising the following components: Waters 2487 Dual λ UV detector, Waters 1515 Isocratic HPLC pump, Waters 410 Differential refractometer (at a temperature of 30 °C), Waters 717 plus autosampler, Waters In-Line degasser. The column setup was as follows: two PLgel 5 μm Mixed-C columns and a PLgel 5 μm guard column; column temperature 30 °C; and eluent system, THF (HPLC-grade, BHT-stabilized) at a flow rate of 1 mL/min at pressure of 941 psi. The concentration of samples is 2 mg/mL. Calibration was done with narrow polystyrene standards with a molar mass range of 580−3 187 000 g/mol.

■ RESULTS AND DISCUSSION

This section is categorized into four chronological subsections, so as to systematically highlight the proficiency of ThFFF-QD in complex polymer analysis. The first subsection describes the inaugural method development process for ThFFF-QD, and the merits of triple detection and DLS are explained using PS samples of different M_w and topologies.

ThFFF-QD Method Development. ThFFF is applied as the separation technique for linear and star PS, and the results are summarized in Table 2 and Figure 2. The samples are chemically homogeneous; therefore, t_R is purely size-based, although linear analogues have been shown to undergo more size changes as a function of temperature.[32] From triple detection and DLS, absolute M_w, R_g, $R_{g\eta}$, R_η, and R_h are obtained. R_g and R_h measurements from light scattering, which are based on the hard sphere size model, are juxtaposed with the respective $R_{g\eta}$ and R_η analogues measured from dVis using the viscosity size model, and the results are found to be comparable.

The logic of combining two intrinsically different size-measuring models allows for (1) a self-compensating analytical

DOI: 10.1021/acs.analchem.9b01384
Anal. Chem. XXXX, XXX, XXX−XXX

Table 2. Triple Detector ThFFF Results for Linear PS250 kDa and 3-Arm Star PS98 kDa

sample	$[\eta]$ (dL/g)	M_w (kg/mol)	t_R (min)	R_g (nm)	R_{gn} (nm)	R_h (nm)	R_η (nm)	$D \times 10^{-7}$ (cm^2/s)	$D_\eta \times 10^{-7}$ (cm^2/s)
PS250 kDa	0.817 ± 0.06	235 ± 4	16.6 ± 0.1	24.6 ± 0.1	19.8 ± 0.2	15.2 ± 0.3	15.1 ± 0.3	0.299 ± 0.003	0.301 ± 0.002
PS98 kDa	0.426 ± 0.02	102 ± 1	10.1 ± 0.1	8.9 ± 0.1	11.5 ± 0.1	8.9 ± 0.2	8.8 ± 0.1	0.511 ± 0.002	0.517 ± 0.001

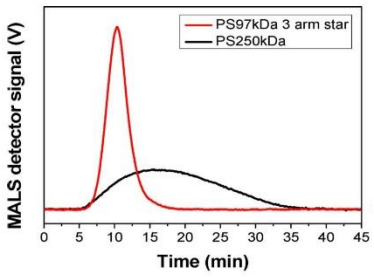

Figure 2. Superimposed MALS fractograms for linear PS250 kDa and 3-arm star PS98 kDa polymers.

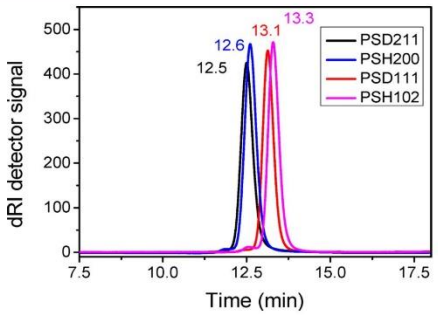

Figure 4. Superimposed SEC-dRI fractograms for isotopic PS analogues in THF.

system that is ideal when one of the two size models becomes unreliable and (2) a self-validating protocol where duplicate results from different techniques are a reflection of precision and reliability.

Fundamentally, $[\eta]$ measurements are shown to be reproducible using ThFFF. Therefore, MH plots can be generated to describe the topology of species separated by ThFFF. The MH plots for branched and linear PS show α values comparable to literature for similar materials (Figure 3).[16,33,34] PS250 kDa has a higher α value of 0.71 as expected for linear chains, compared to 0.41 for the star PS98 kDa. This indicates (as expected) that linear polymeric entities exhibit stronger changes in $[\eta]$ with molar mass when compared to their branched alternatives and, therefore, result in less-dense and less-compact polymer coils in solution.[24,26] The additional significance of coupling dVis to ThFFF shall be explained in the next subsection on the separation of isotopic forms of PS.

Separation of Isotopic PS. Protonated and deuterated polystyrenes (PSH and PSD, respectively) have similar chemical compositions but definite differences in gravimetric properties. PSD is the "heavier" alternative due to the presence of deuterium instead of hydrogen.[35] Insignificant size differences are known to exist between PSD and PSH, and as such, routine size-based separations are not feasible for these isotopes. To highlight this assertion, a comparative study for the separation of isotopic PS analogues was performed using SEC as a size-based separation

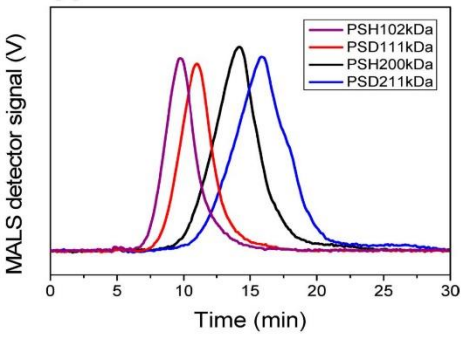

Figure 5. Superimposed ThFFF-MALS fractograms for isotopic PS analogues in THF (thermodynamic good solvent), t_0 = 5.10 min.

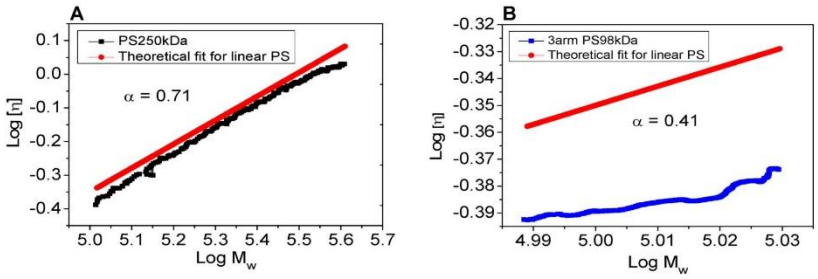

Figure 3. Mark–Houwink plots for (A) linear PS250 kDa and (B) 3-arm star PS98 kDa polymers.

DOI: 10.1021/acs.analchem.9b01384
Anal. Chem. XXXX, XXX, XXX−XXX

Table 3. ThFFF Results for Isotopic PS Analogues (PSD and PSH) Using THF (Thermodynamically Good Solvent)

sample	M_w (kg/mol)	t_R (min)	$[\eta]$ (dL/g)	R_g (nm)	R_{gn} (nm)	R_h (nm)	R_n (nm)	$D \times 10^{-7}$ (cm^2/s)	$D_\eta \times 10^{-7}$ (cm^2/s)	$D_T \times 10^{-7}$ (cm^2/s·K)	$D_{T\eta} \times 10^{-7}$ (cm^2/s·K)
PSH102 kDa	101 ± 1	9.81 ± 0.0	0.440 ± 0.01	13.7 ± 0.2	11.4 ± 0.1	9.2 ± 0.2	8.8 ± 0.2	0.50 ± 0.01	0.52 ± 0.01	0.016 ± 0.02	0.017 ± 0.01
PSD111 kDa	116 ± 1	11.1 ± 0.1	0.502 ± 0.01	15.9 ± 0.3	12.8 ± 0.1	10.3 ± 0.4	9.9 ± 0.1	0.44 ± 0.02	0.46 ± 0.02	0.016 ± 0.02	0.017 ± 0.01
PSH200 kDa	195 ± 4	14.3 ± 0.1	0.730 ± 0.02	20.9 ± 0.4	17.1 ± 0.2	13.5 ± 0.1	13.1 ± 0.1	0.35 ± 0.01	0.34 ± 0.01	0.017 ± 0.01	0.017 ± 0.01
PSD211 kDa	214 ± 2	16.0 ± 0.0	0.808 ± 0.00	21.5 ± 0.2	18.4 ± 0.1	14.9 ± 0.1	14.1 ± 0.1	0.32 ± 0.01	0.32 ± 0.01	0.017 ± 0.01	0.017 ± 0.01

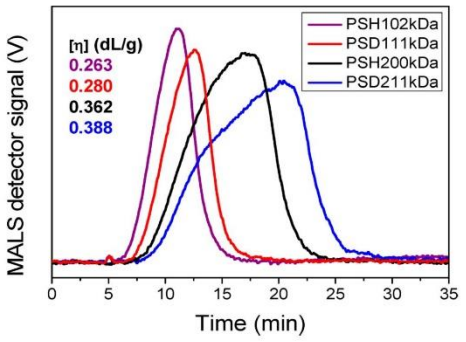

Figure 6. Superimposed ThFFF-MALS fractograms and the respective color coded $[\eta]$ for isotopic PS analogues in cyclohexane (theta solvent), t_0 = 5.12 min.

method.[36] As expected, comparable retention times for PSD and PSH were observed (Figure 4).

In contrast, the application of ThFFF yields unexpected improved resolution, as evident in the overlaid MALS fractograms in Figure 5. Such resolutions cannot emanate exclusively from the minute size differences between the isotopic PS analogues (Table 3), and as expected, the size results recorded from triple detection and DLS are comparable. Subsequently, the respective D and calculated D_T values are also similar for both isotopic analogues. Therefore, the generic reasoning for ThFFF separations solely based on D and D_T becomes limited in this regard. On the other hand, the triple detection aspect of the ThFFF system incorporates $[\eta]$ as fundamentally important extra information, which may help to explain the observed elution trends.

An inspection of the respective $[\eta]$ and t_R values acknowledges a similar trend. Therefore, from such primary evidence, a gravimetric/density sensitivity of ThFFF can be assumed. To further consolidate such an assumption, ThFFF was performed using a theta solvent for PSH, cyclohexane (CH). The utility of a theta solvent ensures the determination of molecular properties in unperturbed dimensions. Once again, the measured $[\eta]$ and t_R are shown to have similar trends as previously seen with the use of THF, a thermodynamic good solvent for PS (Figure 6).

The consolidated utility of the techniques presented herein is cumulatively shown to be critical in comprehensively defining the microstructure and associated ThFFF elution trends of a complex polymer system. In the following subsections, the application of ThFFF-QD for the analysis of SAs is highlighted. All three concepts of the analytical system ascribed to ThFFF-QD are systematically applied for the comprehensive analysis of SAs.

ThFFF-QD of Polymer Self-Assemblies. The ThFFF of 1.4-PBd-PS SAs in heptane is summarized in Table 4 and Figure 7. From triple detection, the normalized aggregation number (Z) can be derived from the quotient of M_w of the SA and the unimer thereof. From R_g and $[\eta]$ measurements, two fundamental M_w dependent probes into SA structure can be presented in the form of the conformation and MH plots. In a good solvent, random linear coils and hyperbranched and hard spheres are known to have ν values of 0.55, 0.3−0.5, and 0.33 for the conformation plot and α values of 0.7, 0.3−0., and 0 for the MH plot.[16,33,37]

DOI: 10.1021/acs.analchem.9b01384
Anal. Chem. XXXX, XXX, XXX−XXX

Table 4. Results for ThFFF-QD of 1.4-PBd-PS Self-Assemblies in Heptane

sample	ρ	$[\eta]$ (dL/g)	Z	t_R (min)	R_g (nm)	$R_{g/l}$ (nm)	R_h (nm)	R_η (nm)
1.4-PBd-PS	1.31 ± 0.08	0.191 ± 0.05	512 ± 10	18.9 ± 0.1	38.8 ± 0.8	44.1 ± 0.4	29.6 ± 1.1	33.8 ± 0.3

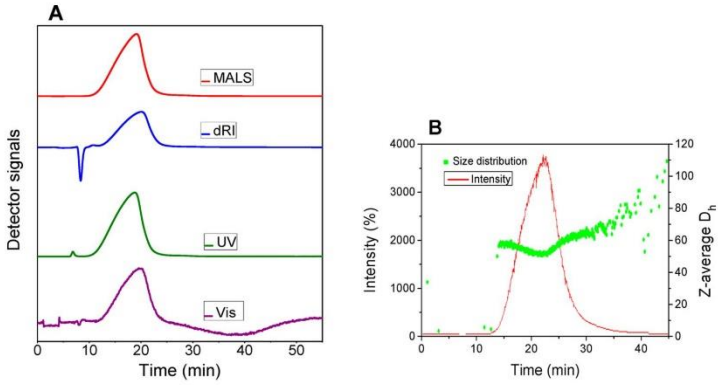

Figure 7. ThFFF-QD fractograms for 1.4-PBd-PS self-assemblies in heptane: (A) MALS (red), dRI (blue), UV (green), and dVis (violet) signals; (B) DLS fractogram, t_0 = 7.1 min.

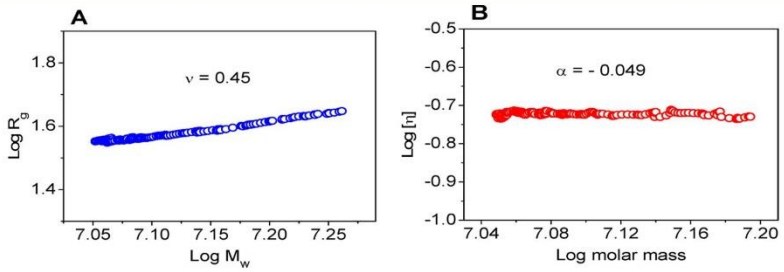

Figure 8. (A) Conformation and (B) Mark–Houwink plots for 1.4-PBd-PS self-assemblies in heptane.

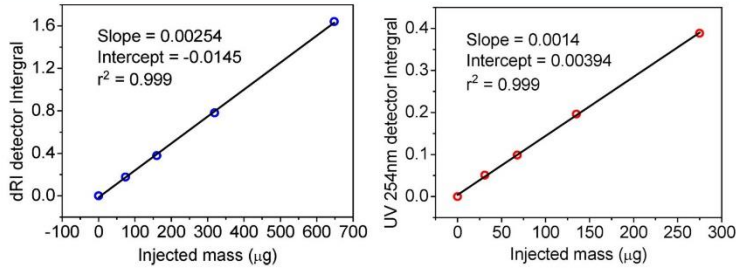

Figure 9. System calibrations using 1,4-PBd-PS SAs: dRI (A) and UV (B) detection.

Table 5. Compositional Analysis of 1.4-PBd-PS SAs Using ThFFF-UV-dRI

sample	dRI integral	SA mass (μg)	UV integral	PS mass (μg)	PS %
1	1.3261 ± 0.002	527.8 ± 2.1	0.3300 ± 0.002	232.9 ± 2.3	44.1 ± 1.4
2	0.459 ± 0.002	186.4 ± 2.9	0.1218 ± 0.003	84.2 ± 1.6	45.2 ± 1.7
3	1.0173 ± 0.003	406.2 ± 1.8	0.2674 ± 0.002	188.2 ± 1.6	46.3 ± 1.1

DOI: 10.1021/acs.analchem.9b01384
Anal. Chem. XXXX, XXX, XXX−XXX

Only with the present ThFFF method and the five-detector setup is it possible to obtain the MH and conformation plots (Figure 8) as well as all the parameters given in Table 4. From the conformation plot in Figure 8A, the ν value of 0.45 describes a species with properties that are the average of a sphere and a random coiled polymer.[38−41] This information alone is inconclusive. Supporting Information is obtained from the MH plot, where α has a value close to zero. This would normally infer the existence of a hard sphere.

However, aggregations and cross-linked polymeric nanoparticles have also been shown to exhibit the same trait, where the characteristic M_w independent behavior of $[\eta]$ is observed.[28,34] To get more explicit topological information, the ratio R_g/R_h (ρ) which is naturally independent of M_w is employed. A value of ~1.31 is obtained that infers the existence of hyperbranched polymers.[16,33] Moreso, similar values have been reported for vesicle-like structures.[42]

Compositional Analysis. In this subsection, an exceptional form of dual concentration detection is introduced for the compositional analysis of 1.4-PBd-PS SAs in heptane using ThFFF-UV-dRI. Unlike the 1.4-PBd shells, the PS cores have chromophores and are thus the only SA microphase potentially detectable by UV, while the entire 1.4-PBd-PS species is projected to be detectable by dRI.[1] Therefore, principles of compositional analysis by dual concentration detection using UV and dRI are applicable. An anomaly arises from PS being insoluble in heptane. However, from the previous subsection (Figure 7), the PS cores for 1.4-PBd-PS SAs were shown to be UV detectable. Therefore, the basic principles of self-assembling can be applied to effectively circumvent solubility challenges. In this respect, the insoluble PS cores are essentially "nanocarried" for analysis within the soluble 1.4-PBd shells. Therefore, the dual concentration detection of BCP SAs presents an unprecedented pathway for acquiring two distinct calibration curves from a single block copolymer SA sample matrix (Figure 9).

Accordingly, a concentration series of 1.4-PBd-PS SAs was prepared from simple dilutions of the bulk sample and then analyzed by ThFFF-UV-dRI, to first get a UV detector calibration curve for PS. The second calibration is from total concentration detection of 1.4-PBd-PS SAs by dRI, to permit compositional analysis as subsequently explained. Samples of 1.4-PBd-PS SAs of unknown concentrations were prepared for ThFFF-UV-dRI analysis, and the results are summarized in Table 5. From the integral of the dRI and UV detector signals, the respective total amounts of SAs and PS injected were determined from the associated linear calibration curves in Figure 9. However, due to systematic errors naturally associated with the technique, the amount of PS measured deviates moderately from the vendor stipulations.

■ CONCLUSIONS

Quintuple detector ThFFF has been presented as a new powerful method combination to obtain quantitative molecular information on complex polymers and polymer self-assemblies. In a single experiment, a multitude of molecular parameters can be analyzed from the simultaneously obtained signals of five information-rich detectors. These include information on molar mass, radius of gyration, intrinsic viscosity, and Mark−Houwink and conformation plots from the combination of dRI, MALS, and dVis. The chemical composition of eluting species can be analyzed by dual concentration detection using dRI and UV. Additional information on hydrodynamic radii and diffusion coefficients can be obtained from online DLS, and shape factors of polymer self-assemblies are accessible from MALS and DLS data.

The present approach is universal and can be applied to polymers with different chemical compositions, microstructures, and molecular architectures as well as to polymer assemblies including micelles, vesicles, and microgels. The analysis of polymer nanocomposites can be considered as one future application.

■ AUTHOR INFORMATION

Corresponding Author

*E-mail: hpasch@sun.ac.za.

ORCID

Upenyu L. Muza: 0000-0003-1397-8932

Harald Pasch: 0000-0003-1132-3393

Notes

The authors declare no competing financial interest.

■ ACKNOWLEDGMENTS

We thank the technical team of Postnova GmbH, Germany, and the National Research Foundation of South Africa (NRF) for supporting this study.

■ REFERENCES

(1) Pasch, H.; Trathnigg, B. *HPLC of Polymers*; Ingo, A., Pasch, H., Eds.; Springer: New York, 1998; DOI: 10.1007/978-3-642-36080-0.
(2) Hiller, W.; Hehn, M. *Anal. Chem.* **2014**, *86*, 10900−10908.
(3) Raust, J.-A.; Brüll, A.; Moire, C.; Farcet, C.; Pasch, H. *J. Chromatogr. A* **2008**, *1203* (2), 207−216.
(4) Grubišic-Gallot, Z.; Sedláček, J.; Gallot, Y. *J. Liq. Chromatogr. Relat. Technol.* **1998**, *21* (16), 2459−2472.
(5) Giddings, J. C. *Science* **1993**, *260* (5113), 1456−1465.
(6) Baalousha, M.; Stolpe, B.; Lead, J. R. *J. Chromatogr. A* **2011**, *1218* (27), 4078−4103.
(7) Zattoni, A.; Roda, B.; Borghi, F.; Marassi, V.; Reschiglian, P. *J. Pharm. Biomed. Anal.* **2014**, *87*, 53−61.
(8) Yohannes, G.; Jussila, M.; Hartonen, K.; Riekkola, M. L. *J. Chromatogr. A* **2011**, *1218* (27), 4104−4116.
(9) Ratanathanawongs Williams, S. K.; Lee, D. *J. Sep. Sci.* **2006**, *29* (12), 1720−1732.
(10) Messaud, F.; Sanderson, R. D.; Runyon, J. R.; Otte, T.; Pasch, H.; Williams, S. K. R. *Prog. Polym. Sci.* **2009**, *34* (4), 351−368.
(11) Schimpf, M. E.; Caldwell, K.; Giddings, J. C. *Field-Flow Fractionation Handbook*; Schimpf, M. E., Caldwell, K., Giddings, J. C., Eds.; Wiley-Interscience: New York, 2000; Vol. *4*.
(12) Kirkland, J. J.; Boone, L. S.; Yau, W. W. *J. Chromatogr.* **1990**, *517*, 377−393.
(13) Cho, K.-H.; Park, Y. H.; Jeon, S. J.; Kim, W.-S.; Lee, D. W. *J. Liq. Chromatogr. Relat. Technol.* **1997**, *20* (16−17), 2741−2756.
(14) Schimpf, M. E.; Giddings, J. C. *J. Polym. Sci., Part B: Polym. Phys.* **1989**, *27* (6), 1317−1332.
(15) Ogendal, L. *Light Scattering Demystified Theory and Practice*; University of Copenhagen: 2013.
(16) Burchard, W. Solution Properties of Branched Macromolecules. In *Advances in Polymer Science*; Springer: Berlin, 1999; Vol. *143*, pp 114−194.
(17) McCrackin, F. L. *Polymer* **1987**, *28* (11), 1847−1850.
(18) Muza, U. L.; Greyling, G.; Pasch, H. *Anal. Chem.* **2017**, *89*, 7216−7224.
(19) Greyling, G.; Pasch, H. *Polym. Int.* **2017**, *66*, 745−751.
(20) Schimpf, M. E.; Giddings, J. C. *Macromolecules* **1987**, *20* (7), 1561−1563.
(21) Rauch, J.; Köhler, W. *Macromolecules* **2005**, *38*, 3571−3573.
(22) Runyon, J. R.; Williams, S. K. R. *J. Chromatogr. A* **2011**, *1218* (38), 6774−6779.

DOI: 10.1021/acs.analchem.9b01384
Anal. Chem. XXXX, XXX, XXX−XXX

(23) Wang, W. J.; Kharchenko, S.; Migler, K.; Zhu, S. *Polymer* **2004**, *45* (19), 6495−6505.
(24) Saunders, G.; Cormack, P. A. G.; Graham, S.; Sherrington, D. C. *Macromolecules* **2005**, *38* (15), 6418−6422.
(25) Pathaweeisariyakul, T.; Narkchamnan, K.; Thitisak, B.; Rungswang, W.; Yau, W. W. *Polymer* **2016**, *107*, 122−129.
(26) Podzimek, S.; Vlcek, T.; Johann, C. *J. Appl. Polym. Sci.* **2001**, *81* (7), 1588−1594.
(27) Ahn, S.; Lee, H.; Lee, S.; Chang, T. *Macromolecules* **2012**, *45* (8), 3550−3556.
(28) Meunier, D. M.; Lyons, J. W.; Kiefer, J. J.; Niu, Q. J.; Delong, L. M.; Li, Y.; Russo, P. S.; Cueto, R.; Edwin, N. J.; Bouck, K. J.; et al. *Macromolecules* **2014**, *47*, 6715−6729.
(29) Plüschke, L.; Mundil, R.; Sokolohorskyj, A.; Merna, J.; Sommer, J.-U.; Lederer, A. *Anal. Chem.* **2018**, *90*, 6178−6186.
(30) Snijkers, F.; Ratkanthwar, K.; Vlassopoulos, D.; Hadjichristidis, N. *Macromolecules* **2013**, *46* (14), 5702−5713.
(31) Abbasi, M.; Faust, L.; Riazi, K.; Wilhelm, M. *Macromolecules* **2017**, *50* (15), 5964−5977.
(32) Greyling, G.; Lederer, A.; Pasch, H. *Macromol. Chem. Phys.* **2018**, *219* (24), 1800417.
(33) Lederer, A.; Burchard, W. *Hyperbranched Polymers: Macromolecules in between Deterministic Linear Chains and Dendrimer Structures*; Royal Society of Chemistry: Cambridge, U.K., 2015; DOI: 10.1016/B978-1-85617-745-0.00001-2.
(34) Striegel, A. M. *Chromatographia* **2016**, *79* (15-16), 945−960.
(35) White, R. P.; Lipson, J. E. G.; Higgins, J. S. *Macromolecules* **2010**, *43* (9), 4287−4293.
(36) Barth, H. G.; Boyes, B. E.; Jackson, C. *Anal. Chem.* **1998**, *70* (12), 251−278.
(37) Burchard, W. *Light Scatt. from Polym.* **1983**, *48*, 1−124.
(38) Cho, E. J.; Holback, H.; Liu, K. C.; Abouelmagd, S. A.; Park, J.; Yeo, Y. *Mol. Pharmaceutics* **2013**, *10*, 2093−2110.
(39) Vagberg, L. J. M.; Cogan, K. A.; Gast, A. P. *Macromolecules* **1991**, *24* (7), 1670−1677.
(40) Roovers, J.; Zhou, L. L.; Toporowski, P. M.; van der Zwan, M.; Iatrou, H.; Hadjichristidis, N. *Macromolecules* **1993**, *26* (16), 4324−4331.
(41) Rowland, S. M.; Striegel, A. M. *Anal. Chem.* **2012**, *84* (11), 4812−4820.
(42) Muza, U. L.; Greyling, G.; Pasch, H. *J. Chromatogr. A* **2018**, *1562*, 87−95.

DOI: 10.1021/acs.analchem.9b01384
Anal. Chem. XXXX, XXX, XXX−XXX

Chapter 5. Conclusions and recommendations

5.1 Conclusions

The work presented herein has not only showcased the successful utility of ThFFF as a competent alternative to classical separation techniques such as SEC, but also highlights that ThFFF may be a much better technique, in particular for the separation and characterization of BCP self-assemblies. Summarised conclusions from three distinct but correlated studies alluded to in Chapter 4 are subsequently presented.

Part 1

The microstructure of core microphase domains (CMDs) is shown to be an essential molecular parameter governing solution behaviour of self-assemblies. Under investigation were two types of vesicles successfully prepared from two symmetrical BCPs of PBd-PS, with either 1.2- or 1.4-PBd, respectively. Using a combination of batch mode ^{1}H NMR, DLS, and ThFFF as a separation technique, core microstructure was shown to impact on M_w, aggregation number and size of the resultant vesicles. Thus, the potential application of microstructural differences for providing designed BCP vesicles is demonstrated. Both PBd cores (1.2- or 1.4-PBd) are shown to be uncharacteristically visible in the ^{1}H NMR spectrum owing to the very low T_g and less compact PBd chains as compared to PS cores. This allows for the detection of chain mobility. Temperature dependent DLS was applied to elucidate crystallinity and elasticity of the PBd cores by measuring size change as function of temperature. Size differences of the vesicles (as imposed by microstructural differences of the cores) were used to explain the ThFFF elution behaviour. Furthermore, it was established

that ThFFF separations are also sensitive to topology, whereupon vesicles with PS shells and PS homopolymers of comparable D_h were shown to have different elution behaviour.

Part 2

In the second part, efforts were directed at designing a system capable of circumventing the typical precipitation effects as a result of stereocomplexation (SC) and, thus, allow for solution analysis of the resultant SC species. In this regard, PMMA-PS BCPs were utilised to design self-assemblies such that the cores were composed of the SC-active block (PMMA), and the shells were composed of a stabilising block (PS). Thermal energy was applied for the SC nanoreactions within the micelle cores. A combination of multiple detection ThFFF (to provide fractionation), DLS and FTIR (to provide size and composition information, respectively), were applied to monitor the SC nanoreactions. These nanoreactions are shown to provide alternative pathways in micelle design and modification, where microstructural differences of the PMMA cores are also shown to affect compactness, thermal stability, degree of elasticity, molar mass (hence aggregation number) and hydrodynamic size of the resultant SC species.

Part 3

The last section summarizes results derived from the unique utility of a five-detector combination to analyse ThFFF separations. The five-detector combination was strategically applied to design a system of three fundamentally different macromolecular analytical techniques. The following three techniques; DLS, dual

concentration detection and triple detection, were applied to derive a wealth of information on size, diffusion coefficient, thermal diffusion coefficient, absolute M_w, aggregation number, intrinsic viscosity, chemical composition, and structure of BCP self-assemblies and nanocarrier systems. Notably, hydrogenated and deuterated PS isotopes were used for the method development process, whereupon uncharacteristically higher resolution was shown for the ThFFF separations. Such resolution was explainable from the intrinsic viscosities, which showcased similar trends with the retention times. As such, ThFFF was concluded to exhibit gravimetric and density sensitivities.

5.2 Recommendations

The introduction of ThFFF-QD allows for detailed analysis of short and long chain branching for high molar mass and complex polymeric entities such as dendrimers, which may be difficult to analyse using column-based techniques. In addition, the morphological evolution of SAs into large aggregates and gels, and the differentiation of such complexities can be studied by ThFFF-QD.

To date, ThFFF separations have been successfully investigated with online FTIR and triple detection, respectively. As such, a combination of FTIR and triple detection presents an unexplored dimension with multiple vantage points for future work on the characterization of branched polymers.

Chapter 6. References

References

(1) Hadjichristidis, N.; Pispas, S.; Floudas, G. *Block Copolymers: Synthetic Strategies, Physical Properties and Applications.*; John Wiley & Sons Ltd, Chichester, UK, 2002. https://doi.org/10.1002/pi.1313.

(2) Yang, J. Viscoelastic Wormlike Micelles and Their Applications. *Curr. Opin. Colloid Interface Sci.* **2002**, *7* (5–6), 276–281. https://doi.org/10.1016/S1359-0294(02)00071-7.

(3) Ning, W.; Jiugao, Y.; Xiaofei, M. Preparation and Characterization of Thermoplastic Starch/PLA Blends by One-Step Reactive Extrusion. *Polym. Int.*

2007, *56*, 1440 – 1447. https://doi.org/10.1002/pi.

(4) Du, J.; O' Reilly, R. K. Anisotropic Particles with Patchy, Multicompartment and Janus Architectures: Preparation and Application. *Chem. Soc. Rev.* **2011**, *40* (5), 2402 – 2416. https://doi.org/10.1039/C0CS00216J.

(5) Antonietti, M.; Briel, A.; Tank, C. Chromatographic Characterization of Complex Polymer Systems with Thermal Field - flow Fractionation. *Acta Polym.* **1995**, *46* (3), 254 – 260. https://doi.org/10.1002/actp.1995.010460307.

(6) Pasch, H.; Trathnigg, B. *HPLC of Polymers*; Ingo, A., Pasch, H., Eds.; Springer: New Yorke, 1998. https://doi.org/10.1007/978-3-642-36080-0.

(7) Baines, F. L.; Billingham, N. C.; Armes, S. P. Synthesis and Solution Properties of Water-Soluble Hydrophilic-Hydrophobic Block Copolymers. *Macromolecules* **1996**, *29* (10), 3416 – 3420. https://doi.org/10.1021/ma951699+.

(8) Rivera, M. R.; Herrera N., R.; R í os G., L. Structure and Properties of Model Polybutadienes and HIPS: Effect of Rubber Microstructure on HIPS Dynamic Mechanical Properties. *J. Elastomers Plast.* **2006**, *38* (2), 133 – 146. https://doi.org/10.1177/0095244306057255.

(9) Snijkers, F.; Ratkanthwar, K.; Vlassopoulos, D.; Hadjichristidis, N. Viscoelasticity, Nonlinear Shear Start-up, and Relaxation of Entangled Star Polymers. *Macromolecules* **2013**, *46* (14), 5702 – 5713. https://doi.org/10.1021/ma400662b.

(10) Raust, J.-A.; Br ü ll, A.; Moire, C.; Farcet, C.; Pasch, H. Two-Dimensional Chromatography of Complex Polymers 6. Method Development for (Meth)Acrylate-Based Copolymers. *J. Chromatogr. A* **2008**, *1203* (2), 207 – 216. https://doi.org/10.1016/j.chroma.2008.07.067.

(11) Alexandridis, P.; Lindman, B. *Amphiphilic Block Copolymers: Self-Assembly and Applications*, 1st ed.; Alexandridis, P., Lindman, B., Eds.; Elsevier: Amsterdam, 2000.

(12) Riess, G. Micellization of Block Copolymers. *Prog. Polym. Sci.* **2003**, *28* (7), 1107 – 1170. https://doi.org/10.1016/S0079-6700(03)00015-7.

(13) Tseng, Y. C.; Darling, S. B. Block Copolymer Nanostructures for Technology. *Polymers (Basel).* **2010**, *2* (4), 470 – 489. https://doi.org/10.3390/polym2040470.

(14) Schacher, F. H.; Rupar, P. A.; Manners, I. Functional Block Copolymers: Nanostructured Materials with Emerging Applications. *Angew. Chemie - Int. Ed.* **2012**, *51* (32), 7898 – 7921. https://doi.org/10.1002/anie.201200310.

(15) Cho, E. J.; Holback, H.; Liu, K. C.; Abouelmagd, S. A.; Park, J.; Yeo, Y. Nanoparticle Characterization : State of the Art , Challenges , and Emerging Technologies. *Mol. Pharm.* **2013**, *10*, 2093–2110.

(16) Miller, A. C. Amphiphilic Block Copolymer Micelles : Creation of Functional Nanocavities and Their Use as Nanocontainers for Controlled Release, Massachusetts Institute of Technology, 2008.

(17) Liu, T.; Liu, L.-Z.; Chu, B. *Formation of Amphiphilic Block Copolymer Micelles in Nonaqueous Solution.*; Woodhead Publishing Limited: Cambridge, UK, 2000. https://doi.org/10.1016/B978-044482441-7/50007-4.

(18) Niu, A.; Liaw, D. J.; Sang, H. C.; Wu, C. Light-Scattering Study of a Zwitterionic Polycarboxybetaine in Aqueous Solution. *Macromolecules* **2000**, *33* (9), 3492 – 3494. https://doi.org/10.1021/ma991622b.

(19) Ford, N.; Havard, T.; Wallace, P. Analysis of Macromolecules Using Low and Right Angle Laser Light Scattering and Photon Correlation Spectroscopy (PCS). *Int. GPC Symp* **1996**, 460 – 483.

(20) Spevacek, J.; Konefal, R.; Cadova, E. NMR Study of Thermoresponsive Block Copolymer in Aqueous Solution. *Macromol. Chem. Phys.* **2016**, *217*, 1370 – 1375.

(21) Godward, J.; Heatley, F.; Price, C. 1H Nuclear Magnetic Relaxation Study of the Phase Structure of Polystyrene-Block-Poly(Ethylene/Propylene) Copolymer Micelles. *J. Chem. Soc. Faraday Trans.* **1993**, *89* (18), 3471. https://doi.org/10.1039/ft9938903471.

(22) Tretinnikov, O. N.; Ohta, K. Conformation-Sensitive Infrared Bands and Conformational Characteristics of Stereoregular Poly (Methyl Methacrylate) s by Variable-Temperature FTIR Spectroscopy. *Macromolecules* **2002**, *35*, 7343 – 7353. https://doi.org/10.1021/ma020411v.

(23) Essenlink, F. .; Dormidontova, E.; Hadziioannou, G. Evolution of Block Copolymer

Micellar Size and Structure Evidenced with Cryo Electron Microscopy. *Macromolecules* **1998**, *31* (9), 2925 – 2932.

(24) Ouarti, N.; Viville, P.; Lazzaroni, R.; Minatti, E.; Schappacher, M.; Deffieux, A.; Borsali, R. Control of the Morphology of Linear and Cyclic PS-b-PI Block Copolymer Micelles via PS Addition. *Langmuir* **2005**, *21* (4), 1180 – 1186. https://doi.org/10.1021/la048944f.

(25) Barnhill, S. a.; Bell, N. C.; Patterson, J. P.; Olds, D. P.; Gianneschi, N. C. Phase Diagrams of Polynorbornene Amphiphilic Block Copolymers in Solution. *Macromolecules* **2015**, *48* (4), 1152 – 1161. https://doi.org/10.1021/ma502163j.

(26) Barth, H. G.; Boyes, B. E.; Jackson, C. Size Exclusion Chromatography and Related Separation Techniques. *Anal. Chem.* **1998**, *70* (12), 251 – 278. https://doi.org/10.1021/a1980015t.

(27) Yu, Y.; Deslauriers, P. J.; Rohlfing, D. C. SEC-MALS Method for the Determination of Long-Chain Branching and Long-Chain Branching Distribution in Polyethylene. *Polymer (Guildf).* **2005**, *46* (14), 5165 – 5182. https://doi.org/10.1016/j.polymer.2005.04.036.

(28) Gaborieau, M.; Castignolles, P. Size-Exclusion Chromatography (SEC) of Branched Polymers and Polysaccharides. *Anal Bioanal Chem* **2011**, *399*, 1413 – 1423. https://doi.org/10.1007/s00216-010-4221-7.

(29) Messaud, F.; Sanderson, R. D.; Runyon, J. R.; Otte, T.; Pasch, H.; Williams, S. K. R.

An Overview on Field-Flow Fractionation Techniques and Their Applications in the Separation and Characterization of Polymers. *Prog. Polym. Sci.* **2009**, *34* (4), 351 – 368. https://doi.org/10.1016/j.progpolymsci.2008.11.001.

(30) Schimpf, M. E.; Caldwell, K.; Giddings, J. C. *Field-Flow Fractionation Handbook*; Schimpf, M. E., Caldwell, K., Giddings, J. C., Eds.; Wiley-Interscience: New York, USA, 2000; Vol. 4.

(31) Glantz, M.; Hakansson, A.; Mansson, H. L.; Paulsson, M.; Nilsson, L. Revealing the Size, Conformation, and Shape of Casein Micelles and Aggregates with Asymmetrical Flow Field-Flow Fractionation and Multiangle Light Scattering. *Langmuir* **2010**, *26* (15), 12585 – 12591. https://doi.org/10.1021/la101892x.

(32) Moon, M. H. Flow Field-Flow Fractionation and Multiangle Light Scattering for Ultrahigh Molecular Weight Sodium Hyaluronate Characterization. *J. Sep. Sci.* **2010**, *33* (22), 3519 – 3529. https://doi.org/10.1002/jssc.201000414.

(33) Hiller, W.; Van Aswegen, W.; Hehn, M.; Pasch, H. Online ThFFF-NMR: A Novel Tool for Molar Mass and Chemical Composition Analysis of Complex Macromolecules. *Macromolecules* **2013**, *46* (7), 2544 – 2552. https://doi.org/10.1021/ma400350y.

(34) Zattoni, A.; Roda, B.; Borghi, F.; Marassi, V.; Reschiglian, P. Flow Field-Flow Fractionation for the Analysis of Nanoparticles Used in Drug Delivery. *J. Pharm. Biomed. Anal.* **2014**, *87*, 53 – 61. https://doi.org/10.1016/j.jpba.2013.08.018.

(35) Runyon, J. R.; Williams, S. K. R. Composition and Molecular Weight Analysis of Styrene-Acrylic Copolymers Using Thermal Field-Flow Fractionation. *J. Chromatogr. A* **2011**, *1218* (38), 6774 – 6779. https://doi.org/10.1016/j.chroma.2011.07.076.

(36) Shiundu, P. M.; Liu, G.; Giddings, J. C. Separation of Particles in Nonaqueous Suspensions by Thermal Field-Flow Fractionation. *Anal. Chem.* **1995**, *67* (15), 2705 – 2713. https://doi.org/10.1021/ac00111a032.

(37) Cho, K.-H.; Park, Y. H.; Jeon, S. J.; Kim, W.-S.; Lee, D. W. Retention Behavior of Copolymers in Thermal Field-Flow Fractionation and Gel Permeation Chromatography. *J. Liq. Chromatogr. Relat. Technol.* **1997**, *20* (16 – 17), 2741 – 2756. https://doi.org/10.1080/10826079708005590.

(38) Schimpf, M. E.; Giddings, J. C. Characterization of Thermal Diffusion of Copolymers in Solution by Thermal Field-Flow Fractionation. *J. Polym. Sci. Part B Polym. Phys.* **1990**, *28* (13), 2673 – 2680. https://doi.org/10.1002/polb.1990.090281313.

(39) Van Batten, C.; Hoyos, M.; Martin, M. Thermal Field-Flow Fractionation of Colloidal Materials: Methylmethacrylate-Styrene Linear Di-Block Copolymers. *Chromatographia* **1997**, *45*, 121 – 126. https://doi.org/10.1007/BF02505548.

(40) Greyling, G.; Pasch, H. Multidetector Thermal Field-Flow Fractionation as a Unique Tool for the Tacticity-Based Separation of Poly(Methyl Methacrylate)-

Polystyrene Block Copolymer Micelles. *J. Chromatogr. A* **2015**, *1414*, 163 – 172. https://doi.org/10.1016/j.chroma.2015.08.023.

(41) Greyling, G.; Pasch, H. Multidetector Thermal Field-Flow Fractionation: A Unique Tool for Monitoring the Structure and Dynamics of Block Copolymer Micelles. *Macromolecules* **2016**, *49*, 1882 – 1889. https://doi.org/10.1021/acs.macromol.5b02634.

(42) Greyling, G.; Pasch, H. Characterization of Charged Polymer Self-Assemblies by Multidetector Thermal Field-Flow Fractionation in Aqueous Mobile Phases. *J. Chromatogr. A* **2018**, *1532*, 175 – 181. https://doi.org/10.1016/j.chroma.2017.12.008.

(43) Cai, S.; Vijayan, K.; Cheng, D.; Lima, E. M.; Discher, D. E. Micelles of Different Morphologies - Advantages of Worm-like Filomicelles of PEO-PCL in Paclitaxel Delivery. *Pharm. Res.* **2007**, *24* (11), 2099 – 2109. https://doi.org/10.1007/s11095-007-9335-z.

(44) Blanazs, A.; Armes, S. P.; Ryan, A. J. Self-Assembled Block Copolymer Aggregates: From Micelles to Vesicles and Their Biological Applications. *Macromol. Rapid Commun.* **2009**, *30* (4 – 5), 267 – 277. https://doi.org/10.1002/marc.200800713.

(45) Vriezema, D. M.; Aragone, M. C.; Elemans, J. A. A. W.; Cornelissen, J. J. L. M.; Rowan, A. E.; Nolte, R. J. M. Self-Assembled Nanoreactors. *Chem. Rev.* **2005**, *105* (4), 1445 – 1489. https://doi.org/10.1021/cr0300688.

(46) Khullar, P.; Singh, V.; Mahal, A.; Kumar, H.; Kaur, G.; Bakshi, M. S. Block Copolymer Micelles as Nanoreactors for Self-Assembled Morphologies of Gold Nanoparticles. *J. Phys. Chem. B* **2013**, *117*, 3028 – 3039. https://doi.org/10.1021/jp310507m.

(47) Deuring, H.; Alberda van Ekenstein, G.; Challa, G. Stereocomplex Formation. *Macromolecules* **1995**, *28*, 1952 – 1958. https://doi.org/10.1021/ma00110a032.

(48) Slager, J.; Domb, A. J. Biopolymer Stereocomplexes. *Adv. Drug Deliv. Rev.* **2003**, *55* (4), 549 – 583. https://doi.org/10.1016/S0169-409X(03)00042-5.

(49) Kumaki, J.; Kawauchi, T.; Okoshi, K.; Kusanagi, H.; Yashima, E. Supramolecular Helical Structure of the Stereocomplex Composed of Complementary Isotactic and Syndiotactic Poly (Methyl Methacrylate) s as Revealed by Atomic Force Microscopy **. *Angew. Chemie - Int. Ed.* **2007**, *46*, 5348 – 5351. https://doi.org/10.1002/anie.200700455.

(50) Muza, U. L.; Greyling, G.; Pasch, H. Characterization of Complex Polymer Self-Assemblies and Large Aggregates by Multidetector Thermal Field-Flow Fractionation. *Anal. Chem.* **2017**, *89*, 7216 – 7224. https://doi.org/10.1021/acs.analchem.7b01445.

(51) Dondi, F.; Guiochon, G. *Theoretical Advancement in Chromatography and Related Separation Techniques*; Springer Science & Business Media: Ferrara, Italy, 2012.

(52) Ratanathanawongs Williams, S. K.; Lee, D. Field-Flow Fractionation of Proteins Polysaccharides, Synthetic Polymers, and Supramolecular Assemblies. *J. Sep. Sci.* **2006**, *29* (12), 1720 – 1732. https://doi.org/10.1002/jssc.200600151.

(53) Giddings, J. C. Field-Flow Fractionation: Analysis of Macromolecular, Colloidal, and Particulate Materials. *Science* **1993**, *260* (5113), 1456 – 1465. https://doi.org/10.1126/science.8502990.

(54) Baalousha, M.; Stolpe, B.; Lead, J. R. Flow Field-Flow Fractionation for the Analysis and Characterization of Natural Colloids and Manufactured Nanoparticles in Environmental Systems: A Critical Review. *J. Chromatogr. A* **2011**, *1218* (27), 4078 – 4103. https://doi.org/10.1016/j.chroma.2011.04.063.

(55) Yohannes, G.; Jussila, M.; Hartonen, K.; Riekkola, M. L. Asymmetrical Flow Field-Flow Fractionation Technique for Separation and Characterization of Biopolymers and Bioparticles. *J. Chromatogr. A* **2011**, *1218* (27), 4104 – 4116. https://doi.org/10.1016/j.chroma.2010.12.110.

(56) Vanasten, A. C.; Stegeman, G.; Kok, W. T.; Tijssen, R.; Poppe, H. Separation Speed in Thermal Field-Flow Fractionation. *Anal. Chem.* **1994**, *66* (19), 3073 – 3080.

(57) Schimpf, M. E.; Giddings, J. C. Characterization of Thermal Diffusion in Polymer Solutions by Thermal Field-Flow Fractionation: Effects of Molecular Weight and Branching. *Macromolecules* **1987**, *20* (7), 1561 – 1563. https://doi.org/10.1021/ma00173a022.

(58) Schimpf, M. E.; Giddings, J. C. Characterization of Thermal Diffusion in Polymer Solutions by Thermal Field-Flow Fractionation: Dependence on Polymer and Solvent Parameters. *J. Polym. Sci. Part B Polym. Phys.* **1989**, *27* (6), 1317 – 1332. https://doi.org/10.1002/polb.1989.090270610.

(59) Nguyen, M.; Beckett, R. Determination of Thermal Diffusion Coefficients Using Thermal Field-Flow Fractionation and Mark-Houwink Constants. *Anal. Chem.* **2004**, *76* (8), 2382 – 2386. https://doi.org/10.1021/ac035311h.

(60) Borchard, F.; de Gennes, P.-G. Mw Independent of Thermal Diffusion. *C. R. Hebd. Seances Acad. Sci.* **1981**, *293*, 1025.

(61) Rauch, J.; Ko, W. On the Molar Mass Dependence of the Thermal Diffusion Coefficient of Polymer Solutions. *Macromolecules* **2005**, *38*, 3571 – 3573.

(62) Shiundu, P. M.; Munguti, S. M.; Williams, S. K. R. P Ractical Implications of Ionic Strength Effects on Particle Retention in Thermal Field-Flow Fractionation. *J. Chromatogr. A* **2003**, *984*, 67 – 79.

(63) Ngaza, N.; Brand, M.; Pasch, H. Multidetector-ThF3 as a Novel Tool for the Investigation of Solution Properties of Amphiphilic Block Copolymers. *Macromol. Chem. Phys.* **2015**, 1355 – 1364. https://doi.org/10.1002/macp.201500070.

(64) Greyling, G.; Pasch, H. Tacticity Separation of Poly(Methyl Methacrylate) by Multidetector Thermal Field-Flow Fractionation. *Anal. Chem.* **2015**, *87* (5), 3011 – 3018. https://doi.org/10.1021/ac504651p.

(65) Greyling, G.; Pasch, H. Multidetector Thermal Field-Flow Fractionation as a Novel Tool for the Microstructure Separation of Polyisoprene and Polybutadiene. *Macromol. Rapid Commun.* **2014**, *35* (21), 1846 – 1851. https://doi.org/10.1002/marc.201400405.

(66) Hiller, W.; Hehn, M. Investigations of Multiple Detection of Polymers. *Anal. Chem.* **2014**, *86*, 10900 – 10908. https://doi.org/10.1021/ac5031607.

(67) Gaborieau, M.; Gilbert, R. G.; Gray-Weale, A.; Hernandez, J. M.; Castignolles, P. Theory of Multiple-Detection Size-Exclusion Chromatography of Complex Branched Polymers. *Macromol. Theory Simulations* **2007**, *16* (1), 13 – 28. https://doi.org/10.1002/mats.200600046.

(68) Ratanathanawongs Williams, S. K.; Shiundu, P. M.; Giddings, J. C. Size and Compositional Studies of the Core Shell Latexes Using Flow and Thermal Fff.Pdf. *Colloids Surfaces A Physicochem. Eng. Asp.* **1995**, *105*, 243 – 250.

(69) Kassalainen, G. E.; Williams, S. K. R. Coupling Thermal Field-Flow Fractionation with Matrix-Assisted Laser Desorption/Ionization Time-of-Flight Mass Spectrometry for the Analysis of Synthetic Polymers. *Anal. Chem.* **2003**, *75* (8), 1887 – 1894. https://doi.org/10.1021/ac020594j.

(70) Greyling, G.; Pasch, H. Multidetector Thermal Field-Flow Fractionation: A Unique Tool for Monitoring the Structure and Dynamics of Block Copolymer Micelles. *Macromolecules* **2016**, *49*, 1882–1889. https://doi.org/10.1021/acs.macromol.5b02634.

References

(71) Ebrahim Attia, A. B.; Ong, Z. Y.; Hedrick, J. L.; Lee, P. P.; Ee, P. L. R.; Hammond, P. T.; Yang, Y. Y. Mixed Micelles Self-Assembled from Block Copolymers for Drug Delivery. *Curr. Opin. Colloid Interface Sci.* **2011**, *16* (3), 182 – 194. https://doi.org/10.1016/j.cocis.2010.10.003.

(72) Owen, S. C.; Chan, D. P. Y.; Shoichet, M. S. Polymeric Micelle Stability. *Nano Today* **2012**, *7* (1), 53 – 65. https://doi.org/10.1016/j.nantod.2012.01.002.

(73) Li, G.; Song, S. E. N.; Guo, L. E. I.; Ma, S. Self-Assembly of Thermo- and PH-Responsive Poly (Acrylic Acid) - b -Poly (N -Isopropylacrylamide) Micelles for Drug Delivery. *J. Polym. Sci. Part A Polym. Chem.* **2008**, *46*, 5028 – 5035. https://doi.org/10.1002/pola.

(74) Bakshi, M. S. Colloidal Micelles of Block Copolymers as Nanoreactors , Templates for Gold Nanoparticles , and Vehicles for Biomedical Applications. *Adv. Colloid Interface Sci.* **2014**, *213*, 1 – 20. https://doi.org/10.1016/j.cis.2014.08.001.

(75) Saunders, G.; Cormack, P. A. G.; Graham, S.; Sherrington, D. C. Use of Rapid Triple Detection Size Exclusion Chromatography to Evaluate the Evolution of Molar Mass and Branching Architecture during Free Radical Branching Copolymerization of Methyl Methacrylate and Ethylene Glycol Dimethacrylate. *Macromolecules* **2005**, *38* (15), 6418 – 6422. https://doi.org/10.1021/ma0501693.

(76) Ahn, S.; Lee, H.; Lee, S.; Chang, T. Characterization of Branched Polymers by

Comprehensive Two-Dimensional Liquid Chromatography with Triple Detection. *Macromolecules* **2012**, *45* (8), 3550 – 3556. https://doi.org/10.1021/ma2021985.

(77) Wang, W. J.; Kharchenko, S.; Migler, K.; Zhu, S. Triple-Detector GPC Characterization and Processing Behavior of Long-Chain-Branched Polyethylene Prepared by Solution Polymerization with Constrained Geometry Catalyst. *Polymer (Guildf).* **2004**, *45* (19), 6495 – 6505. https://doi.org/10.1016/j.polymer.2004.07.035.

(78) Kirkland, J. J.; Rementer, S. W. Polymer Molecular Weight Distributions by Thermal Field Flow Fractionation Using Mark-Houwink Constants. *Anal. Chem.* **1992**, *64* (8), 904 – 913. https://doi.org/10.1021/ac00032a014.